Progress in Energy and Combustion Science 60 (2017) 68–96

Contents lists available at ScienceDirect

Progress in Energy and Combustion Science

journal homepage: www.elsevier.com/locate/pecs

Removal of non-CO_2 greenhouse gases by large-scale atmospheric solar photocatalysis

Renaud de_Richter[a,*], Tingzhen Ming[b,*], Philip Davies[c], Wei Liu[d], Sylvain Caillol[a]

[a] Institut Charles Gerhardt Montpellier – UMR5253 CNRS-UM2 – ENSCM-UM1 – Ecole Nationale Supérieure de Chimie de Montpellier, 8 rue de l'Ecole Normale, 34296 Montpellier Cedex 5, France
[b] School of Civil Engineering and Architecture, Wuhan University of Technology, No. 122, Luoshi Road, Wuhan 430070, China
[c] Sustainable Environment Research Group, School of Engineering and Applied Science, Aston University, Birmingham B4 7ET, UK
[d] School of Energy and Power Engineering, Huazhong University of Science and Technology, Wuhan 430074, China

ARTICLE INFO

Article History:
Received 21 May 2016
Accepted 12 January 2017

Keywords:
Atmospheric greenhouse gas removal
GHG photocatalysis
Solar-wind hybrid
Negative emissions technology
Solar chimney power plant
Giant photocatalytic reactor
Large scale atmospheric air cleansing

ABSTRACT

Large-scale atmospheric removal of greenhouse gases (GHGs) including methane, nitrous oxide and ozone-depleting halocarbons could reduce global warming more quickly than atmospheric removal of CO_2. Photocatalysis of methane oxidizes it to CO_2, effectively reducing its global warming potential (GWP) by at least 90%. Nitrous oxide can be reduced to nitrogen and oxygen by photocatalysis; meanwhile halocarbons can be mineralized by red-ox photocatalytic reactions to acid halides and CO_2. Photocatalysis avoids the need for capture and sequestration of these atmospheric components. Here review an unusual hybrid device combining photocatalysis with carbon-free electricity with no-intermittency based on the solar updraft chimney. Then we review experimental evidence regarding photocatalytic transformations of non-CO_2 GHGs. We propose to combine TiO_2-photocatalysis with solar chimney power plants (SCPPs) to cleanse the atmosphere of non-CO_2 GHGs. Worldwide installation of 50,000 SCPPs, each of capacity 200 MW, would generate a cumulative 34 PWh of renewable electricity by 2050, taking into account construction time. These SCPPs equipped with photocatalyst would process 1 atmospheric volume each 14–16 years, reducing or stopping the atmospheric growth rate of the non-CO_2 GHGs and progressively reducing their atmospheric concentrations. Removal of methane, as compared to other GHGs, has enhanced efficacy in reducing radiative forcing because it liberates more ·OH radicals to accelerate the cleaning of the troposphere. The overall reduction in non-CO_2 GHG concentration would help to limit global temperature rise. By physically linking greenhouse gas removal to renewable electricity generation, the hybrid concept would avoid the moral hazard associated with most other climate engineering proposals.

Contents

Abbreviations: Bioenergy with carbon sequestration and storage, BECCS; Carbon sequestration and storage, CCS; Carbon dioxide removal, CDR; Methane, CH_4; Chloro fluoro carbons, CFCs; Carbon dioxide, CO_2; Giant photocatalytic reactor, GCR; Greenhouse, GH; Greenhouse gas, GHG; Greenhouse gas removal, GHGR; Global warming potential, GWP; Hydro chloro fluoro carbons and hydro fluoro carbons, HFCs; Intergovernmental Panel on Climate Change, IPCC; Metal organic framework, MOF; Nitrous oxide, N_2O; Parts per billion, ppb; Parts per million, ppm; Photocatalytic reactor, PCR; Relative humidity, RH; Solar chimney power plant, SCPP; Solar radiation management, SRM; Ultraviolet, UV; Volatile organic compound, VOC

* Corresponding authors.
E-mail address: renaud.derichter@gmail.com (R. de_Richter), tzming@whut.edu.cn (T. Ming), p.a.davies@aston.ac.uk (P. Davies), w_liu@hust.edu.cn (W. Liu), sylvain.caillol@enscm.fr (S. Caillol).

http://dx.doi.org/10.1016/j.pecs.2017.01.001

1. Introduction

1.1. The need for hybrid renewable energy and greenhouse gas reduction technologies

Even if humans stop combusting fossil fuels and discharging CO_2 into the atmosphere, the average global temperature of the Earth will continue to increase for the rest of the century –for several reasons. Firstly, the long lifetime of CO_2 (estimated in the 100–300 year range [1]) means that the excess atmospheric stocks (515 Gt Carbon) would continue to drive radiative forcing and global warming for many decades [2]. Secondly, even if atmospheric concentrations were to decrease, CO_2 would outgas from the oceans and offset this decrease, because of the dynamic equilibrium between the CO_2 in the atmosphere and the (bi)carbonates HCO_3^-/CO_3^{2-} dissolved in the oceans [3].

Thirdly, there is the contribution of other GHGs, besides CO_2, which together account for about 34% of radiative forcing [4]. Even if all excess anthropogenic atmospheric CO_2 were removed, radiative forcing would only be reduced by half [5].

The insufficiency of mitigation measures based just on fossil fuel replacement has prompted research in carbon capture and sequestration (CCS), greenhouse gas removal (GHGR), and solar radiation management (also called solar reflection methods: SRM). But each of these approaches suffers drawbacks. CCS [6,7] may restrict release of CO_2 from stationary fossil-fuel power plants, but not from vehicles. It also carries significant water and energy penalties and a number of environmental risks associated with transport and storage of the CO_2 [7,8].

In order to stabilize the Earth surface temperature alternative processes are needed to decrease the level of atmospheric GHGs. Of the over 100 climate modeling simulations consistent with the Paris Agreement goals, as analyzed by the IPCC scientists, 87% involve net-negative emissions [9] by the end of the century: this can only be accomplished through the large-scale deployment of GHGR solutions.

According to the United Nations Environment Program [10], as shown in Fig. 1, the CO_2 emissions will have to be stopped by mid-century and by the second half of the century, GHGs will have to be removed from the atmosphere and among them non-CO_2 GHGs which have a significant contribution to the global anthropogenic radiative forcing (nearly 1/3rd).

Among GHGR technologies, those most frequently discussed target CO_2. Carbon dioxide removal (CDR) technologies include afforestation, reforestation, biochar [11,12], bioenergy with carbon capture and sequestration (BECCS) [13,14], direct air capture (removing the CO_2 from ambient air rather than from a smoke stack) [15], accelerated mineral weathering [16], ocean iron fertilization and several others [17]. Each incurs significant penalties with regard to land, energy and water usage [18]. BECCS offers the benefit of net energy production, but requires very large land usage which would impact on world food production [19].

SRM technologies include atmospheric aerosol injection using sulphur dioxide or other agents to induce negative radiative forcing by reflecting back to space incoming sunlight. Such interventions raise perplexing issues of international governance and security, prompting discussions about militarization, vulnerability to sabotage, and the risks of sudden termination causing catastrophic warming should the technology fail for any reason [20]. Over-reliance on SRM and CDR generally, and fear of resulting complacency as regards emissions reduction, has been referred to as *moral hazard* in debates about both these climate engineering measures.

The moral hazard can be avoided, however, if GHGR is physically linked to emissions reduction, thus making sure that the former does not neglect the latter. While BECCS achieves such linkage, another approach so far less discussed and evaluated is to hybridize Solar Chimney Power Plants (SCPPs) with Photocatalytic Reactors (PCRs) – see Fig. 2 and chapter 2. The idea of hybrid SCPP-PCR was introduced at the recent Oxford (UK) GHGR conference [21] and earlier at a SCPP conference in Bochum (DE) [22]. Like BECCS, SCPP-PCR would provide renewable electricity while removing GHGs; but

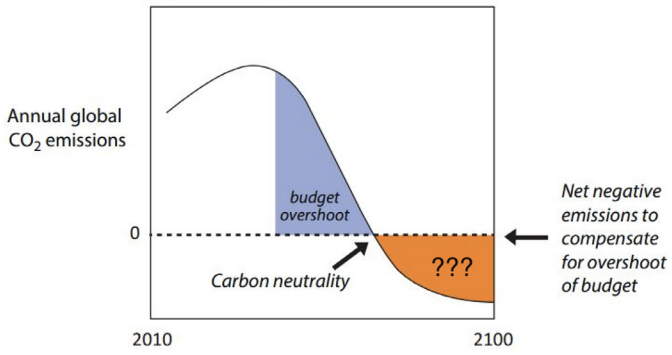

Fig. 1. CO_2 emissions pathway [10].

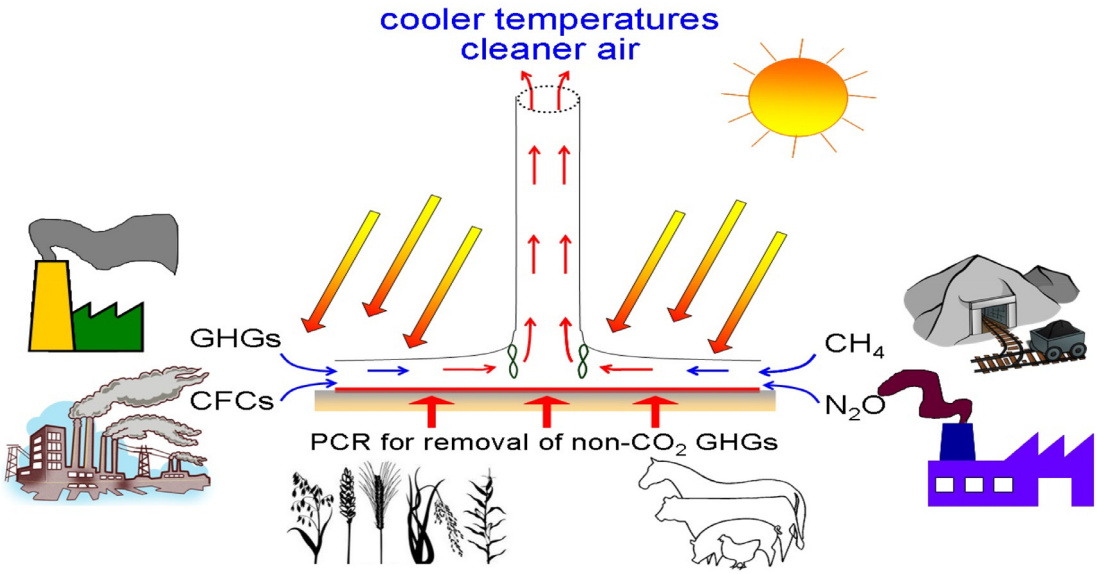

Fig. 2. Hybrid SCPP-PCR for renewable electricity generation and greenhouse gas removal (reproduced from [21]).

instead of removing CO_2 it would remove other GHGs including methane, nitrous oxide and halocarbons.

The SCPP is an established concept that generates electricity in a solar updraft tower incorporating axial-flow turbines [23]. Hot air is supplied to the tower by a large solar air heater (solar collector) similar to a horticultural greenhouse (GH). The function of a PCR can be incorporated in the SCPP by coating its collector with a photocatalyst, such as TiO_2, which is able to transform non-CO_2 GHGs into less harmful products.

1.2. Why focus on removing non-CO_2 greenhouse gases?

Though CO_2 currently contributes the largest part (65%) to radiative forcing, with CH_4 in second place at 17%, reduction of CH_4 may have a disproportionately large effect in arresting future global warming. This is because of the role of methane in tropospheric ozone chemistry. Methane reduces the oxidizing capacity of the atmosphere when reacting with hydroxyl radicals ($^{\circ}OH$) which produces tropospheric ozone, a harmful compound for humans, livestock and plants. The chemical coupling between $^{\circ}OH$ and CH_4 leads to a significant amplification of an emission impact; that is, increasing CH_4 emissions decreases tropospheric $^{\circ}OH$ which in turn increases the CH_4 lifetime and therefore its burden.

Moreover, the last report of IPCC revised upwards the estimates of global warming potential (GWP) of CH_4. Per kg, CH_4 causes 28–34 times more global warming than CO_2 over a 100-year time horizon according to the IPCC 5th report of 2013 [24]. This represents a significant increase over the earlier estimate of $GWP_{100}=25$ in the 4th IPCC report of 2007. Furthermore, over a 20-year horizon, the IPCC now attributes $GWP_{20}=86$ to methane, bringing new urgency to the control of CH_4 levels. Photocatalysis would transform CH_4 into equimolar quantities of CO_2 so comparisons should be made on a molar basis (rather than per kg). Thus GWP values for methane are effectively reduced by a factor of 2.75 leading to modified values in the range 10–30 approximately. Even so, transforming methane and other GHGs into CO_2 is almost as good as removing them altogether. For example, based on GWP = 28, transformation of 1 kg of methane into 2.75 kg of CO_2 reduces its climate change effect by 90%, and is equivalent to removal of 25.25 kg of CO_2 from the atmosphere. In summary, transforming atmospheric CH_4 into equimolar amounts of CO_2, as discussed in this review, would have a significant impact in fighting global warming.

It should be remembered that radiative forcing is conventionally measured relative to 1750 baseline estimates of GHGs concentration. As highlighted by Ruddiman [25], a reframing of timescales to span back to about 6000 BCE, would lead to further upward estimate in the radiative forcing of methane.

1.3. The need for this review

Though CO_2 reduction is more frequently the subject of scientific study, some technological options for reducing *non*-CO_2 emissions have already been reviewed [26]. But few options have been presented for removal at global scale. By way of exception, Boucher [27] considered molecular sieves, adsorption filters (zeolite minerals), cryogenic separation and in-situ CH_4 oxidation techniques (rather than capture it) with enzymatic systems, methanotrophic bacteria hosted in bio-rectors, bio-inspired catalytic oxidation in aqueous phase and using precious metal-based catalysts. Boucher suggested carefully assessing all suitable technologies for CH_4 air capture against their energetic cost and scalability. But none of the proposals appeared energetically or economically suitable to be applied on a large scale. Most of them would require an energy supply, which is strong disincentive to their application, and none of them explicitly addresses issues of implementation at the scale necessary to avert disastrous climate change.

Stolaroff [28] found that any strategy to reduce significantly atmospheric CH_4 concentrations needs to process nearly 1/10 of the atmosphere each year. According to Stolaroff, with catalytic aerosols dispersed in the atmosphere this might be feasible; although a suitable aerosol material was not identified by this author.

Though reduction of CO_2 emissions will not alone suffice to stabilize global warming, an overall reduction in concentrations of CO_2 and other GHGs could limit global temperature rise to the ceiling of 1.5–2 °C mandated at the recent COP 21 meeting in Paris [29]. This makes a hybrid approach for renewable energy (avoiding CO_2) and removal of GHGs highly interesting as a potentially effective solution and a negative emissions technology. Furthermore, the economics of power generation could help pay for the GHGR. These advantages are also a feature of BECCS, which has so far attracted much research and review of literature [30–32].

In contrast to BECCS, the hybrid SCPP-PCR concept has only been subject to an academic review for N_2O and halocarbons [33,34]. This review aims to redress this situation and provide a sound literature

background for future research of this promising new concept, especially for CH_4 removal. No SCPP-PCR has ever been built; therefore the review must focus on the parent technologies of the PCR and SCPP, of which examples have been built (though not yet of sufficient scale), in order to draw inferences about the potential of the hybrid concept.

The review is structured as follows. Section 2 covers the background of SCPPs; then Section 3 covers the types of photocatalysts and reactors, their environmental and large scale applications, and issues associated with lifetime of the catalysts. Section 4 discusses specific photocatalytic reactions: firstly, photoreduction of nitrous oxide into nitrogen and oxygen according to the reaction scheme of Eq. (1); then the photocatalytic oxido-reduction of several halocarbons generally (but not always) into carbon dioxide and mineral halo-acids according to the generic reaction scheme of Eq. (2); and finally the photocatalytic oxidation of methane into carbon dioxide and water, according to the reaction scheme of Eq. (3):

$$2N_2O \rightarrow 2N_2 + O_2 \quad (1)$$

$$\text{Halocarbon} + \text{oxygen}\wedge \rightarrow CO_2 + \text{hydrofluoric}\wedge \quad (2)$$

$$CH_4 + 2O_2 \rightarrow 2H_2O + CO_2 \quad (3)$$

In Section 5, we discuss coupling of a PCR with the SCPP. The synergies between these two disruptive technologies are then listed before the examination of the possibilities for night operation of the non-CO_2 GHGs removal process; and then a discussion (Section 5) and concluding remarks are given.

2. Solar chimney power plants background

This section reviews work up till now on SCPPs, as this will be relevant to their proposed coupling to photocatalytic reactors. It makes special reference to the experimental plant operated in Spain in the 1980s and the following theoretical studies and design initiatives.

The rationale in combining SCPPs with PCR for non-CO_2 GHGR is as follows. First, we note that to be able to remove, transform, or destroy significant amounts of non-CO_2 GHGs (halocarbons, N_2O and CH_4) from the earth's atmosphere in air, at ambient temperature and ambient RH% several materials and conditions are required:

- efficient visible light photocatalysts able to transform non-CO_2 GHGs;
- strong sunlight radiation during numerous hours to activate very large surface areas of the photocatalysts;
- strong and continuous air fluxes to put in contact the photocatalysts under the sunlight and the polluted air containing CH_4, N_2O, CFCs and HFCs.

Second, we note that a SCPP (Fig. 2) can bring all these conditions together.

A conventional SCPP is composed of 4 principal components [35]:

- a very large GH collector, for GH effect;
- a tall chimney for stack effect;
- a thermal energy storage layer to store the solar radiation for night time operation;
- and several turbines to generate renewable electricity which is carbon-free. By transforming sunlight radiation received under several km^2 of greenhouse (GH) collector (made of glass or plastic) a SCPP produces sustainable decarbonized renewable energy.

When linked with photocatalysis, the SCPP therefore becomes a negative-emissions technology with power generation (whereas CCS and DAC technologies consume energy).

Typically, the area of the GH collector for a model SCPP of 200 MW is 38 km^2 and the daily airflow passing through it is 17 km^3 per day, SCPPs being located in regions receiving usually >2200 kW m^{-2} $year^{-1}$ of solar radiation [36]. SCPPs appear to be good candidates for large scale GHGR as they can share several km^2 of illuminated area to perform photocatalytic reactions in synergy. The energy pay-back time of a SCPP is estimated to ~2 years [37] (compensation of the CO_2 emissions due to the production of construction materials and the construction of a structure reimbursed by the CO_2 emissions avoided by renewable energy production).

Though SCPPs have hardly been studied for non-CO_2 GHGR, there are other studies for air cleaning that are worth noting. Recently Cao, et al. [38] proposed a large-scale urban air remediation with a solar chimneys equipped of filters inside as a cleaning system to remove particulate matter thanks to the air flux it can provide. This modified solar chimney is devoted to air purification and does not produce electricity, as an average pressure drop of 500 Pa is used by Cao in the numerical simulation, because the filter has to remove small particles.

Similarly, direct CO_2 capture from the atmosphere using alkali resin solid sorbents has also been proposed [39], taking profit from the very important air flux provided "almost for free" by SCPPs.

2.1. SCPP pilot plant at Manzanares, Spain

In 1982, a 50 kW SCPP prototype with collector radius 122 m and chimney height 195 m was built in Spain by the German company Schlaich Bergermann and Partners [40,41]. Key technical data and design criteria of this pilot are shown in Table 1. The SCPP pilot was fully tested and validated over seven years [23,35] attracting worldwide attention.

Advocates of the technology have pointed to the following benefits: (1) ease of collecting large amounts of solar radiation; (2) thermal energy storage using cheap storage material which can realize continuous and steady generation of electricity; (3) artificial strong unidirectional upwind caused by the GH effect and the stack effect, which avoid the application of complex controlling systems necessarily used in free wind farms; (4) easily combing natural wind by introducing the natural wind via the collector inlet; (5) technical feasibility and cost-reduction possibilities by using ETFE for the collector canopy [37] and self-standing fabric chimney to replace the conventional concrete tower [42–44].

Under the GH, the thermal inertia of the ground can be enhanced, to store heat during the day and to release sensible heat at night, allowing electricity production 24 h/day with no-intermittency [45].

Table 1
Technical data and design criteria of the Spanish SCPP prototype [40].

Chimney height	194.6 m
Chimney radius	5.08 m
Mean collector radius	122 m
Average collector height	1.85 m
Number of turbine blades	4
Blade radius	5 m
Turbine speed in grid connection mode	100 rpm
Gear ratio	1:10
Design irradiation	1000 W/m^2
Design free-air temperature	302 K
Ambient temperature	29 °C
Temperature collector outlet	49 °C
Ground temperature [40]	70 °C
Temperature increase	20 K
Collector efficiency	32%
Turbine efficiency	83%
Upwind velocity under load condition	9 m/s
Upwind velocity on release	15 m/s
Power output at design point	50 kW
Power production per unit of land area	0.1 W/m^2

2.2. Theoretical analysis of the SCPP

A very comprehensive mathematical model to describe the GH effect of a SCPP pilot based upon the thermal network theory was firstly advanced by Pasumarthi and Sherif [46], where they considered: (1) the effect of single and double canopy to avoid excessive thermal energy releasing to the ambience; (2) the effect of the area of an energy storage layer on the overall performance of SCPP. Later, the same group further studied the performance of a backyard SCPP pilot [47,48]. The thermal network model for SCPP was further developed by Bernardes et al. [49] to analyze the large scale SCPP with the ambient pressure, temperature, and density varying with altitude. To calculate the heat transfer characteristics of the collector with a single channel and an energy storage system, a 7×7 matrix comprehensively considering the heat transfer between the energy storage system, air flow, the canopy, and the ambience is shown in Eq. (1), with the Latin and Greek symbols as defined in [49]. In this equation, all the coefficients in the matrix on the left side were confirmed according to the empirical formula from classic textbook being verified at various working conditions.

Eq. (2) is partial differential equation representing the transient energy transfer and storage mechanism inside the energy storage layer [50], where the solar radiation was regarded as an effective heat source being imposed upon the ground surface with a thickness of 0.2 mm [45,51]. The average efficiency of the collector is less than 60% [41,46], as a result, in order to further improve the thermal performance of the collector, Ming [52] advanced a helical heat-collecting SCPP by adding several helical transparent walls within the collector which could extend the flowing time and hence increase the air temperature rise in the collector. But this method might decrease the power output during the night time as a larger part of the stored energy is used in the daytime.

$$\rho c\frac{\partial T}{\partial \tau}=\frac{1}{r}\frac{\partial}{\partial r}\left(\lambda r\frac{\partial T}{\partial r}\right)+\frac{\partial}{\partial z}\left(\lambda\frac{\partial T}{\partial z}\right)+\dot{Q} \tag{2}$$

The chimney at the center of the SCPP induces the air to flow from the collector inlet and also increases the flow velocity due to the stack effect: the higher the chimney, the faster the fluid flows. The pressure difference caused by the chimney is generally the function of gravitational acceleration, chimney height, and the density difference between the ambience and inner tower [40,49,53].

The maximum theoretical efficiency is equal to the Carnot's efficiency in the following Equaztion.

$$\eta=1-(T_{\text{in}}/T_{\text{out}}) \tag{3}$$

where T_{in} and T_{out} are respectively the temperatures at the engine inlet and exhaust.

The tower's efficiency is proportional ($\propto$) to its height h_{t} and the collector efficiency is proportional to the collector area A_{coll} and the heat received, therefore in Eq. (4) the power output P_{elec} is proportional to the volume included within the chimney height and the collector area:

$$P_{\text{elec}}\ \propto\ h_{\text{t}}\ .\ A_{\text{coll}} \tag{4}$$

Later, Ming et al. [54] conducted a comprehensive analysis on the stack effect of SCPP and presented a detailed mathematical model to describe the driving force of the SCPP system (Eq. (5)), in which, the effects of all SCPP dimensions on the driving force were included (with the symbols signification as defined in [54]).

$$\Delta p=\left(\frac{g^2}{2c_p}\right)^{\frac{1}{3}}\cdot\left(\frac{{\rho_0}^2{\beta_0}^2}{\rho}\right)^{\frac{1}{3}}\cdot\left(\frac{H}{{r_{\text{chim}}}^2}\right)^{\frac{2}{3}}\cdot{R_{coll}}^{\frac{4}{3}}\cdot q^{\frac{2}{3}} \tag{5}$$

The design of turbine is an interesting topic in the research of SCPP, as it differs to that of wind turbines in free wind farms, and to hydraulic turbines [40]. Gannon and von Backström [55] presented

$$\begin{bmatrix}
\begin{pmatrix}h_3\\+h_{r21}\\+U_t\end{pmatrix} & -h_3 & -h_{r32} & 0 & 0 & 0 & 0\\
h_3 & -\begin{pmatrix}h_3\\+h_4\\+\Gamma\end{pmatrix} & h_4 & 0 & 0 & 0 & 0\\
-h_{32} & -h_4 & \begin{pmatrix}h_4\\+h_{r32}\\+h_{r43}\\+h_5\end{pmatrix} & -h_5 & -h_{r43} & 0 & 0\\
0 & 0 & h_5 & -\begin{pmatrix}h_5\\+h_6\end{pmatrix} & h_6 & 0 & 0\\
0 & 0 & -h_{r43} & -h_6 & \begin{pmatrix}h_6\\+h_{r43}\\+h_7\\+U_w\end{pmatrix} & -h_7 & 0\\
0 & 0 & 0 & 0 & 0 & -\begin{pmatrix}h_7\\+h_8\end{pmatrix} & h_8\\
0 & 0 & 0 & 0 & 0 & -h_8 & \begin{pmatrix}h_8\\+U_b\end{pmatrix}
\end{bmatrix}
\begin{bmatrix}T_2\\T_{f2}\\T_3\\T_{f3}\\T_4\\T_{f4}\\T_5\end{bmatrix}=
\begin{bmatrix}s_2+h_wT_\infty+h_{rs}T_s\\-\Gamma T_{f2,i}\\S_3\\0\\S_4+U_wT_{4,0}\\0\\U_bT_{5,0}\end{bmatrix} \tag{1}$$

an interesting design of the turbine system used in SCPPs and an experimental investigation was conducted to assess the performance of a SCPP turbine. Later, von Backström and Gannon [56] presented an analytical model to express the influences of turbine flow, load coefficient, and degree of reaction on turbine efficiency. Subsequently, Fluri and von Backström [57] conducted an analysis on the performance of the power conversion unit (PCU, consisting of one or more turbo-generators, power electronics, a grid interface, and the flow passage from collector exit-to-chimney inlet), explored the interaction between the PCU and the SCPP, and compared the efficiency and output power of three PCU configurations.

In the field of CFD simulation with turbine, Pastohr et al. [58] were the first to carry out a two-dimensional numerical analysis on a SCPP coupled with turbine. In their research, the pressure drop at the turbine was imposed as a working condition. No three-dimensional (pressure, velocity, and temperature) distributions can be represented with this model, resulting in certain divergence from actual operating conditions. Nonetheless their research introduced a valuable approach, enabling subsequent researchers to numerically analyze the SCPP coupled with turbine. Ming et al. [59] developed a mathematical model to describe the turbine rotation, fluid flow, and heat transfer mechanism in the turbine area, conducted a 3-dimensional numerical simulation on a SCPP coupled with a turbine based on the above mathematical model, and analyzed the temperature, mass flow rate, output power and efficiency with turbine rotation speed. Validation of the numerical model was made thanks to the Spanish SCPP pilot and a MW-graded medium scale SCPP was analyzed. Recently, the optimal ratio of pressure drop across the turbine in SCPP was also considered [60–62].

However, no commercial SCPP has yet been built since the Spanish SCPP pilot was built in the beginning of 1980s. One key reason might be that the initial investment required is quite high for government funding and for enterprises [48,63–70]. Currently there are two methods to reduce the construction cost of a tall chimney. One is the “floating solar chimney” concept advanced by Papageorgiou et al. [43,71–75], which consists in a self-sustained chimney made of fabric ring balloons filled by Helium, and could greatly decrease the initial investment of the tower without significantly decreasing the overall efficiency [42,44]. The other is the “sloped chimney” which is built along a high mountain [76–84]. Experimental results indicate that a sloped solar chimney also has good overall performance [85].

2.3. The effect of dimensions on SCPP

Intensive research has been conducted to optimize the different constituents of MW scaled SCPPs, for instance the chimney shape [86] and the turbines [87]. To evaluate the performance of a SCPP, several small prototypes have been built and the operation parameters measured were compared to theoretical analysis using numerical simulations, mathematical models and CFD, carried out by numerous teams [54,88].

Many parameters have been studied for SCPPs: ambient conditions [89], collector inlet opening and height, outlet diameter, chimney throat diameter, chimney divergence angle [90]. The power output of a SCPP greatly depends on chimney height and collector diameter allowing scale economies: multiplying both by 2 increases power by 4 meanwhile the construction costs are almost only doubled [23,89].

A comprehensive review of scientific literature on SCPP was written by Zhou [91], describing pressure drop under the GH and inside the tower, optimal sizes, chimney resistance, effects of cross wind, collector performance, types of thermal energy storage layers, etc.

The technological challenges facing SCPP were recently described by Lupi, et al. [92] who noted that, due to the very large dimensions involved, the wind loading process and the structural behavior of the tower require multi-physics modeling.

A realistic growth path from the 50 kW prototype of Manzanares (Spain) with a chimney 200 m high to 200 MW SCPPs with 1000–1500 m high towers was proposed by Francke, et al. [93] who suggested that only one more prototype with a 400 m high chimney is necessary before industrially-scaled SCPPs enter in operation. The design of commercial SCPPs was first provided by Schlaich and resulted in the 200 MW model design SCPP studied by many researchers. Zongker [37] performed a life cycle assessment (LCA) for SCPPs. He found that the largest contributor to life cycle impacts is the GH collector, although ethylene tetrafluoroethylene (ETFE) sheets and glass offer favorable recyclability and durability combinations. Using ETFE, the ratio of “Energy Returned over Energy Invested” found by Zongker is 14, meanwhile for glass it is only 7. A cost assessment was published by Fluri et al. [94] who found prices for the electricity produced 2 to 3 times higher than initially proposed by Schlaich [35]. But recently an actualized cost assessment by Krätzig, et al. [89,95] confirmed for a SCPP 750 m high with a collector of 3500 m diameter similar cost competitive electricity generation, in the order of 63 to 75 £/MWh (99 to 131€/MWh). The differences between the academic authors with the structural engineers and architects come from construction costs (found higher by the academics) and lower provisional power output. Of course for all renewables, local solar irradiation and wind characteristics are important, as well as the size of the plants and their local configuration. Nonetheless, compared with the levelized costs of other types of renewable energy technologies as shown in Table 2, the results are promising for all SCPPs. We note that certain assumptions have been made in these calculations. On the one hand, the authors estimated that the desert site is provided cost-free by the client; on the other hand, the depreciation time for calculations was 30 or 33 years, while the life expectancy of the plant is estimated in between 80–100 years.

Bergermann and Weinrebe [98] investigated SCPPs with 1 km high chimney and collector radius of 3500 m and calculated a LECs of 103 € MWh^{-1} with plant locations in North Africa and a total investment of 750 M€.

Krätzig [89] concentrated his cost-estimations on optimized smaller plants with double glazed collector. For the smallest plant with 500 m high chimney and collector radius of 1000 m, a total investment of 111.0 M€ was calculated; whereas for a larger one with a 750 m high chimney and 1750 m collector radius, the investment rose to 337.6 M€. The corresponding LECs are 131 € per MWh and 99 € per MWh

The power production per unit of land area or water area was introduced by MacKay [96] as a useful parameter to assess the performances of renewable energy technologies as shown in Table 3, based on the energy resources in UK and in European countries. For

Table 2
Levelized electricity cost (LEC) of various renewable energy power plants.

Renewable energy technologies	Levelized cost (£ MWh^{-1}) in UK in 2007 [96]	Levelized cost (€ MWh^{-1}) in Germany in 2013 [97]
Offshore wind	92	119–194
Onshore wind	65–89	45–107
Co-firing of biomass	53	
Large-scale hydro	63	
Sewage gas	38	
Solar PV	571	78–142
Wave	196	
Tide	177	
200 MW SCPP [36, 37]		99–131

Table 3
Power production per unit of land-area or water-area [96].

	Renewable energy technologies	Power production per unit of area in W m^{-2}
	Wind	2
	Offshore wind	3
	Solar PV panels	5–20
	Hydroelectric facility	11
	Rainwater(Highlands)	0.24
	Geothermal	0.017
	Concentrating solar power (desert)	8–15
SCPP	50 kW Spain Prototype [40]	0.1
	200MW industrial Model [35]	2

different scales of SCPPs, the values of the power production per unit of land area vary greatly. For the 50 kW Spanish SCPP prototype with collector radius of 122 m [40], the power production per unit of land area was about 0.1 W m^{-2}. However, for the 200 MW commercial SCPP with collector radius of 3500 m [23,35] receiving a solar radiation of 2200 kWh m^{-2} yr^{-1} (Sahara Desert for instance), the power production per unit of land area can be calculated as 2 W/m^2 which is comparable to inland wind farms, but lower than for solar PV panels or for CSP.

The figures given by MacKay [96] compare well to the average total land-use requirements evaluated by NREL in the USA for PV and for CSP power plants [99]: 1.46 ha GWh^{-1} yr^{-1} for PV and 1.42 ha GWh^{-1} yr^{-1} for CSP, which gives an average power production per unit of area of 7.8 W m^{-2} for PV and 8,1 W m^{-2} for CSP.

Dozens of PhD theses and hundreds of scientific publications have been published, all showing that SCPPs with kilometer high chimneys can be competitive with wind energy or with PV, also giving the advantage of no-intermittency thanks to thermal storage [45,93]. Nonetheless, no commercial scale SCPP has yet been built. Alternative uses of SCPP have now been published, allowing complementary revenue or reduced investment by synergies with complementary technologies [33,34,39].

On the one hand, the original pilot plant in Spain proved the concept and showed up new potential such as operating into the night thanks to natural thermal energy storage in the ground (and latter in water bags), which can allow this renewable energy power plant to work 24 h with no intermittency. It also demonstrated the importance of preventing rain or water to enter under the collector where the latent heat of evaporation will reduce the thermal energy available. The pilot plant also allowed testing of different collector materials and investigation of techniques for improving the collector efficiency and optimizing mounting and construction techniques.

On the other side, the pilot plant also showed up some design flaws like the turbine design (turning in the horizontal plan) that was not suited to that plant. It also become evident that the collector can be slightly sloped from the collector entrance towards the chimney, in order to guide the rising hot air and reduce friction by keeping an almost constant cross section. The current complexity of today's solar plants with thermal storage, make us regret that the pilot SCPP plant was not used to investigate relatively simple techniques of improving thermal storage, prior to being decommissioned in 1989. The first numerical simulations (validated against experimental measurements) quickly showed the possible economies of scale; and the data gathered from the pilot plant are still being used to validate more and more complex CFD models and numerical simulations using a variety of novel components.

A SCPP installed in urban areas has been proposed by Negishi [100] for the elimination of a low concentration of VOCs. The authors performed Computational Fluid Dynamic (CFD) study of the effect of a filter placed inside the chimney. Land price is expensive and the area available for the GH is generally small in urban areas; so the SCPP can be driven by waste heat from thermal power plants, or by geothermal heat, instead of solar energy [101].

To summarize this section, it has been seen that substantial experimental experience obtained with the 50 kW plant in Spain has helped to spur the development of theories and models of SCPPs. Energy storage is an area of keen interest; and alternative uses of SCPPs have been discussed including elimination of VOCs. On the other hand, the performance and costs of larger SCPPs is still somewhat uncertain due to the lack of practical scale ups. Though there are many promising predictions, these could be subject to bias where undertaken by researchers or industrialists wishing to justify new projects. SCPPs incorporating PCR have not been built at all. In the next chapters, we review the possible synergies between SCPPs and photocatalysis for CH_4, N_2O and halocarbon removal from the atmosphere, because these important long lived well mixed GHGs all together have a current RF of almost half of the RF of CO_2 (RF of CO_2 is nearly $^2/_3$ of total RF, and cumulated non-CO_2 GHGs RF is $^1/_3$ of total RF).

3. Photocatalysis

In this section, after introducing the photocatalysis process, we review the main options for catalysts and review experiments in their environmental uses for air cleaning. Means of contacting photocatalysts with the air will also be reviewed.

The IUPAC 2011 [102] definition of photocatalysis is: "*Change in the rate of a chemical reaction or its initiation under the action of ultraviolet, visible, or infrared radiation in the presence of a substance—the photocatalyst—that absorbs light and is involved in the chemical transformation of the reaction partners*." Using a catalyst allows to accelerate and/or reduce the temperature of a particular chemical reaction, that usually requires heat for its activation. Using a photocatalyst allows generally the chemical reactions to occur at room temperature thanks to visible light or UV. By harnessing solar energy, photocatalytic processes avoid the costly heat input of conventional thermal catalytic methods.

Since scientific studies on photocatalysis started four decades ago, titanium dioxide (TiO_2), a common material in our daily lives, has emerged as a very good photocatalyst for environmental purification. Upon photoactivation of the catalyst, adsorbed gases like oxygen (O_2), hydroxide radical ($^{\circ}OH$) and contaminant species can participate in surface-mediated reactions [103]. The product species, notably CO_2 and H_2O according to Eq. (3) for CH_4 photooxidation, or N_2 and O_2 for N_2O photoreduction according to Eq. (1) then desorb easily from the metal oxide surface due to little affinity.

It can be deduced from these equations that the reagents (non-CO_2 GHGs) need to have some affinity for the photocatalyst in order to be absorbed and react. In case of generation of acidic or alkaline by-products for example according to Eq. (4), it is necessary to neutralize the by-product, or if it stays on the photocatalyst surface, the active sites will be de-activated until rinsing with water regenerates them.

3.1. Types of photocatalytic reactors and types of photocatalysts

Many types of photocatalytic reactors (PCRs) exist each having individual advantages and disadvantages [104]. For laboratory research, PCRs can be divided in 3 main categories [105]: tubular, plate or honey-comb. Among fixed-bed designs, thanks to their higher volumes and lower pressure drop, annular reactors and honeycomb monoliths are the most common and useful for photocatalytic reactions with gases. Though procedures for scale up of PCRs have been described [106], few larger PCRs have been developed

except for wastewater decontamination using photocatalyst suspensions. Besides usual reactor scale-up factor parameters, like mass transfer and mixing, uniform light distribution for high surface area of illuminated photocatalyst has also to be taken into account [107], in particular for solar PCRs [108].

The proposals described in this review concern heterogeneous reactions between a solid photocatalyst and gaseous pollutants diluted in air. As will be seen in next two sub-chapters, numerous open field outdoor trials have been conducted, but without outdoors real-world PCR application (streets, highway lanes, tunnels, etc.), except for the primary laboratory experiments which validated the photocatalyst efficiency.

Many types of photocatalysts exist for heterogeneous photocatalysis under UV light and they are generally based on mineral semiconductor metal oxides [109], of which TiO_2 is the most used [103]. Some types of photocatalysts are mentioned in Table 4 and these will be covered more in detail in Section 3 with reference to the mineralization of CH_4, N_2O and halocarbons.

Photocatalysts with organic ligands have also been developed [110], usually in the form of metal-organic frameworks [111]. Many ways of doping or modifying the photocatalyst are employed, usually to prolong the functional life-time, to enhance the red-ox activity and the electron–hole charge separation, as well as to enhance the light absorption and confer visible-light activity to the photocatalyst [112]. The photocatalytic activity can also be enhanced by supporting the photocatalyst particles on porous materials like zeolites [113]. The photocatalyst can be incorporated in porous materials, or coated as thin films (single or multiple layers) on quartz, glass, polymeric substrates or fibers [114].

3.2. Self-cleaning applications

Self-cleaning materials are becoming an integral part of daily life, because of their utility in various applications [125], and an important number of products are on the market today. The oldest large commercial application of photocatalysis is probably for self-cleaning glasses [126], typically used for skyscrapers, high-rise hotels and office-buildings where the access for window-cleaning is difficult. Under the action of the sunlight on a photocatalytic film coated on the glass, the organic dirt breaks down and sticks less to the glass [127]; the organic matter in contact with the photocatalyst is oxidized at an increased rate and is decomposed. Then when it rains, the photo-induced hydrophilicity [128,129], allows the water to spread evenly across the surface of the glass like a thin film that cleans the glass of dirt and minerals and dries off fast without leaving streaks.

In 2004, Lee [130] performed experiments of photocatalytic soot destruction by titania. Lee succeeded in demonstrating that the photo-generated oxidizing species are both surface mobile and capable of air-borne diffusion. Experiments conducted with two thin titania film strips separated by a small 'titania free' gap of 0.7 mm. A continuous soot layer (0.5 μm) was deposited on the titania film strips and in the gap between them. Photos were taken as a function of irradiation time of the soot with ultraviolet (UV) light, which visually demonstrated that the *direct* photocatalytic soot destruction can be performed in 4.5 h on thick titania surface films. A prolonged irradiation (155 h) allowed removal of the soot in the 'titania free' gap of 0.7 mm between the two TiO_2 strips. This provided visual evidence of the *lateral* destruction of soot by UV irradiation that produces highly oxidizing photogenerated species on the TiO_2 photocatalyst. The *lateral* oxidation of this pollutant was attributed to the spill-over of hydroxyl radicals or other photogenerated oxidizing species. Other experiments with 305 h of irradiation allowed these authors to also demonstrate *remote* destruction of soot, 175 μm away from the photocatalyst.

Nitrogen oxides are mainly formed by the combustion of fossil fuel vehicles, together with sulphur dioxide, carbon monoxide, volatile organic compounds (VOCs), particulate matter and soot. In areas with heavy traffic, this type of pollution not only affects the heath [131], but is also involved in the formation of tropospheric ozone and summer-smog, and deteriorates building facades. Photocatalytically active building materials such as house paints, paving stones, saddle stones, and roofing tiles have been tested to improve the air quality in cities, and are able to remove nitrogen oxides pollution in urban areas. An ISO method ISO 22,197–1:2007 has been established to evaluate NO removal-based air-purification.

Photoactive interior textiles, paints, and plasters with antibacterial and antimicrobial properties are used in hospitals [132,133]. They are also used to prevent mould infestations. Air cleaning apparatus with filter systems and photocatalytic systems are also commercially available. Fig. 3 summarizes some of the commercial uses of photocatalysis.

In addition to the reduction of pollutants, photoactive construction materials exhibit an improved soiling resistance [134]. A positive side-effect of photoactive products is also the conservation of value, as the risk of a microbial infestation with algae, fungi or mildew is significantly reduced.

3.3. Large-scale photocatalysis for environmental remediation

The interest in heterogeneous photocatalysis for industrial applications, such as treatment of gas streams, deodorization and pollution removal is shown by many indoor-air applications [135] and large scale worldwide use of photocatalytic self-cleaning cements, coatings, paints and glass with no unintended consequences yet reported.

Many experiments carried out outdoors and at large scale showed that significant reduction in NO_x air pollutants can be obtained with photocatalytic road materials [136]. Photocatalytic methods for NO_x removal are currently very intense areas of scientific research and full-scale cases of the application of photocatalysts and photo-processes for NO_x abatement are reported [136,137]. Although results are highly variable [138–140], the large number of issued patents [141] for photocatalytic removal of NO_x reveals the fast-growing development of these methods.

More and more publications describe full-scale demonstration of the effectiveness of TiO_2-containing construction material in reducing air pollutants, or in reducing deposition of pollutants on

Table 4
Examples of photocatalysts for mineralization of non-CO_2 GHGs.

GHG (formula)	GWP_{100} (AR5) (and Lifetime)	Radiative forcing (W/m^2)	Examples of photocatalysts for GHG mineralization except CO_2	Authors and references
Methane (CH_4)	28–34 (12 yr)	0.50	Polytungstate on TiO_2 TiO_2 on Mo UO_2^{2+} on MCM-41 zeolite Ag on ZnO	Graetzel [115] Thampi [116] Krishna [117] Chen [118]
Nitrous oxide (N_2O)	265 (114 yr)	0.187	Cu, Ag, Ti, V, Mo or Cr in ZSM-5 zeolite 1% Ag on TiO_2 films ZnS - montmorillonite	Matsuoka [119] Obalová [120] Obalová [121]
CFC-12 (CCl_2F_2)	10,200 (100 yr)	0.166	TiO_2	Tennakone [122]
CFC-11 (CCl_3F)	4660 (58 yr)	0.058	ZnO	Filby [123]
HCFC-22 ($CHClF_2$)	1760 (12 yr)	0.045	TiO_2	Minami [124]

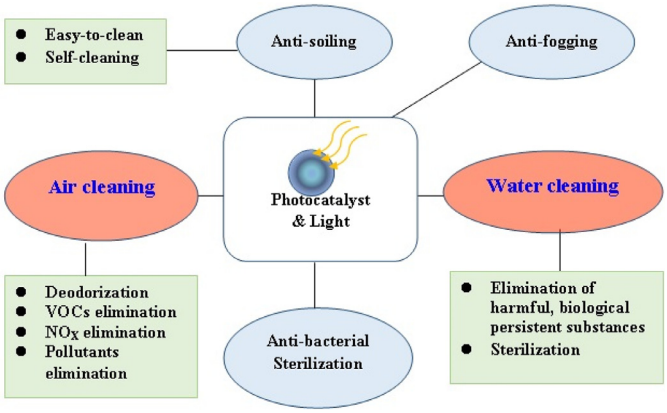

Fig. 3. Some to the commercial uses of photocatalysis.

buildings and preserving the cleanliness of buildings or their corrosion by acids. Some results are good and others are not, as it will be seen later [140,142,143].

Maggos, et al. [144] reported for instance experiments on three mini-canyon streets (produced at a scale of $^1/_5$), with a width of 2 m, length of 18 m, and wall height of 5 m. The walls were: bare for the first canyon, covered with TiO_2-treated mineral paint for the second canyon, covered with the same paint material, except it did not contain TiO_2 for the third canyon (reference canyon). An example of canyon street is on Fig. 4. The measured NO_x levels in the canyons varied as expected with the time of the day and wind direction, as well as the orientation of the canyon wall. However, the overall NO_x concentrations measured in the TiO_2 canyon were 36.7–82.0% lower than those measured on average in the reference canyon.

In order to evaluate the depolluting effect by photocatalytic coverings in street canyons, Moussiopoulos, et al. [145] performed comparisons of numerical and experimental results. Their numerical simulations included a wide range of factors: flow field, dispersion mechanism, the depollution efficiency depending of the length of the street canyon, the wind direction, and the thermal exchange between the air and the heated street canyon walls. The model simulations results revealed the dependence of the concentration fields inside the street canyon and developing flow with the direction of the approaching wind.

Solar intensity, wind speed and direction and relative humidity are outdoors environmental factors with significant impact on photocatalytic efficiency [146]. The authors think that it needs also to be taken into account for vehicles passage, which turbulences change locally wind direction and speed, and light intensity by their shadow.

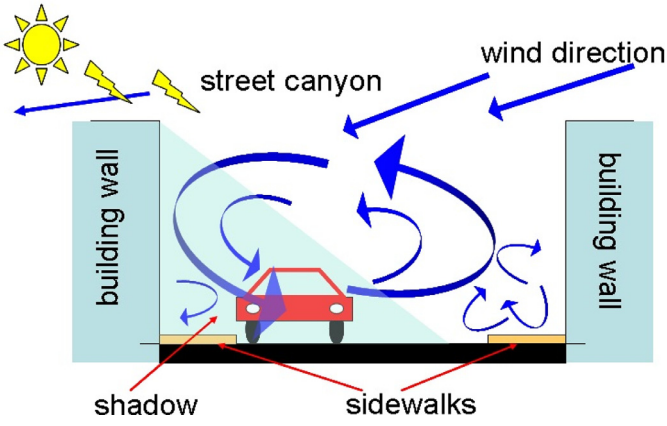

Fig. 4. Front view of a canyon street: only the photocatalyst on the sidewalks and on the building walls receiving sunlight might be efficient on pollution mineralization.

The photocatalytic degradation of NO_x from field studies has been measured by two techniques: (i) by measuring the reduction of the ambient air pollution, which is difficult to estimate when, in the reference site the NO_x concentration is highly variable; or (ii) by measuring the by-products created by the degradation process on the photocatalyst surface, i.e. rinsing the photocatalyst with water and measuring the nitrate content. As reported by Dylla [146], the nitrates collected onto the pavements coatings show the evidence of NO_x reduction.

The photocatalytic activity of cementitious materials containing TiO_2 is also influenced by the size and the nature of the photocatalyst aggregates [147]: a nano-sized TiO_2 was expected to perform better than a micro-sized TiO_2 (respective averages particle size 18 nm and 154 nm) due to its much higher specific surface area, but degradation of rhodamine B under UV light conducted to the opposite results as, by a phenomena of aggregation / flocculation, the nano-particles leads to much bigger secondary particle size.

Large-scale indoor and outdoor experiments have been conducted in Japan [138,148], Europe [149] and the US [150] for the in-situ large scale destruction of NO_x [149,151] and VOCs [152,153] and the principal method limitation is the transport of the pollutants towards the active surfaces. The environmental factors with significant impact are wind direction and speed, solar intensity and relative humidity [154,155].

Several of the environmental important parameters for photocatalytic reactions can be controlled under a SCPP (some parts warmer, some parts with lower air flux speed, always the same air direction, low level of urban pollutants in deserts, RH% is naturally low and decreases as temperature inside the collector increases) depending on where the photocatalyst is installed. In view that numerous laboratory scale results, obtained with numerous different photocatalysts, as it is shown in the next section, can transform CFCs, N_2O and CH_4 and thanks to the very large area available ($2 \times 38\ km^2$) and the large amount of sunlight (UV+visible-light), high transformation rates might be possible, as it will be shown by calculation in Section 5.

Recently an international team from Italy, Germany, Greece, France and Belgium [140,156] conducted inside a Brussels tunnel a fully comprehensive assessment and real world tests of air-purifying photocatalytic materials for $NO+NO_2$ (NO_x) pollutant abatement.

But poor results were obtained in some experiments [142] (developed later in the discussion of Section 5). The authors reported that the poor results are due to transport limitations of the pollutants towards the active surfaces. As a matter of fact, the relatively concentrated NO_x generated at vehicle exhausts is rapidly diluted in the surrounding air and local wind speed due to the vehicles movement, so very small amounts of pollutants reach the photocatalysts surfaces installed nearby. The good photocatalytic NO_x remediation results from some previous studies by the same authors can be explained by differences in sampling positions, in sampling periods and in the geometry of the field sites or by differences between the reference and the active sites.

A first set of experiments was performed on a 70 m tunnel section (the total photocatalytic area is not indicated but is probably of nearly $1500\ m^2$) and UV illumination in the 315–420 nm range of $\sim 0.6\ W\ m^{-2}$. A second set of experiments was conducted on a 160 m tunnel section (probably $3500\ m^2$ of total photocatalytic area, not indicated in the article), with a more efficient commercial photocatalyst and UV illumination of $\sim 1.6\ W\ m^{-2}$. The new results published are quite disappointing, despite good results reported from outdoor experiments of numerous publications from the last 15 years (many of these articles are reviewed in the two publications just cited, and some are from the same researchers).

To give just an illustration among the numerous examples available, Guerrini [157] reported 20% pollution abatement in the center of a city tunnel in Rome, meanwhile only an upper limit of 0.4–2% NO_x abatement was detected in the Brussels tunnel (comprised in the 2% uncertainty of measurement) [140,156]. Similar disappointing results were obtained by the same international team in a model street canyon [142].

The best-case pollutants abatement scenario was evaluated by this international team with various deposition models and numerical simulations using CFD. The calculations indicate that at best the NO_x removal can only be of 3% in the 160 m of the Brussels tunnel section and of 12% if the 3 km of the tunnel were equipped with the UV lamps and the photocatalytic coating [143], and under the assumption that ventilation, wind, humidity, temperature stay close to the ideal conditions and do not affect the reaction rates and that the photocatalyst deactivation by pollution do not occur. It is reported by Gallus [140,156] that in the 160 m tunnel section (with 3500 m^2 of photocatalyst) and under ideal experimental conditions (without passivation of the photocatalytic surfaces, and with RH%<50%, wind speed<1 m s^{-1} and 10 W m^{-2} illumination by UVA), a 20% NO_x reduction might have been possible. During the tests that were conducted, the wind speed went up to 3 m s^{-1} and the RH% was 80–90%, and also the temperatures were cold, all parameters which reduce the abatement efficiency of the TiO_2 photocatalyst used. Just to fix ideas, in Section 4, we will see that the area of the visible-light active photocatalyst proposed is 20 km^2, with locations where RH% is almost always <40% and where visible light illumination in the order 700–900 W m^{-2}, with UV light representing in the order of 30 W m^{-2} (i.e. 4–5% of total as latitude is well below 35°).

As expressing findings in terms of percent pollution abatement can be misleading, the following example expressing the pollutant reduction in grams or moles of removal per mile of road lane provides a better illustration: for a highway, Sikkema [158] observed NO oxidation rates by the photocatalytic coating ranging from 6.2 to 57 nmole·m^{-2} s^{-1} (4.0 –36 g·lane-$mile^{-1}$ h^{-1}), while vehicles emissions were estimated to be 720 g·lane-$mile^{-1}$ h^{-1} thus NO oxidation rates ranging from 0.5% to 5%.

Fig. 5 shows a wall coated with photocatalyst along a multiple lane urban street. Depending on wind direction, the pollution can be dispersed and reach the buildings behind. Depending on the wall orientation, on the hour of the day, and on cloud cover the photocatalyst will receive variable amounts of sunlight.

The extent of the photocatalyst deactivation (by adsorption of "organic grime" volatile organic hydrocarbons and deposition of brake dust, soot and other sticking particles) was almost unexpected, as under laboratory conditions deactivation is much lower and under previous open field tests it usually appears slowly. But the tunnel where the experiments were conducted is described as highly polluted with concentrations of 1000 and 400 mg m^{-3} annual average half-hour respectively for NO and NO_2.

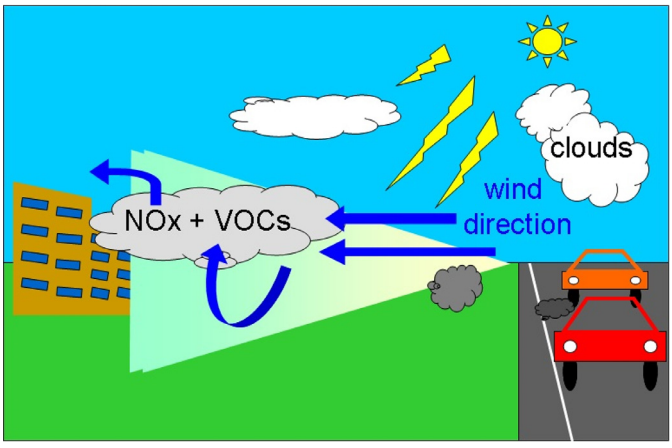

Fig. 5. Multiple lane urban street: sunlight and pollution (NO_x, VOCs) hardly reach the photocatalytic wall.

As explained by Kleffmann the discrepancy in the results might come from the extremely high variability of the outdoors concentrations of atmospheric pollutants and/or the meteorological conditions, also to crosswind and turbulences due to vehicles speed and to the rapid dilution of the vehicles exhaust pollution by convection and dispersion. The analysis of the discrepancy between previously published results and new ones was made by Kleffmann [159] who studied results obtained by Folli [136] and demonstrated by two different methods that the maximum NO_x removal can be in the order of 0.8% under the experimental conditions set. Using the same equations and parameters than Kleffmann, but considering that only 400 m^2 area out of the 3000 m^2 available of the canyon street were covered by the photocatalyst, a calculation shows that the upper limit of NO degradation can be 6%.

In deserts where the SCPPs can be built, there is no NO_x, but well mixed, long lived GHGs, thus the same calculation has no sense, but the 20,000,000 m^2 of photocatalyst area and an UV illumination at least 3 times higher should provide better results. As will be seen later, in Section 5.3.3 is has been calculated [21] that for CH_4 it can be removed up to 67% under a SCPP (Table 7).

It is often written that UV is in the range 3–5% of the total solar irradiance [160]. By modeling solar irradiance as a function of location Folli [161] showed that even at the best solar irradiation conditions (the solar noon) this range is applicable only to latitudes below 35°, which is not the case of Europe. Folli showed that significant NO oxidation with anastase TiO_2 is only achieved in a test site in Copenhagen (55.68°N) when the UV intensity exceeds 600 kJ/m^2/day at this site (~2% of total solar irradiance at noon). Adequate performances of the photocatalyst depend on solar light conditions rigid limits outside which it simply does not receive enough UV photons [162]. The use of photocatalysts active under visible light solves these problems. For example, Zhao [163] developed a Bi/TiO_2 nanocomposite hybrid with the most efficient visible light photocatalytic activity reaching a NO removal ratio of 50.0 %, superior to that of well known N-doped TiO_2 (36.5%) and C-doped TiO_2 (21.8%) and with 27% NO removal capacity at 500 nm (which is in the visible light range).

Some explanations of the discrepancies might also come from total NO_x measurement, while NO concentration often decreases, in an urban environment polluted by ozone, NO_2 concentration might increase (and yet it is more toxic). For instance at the photocatalytic measurement active site, a 0.5 NO/NO_x ratio can be measured although for fresh vehicle emissions the NO/NO_x ratio is typically of 0.85, because the pollutants pass first the reference measurement site, meanwhile NO is oxidized into NO_2 by atmospheric O_3 on its way to the photocatalytic active site, conducting to erroneous estimations of the NO_x abatement. NO_2 might also be a by-product of the incomplete oxidation of NO on the photocatalyst, or even come from the nitrate deposited on the photocatalyst. Thus selectivity of the photocatalyst matters and for instance to oxidize nitric oxide to nitrate selectivity can be obtained with W/N- or Nb/N- co-doped titanium dioxide photocatalysts [164–166] which have the ability of generate very low amounts of NO_2.

The experiments reported above were made at an already significant scale and are based on hundreds of NO_x photocatalytic oxidation studies at laboratory scale, but also from tens of indoors and outdoors experiments.

3.4. Lifetime of photocatalysts and possible regeneration

Chabas [127] analyzed the self-cleaning mechanism of two hydrophilic photocatalytic TiO_2-coated industrial glasses and a traditional float glass (the reference glass), in a site representative of background urban pollution in Paris. The glasses were exposed in unsheltered (where rain washing can occur) and under sheltered condition for various time duration. A moderate weathering of the glass surfaces was only detected after 24 months of exposure. A significant decrease of the organic fraction deposited on the TiO_2-coated glasses evidenced the self-cleaning mechanism. Years later, Chabas [167] performed a comparative assessment of the long term exposure (100 months) and short term (12 months) of self-cleaning and reference glass in an urban environment. The affinity of the self-cleaning glass for water vapor and the properties of super hydrophilicity were maintained after long exposures. Thus in urban and polluted environments, the life time of a photocatalytic coating in vertical position can at least be expected in the order of tens of years with maintained activity if some regular washing (by rain) can occur. The article did not precise at which floor or height were located the self-cleaning windows studied, but pollution is clearly more concentrated close to the ground were NO_x removal experiments take place.

Several studies report a decrease of photocatalytic activity (for NO_x removal) in outdoor environment: 50% after 5-months [168]; from 36% to 78% after 4-months and from 22% to 88% after a 12-months period [169]. In the case of NO_x removal, as nitrate and nitrous acid are formed and progressively reduce the amount of photocatalytic sites available, the outdoor photocatalysts activity recovery is obtained by rainfall or clear water surface washing [170,171].

Not only water soluble reaction products (nitrate and nitrous acid) accumulate on the photocatalyst and the substrate. If the photocatalyst is located on horizontal surfaces like roads or sidewalks, also urban and traffic generated pollution like motor oil, chewing gum, de-icing salt, gum tire soot, unburned fuels and particulate matter will also deposit on the photocatalytic pavements or asphalt. Many of these pollutants are hydrophobic and reduce significantly the photocatalytic activity as they block the active sites preventing the light and the NO and NO_2 pollutants to reach them. Pavements located 1 m above the roadway exhibited almost double photocatalytic activity than the ones on the road even after substantial field exposure [158]. Placing the photocatalytic coating or paint on vertical surfaces like walls or glass windows well above the road and the side-walks should allow better cleaning and less dirt to deposit. Inside the laboratory, a reduction of the photocatalytic activity of aged slabs (stored in plastic bags and unexposed to outdoor pollution) was explained by calcium carbonate formation and loss of slab water content. Sikkema [172,173] tested photocatalytic mortar slabs in a laboratory and outdoors in a roadway field test at Missouri route 141 and also tested several regeneration procedures (brushing and washing) which were inefficient for many of these contaminants. The NO_x pollution removal rate capacity was more or less 60 times lower than the NO_x estimated emissions by vehicles traffic conducting to the conclusion that it is difficult to talk of mitigation of this pollution. As will be seen later in Section 4, the situation is different in the system proposed here for GHGR of non-CO_2 GHGs, mainly because there is no air-dilution of the targeted pollutants, the areas of photocatalyst as well as light intensity are much larger and there are almost no other pollutants in deserts.

To summarize this section, while titania is the main photocatalyst in use, there is also interest in using a wider variety of modified photocatalysts for NO and NO_2 destruction. Photocatalysis in outdoor applications has been used mainly for self-cleaning and in local air pollution control. Mounting surfaces include tiles, road surfaces, and painted walls. Reports on catalyst lifetime vary considerable – lifetime may be shortened rapidly by exposure to grimes, and much depends on the sitting relative to specific pollution sources. The comparison of the performance of outdoor systems is hampered by the complexity of monitoring trace concentrations in the open environments.

4. Photocatalysis of non-CO_2 GHGs

In the previous section a general overview of photocatalysis, its possibilities and its applications to air remediation in particular for large-scale outdoors NO_x de-pollution has been given. This section reviews photocatalysis literature specifically applied to the major GHGs other than CO_2. As two recent articles reviewed the possibilities of photocatalytic elimination of N_2O [33] and of CFCs and HFCs [34], in this section the photocatalytic transformation of CH_4 will be covered in more detailed than N_2O and halocarbons.

4.1. Photocatalysis of nitrous oxide

At the beginning of the 1970′s some dissociation of N_2O was discovered in the dark on activated Fe_2O_3 and ZnO [174], and N_2O photodecomposition was demonstrated under UV illumination at room temperature [175,176]. The photocatalytic N_2O reduction into N_2 and O_2 at 293 K was obtained by many authors on numerous photocatalysts, for instance: on Cu-exchanged ZSM-5 zeolites [177–181]; on Cu^+/Al_2O_3, Cu^+/SiO_2 and $Cu^+/(SiO_2/Al_2O_3)$ photocatalysts [182,183]; on calcined and on modified TiO_2 [184]; on Ag doped TiO_2 powder [185] and Cerium-doped TiO_2 [186]; on photocatalytic nanocomposite of TiO_2/g-C_3N_4 (ratio 1:2) under UVA ($\lambda = 365$ nm) irradiation [187] and on many different modified ZSM-5 zeolites with metal oxides or with transition metal ions [119,188–193].

The photocatalytic reduction of N_2O is also obtained using reducing agents like CO (which oxidizes into CO_2) with Ti/USY zeolite [194]; like methanol (which oxidizes into CO and CO_2) using Ag^+ ions dispersed on TiO_2 [195]; like propane using Pb^{2+}/ZSM-5 zeolites [188,189]; or like water and methanol on Cu- and Ag- supported TiO_2 [196].

An almost exhaustive review has been recently published [33] in which details of the reaction mechanisms suggested in the literature are given.

Obalová [120] successfully reduced N_2O into N_2 and O_2 on TiO_2, Ag–TiO_2 thin films and ZnS- montmorillonite at 254 nm using 8 W Hg lamps at room temperature, under a neutral gas (He or N_2), but also under a gas mixture containing water vapor and / or excess oxygen. The yields were improved when water vapor was added, as the possible photocatalytic water splitting gives hydrogen and oxygen and then, the nitrous oxide reduction with hydrogen produces nitrogen and water.

As shown previously, successful research has been made on the photocatalytic mineralization of N_2O using currently available TiO_2-based photocatalysts or modified zeolites [197]. The experiments conducted by Obalová in the gaseous phase in presence of excess oxygen (as in air) and at room temperature prove that the direct photocatalytic reduction of N_2O in air is possible. It is still possible that photocatalysts active under visible light may be developed for N_2O reduction.

Field experiments were carried out [198–200] with TiO_2 photocatalytic paints on the walls of animal husbandries and in particular of pig houses, in order to decrease NH_3, CH_4 and the N_2O concentrations. The experiments were carried out in real conditions, in air and at ambient temperature with a ventilation flow in the order of 3000 $m^3\,h^{-1}$. Even if the results obtained were modest: 4–11% decrease of N_2O emissions, the results are encouraging as the photocatalyst used was un-doped and unmodified, which was not active under visible-light and that was progressively deactivated by the

adsorption of HNO_3 a by-product of the oxidation of NH_3 that can be easily washed out with clear water.

4.2. Photocatalysis of several CFCs and HFCs

The photodegradation of HFCs on several metal oxides was described by Tanaka [201] who found that the mineralization rate was higher on TiO_2–ZnO (semiconductors), than on SiO_2–Al_2O_3 (insulators). Chlorine and fluorine ions and CO_2 were the main degradation products obtained.

An almost exhaustive review of photocatalytic oxido-reduction of halogenated compounds was recently published [34] thus only a rapid overview of CFCs and HFCs removal is given.

The photomineralization of CFCs with TiO_2 and UV radiation at 366 nm has been described by Tennakone and Wijayantha [122]. The products detected were chlorine Cl_2 (gas) and CO_2 together with Cl^- and F^- ions.

Kutsuna [202] described the CFC-11 adsorption and its surface induced degradation in air, on several metal oxides under UV photo-irradiation (>310 nm) and at room temperature. Wylie [203] also described the decomposition of HFC-22, CFC-12 and CFC-11 on oxide surfaces under UV light (>300 nm) and/or under thermal treatment.

Minami [124] reported that by using TiO_2 the decomposition rate was the lowest for CCl_4, and the highest for HFC-22, with the mineralization of CH_4 in between. The photodegradation of HFC-152a was studied by Sangchakr [204] at 185 nm by photolysis and by photocatalysis at 254 nm with TiO_2.

Jo [205] found that the destruction of low-ppb concentrations of chlorinated VOCs was nearly 100% effective by applying TiO_2 photocatalysis (the atmospheric concentration of halocarbons goes from nearly 3 ppt for CFC-13 up to 528 ppt for CFC-12).

Zhou [206] studied the photodegradation of CCl_4 using MgO, Balko [207] using zero valent iron and Choi [208] using TiO_2. Wiltowski [209] also employed TiO_2 for the photooxidation of CCl_4 and of 1,1,1-trichloroethylene. Meanwhile Hsu [210] succeed the photoreduction of 1, 2-dichloroalkanes and 1, 2-dichloroalkenes using molybdenum derivatives.

The gas-phase TiO_2 photocatalytic destruction in air of 17 VOCs was studied by Alberici [211], with the following conversion yields: nearly 100% for $CHCl=CCl_2$, 90% for CH_2Cl_2, 70% for $CHCl_3$, 67% for $CCl_2=CCl_2$ and 20% for CH_3CCl_3.

Using TiO_2 as photocatalyst, Calza [212,213] investigated the photo-dehalogenation of $CBrCl_3$, $CHBrCl_2$, CH_2BrCl and of other halomethanes and halons containing bromine and chlorine or bromine and fluorine (CBr_3F).

Yin [214] obtained a rapid decomposition of several HFCs using bismuth oxide as photocatalyst under visible light irradiation (>420 nm). Compared with direct photolysis and with a nano-TiO_2 photocatalyst, Yin found that the photocatalysis by bismuth oxide removes more efficiently the hydrofluorocarbons tested.

The photocatalyzed transformation of 1,1- and 1,2-dibromoethane to CO_2 and HBr was realized by Nguyen [215], and the photocatalyic oxidation to CO_2 and HCl of $CHCl_3$ by Martin [216] and of CH_2Cl_2 by Borisch [217].

Photogenerated trihalomethyl radicals were discovered by Choi and Hoffmann [218], during the TiO_2 photodegradation of $CHCl_3$, $CHBr_3$, and CCl_3—CO_2H.

Neutralization of halo acids or removal by water rinsing might be necessary as deactivation of the photocatalysts may occur by F^-, Cl^- or Br^- contamination [219]. The regeneration of photocatalysts by rinsing them with clear water has been described [169,220,221] after deactivation of catalysts by NO_3^- or SO_4^{2-} during the photocatalytic oxidation of nitrogen oxides ($NO+NO_2$) or sulphur containing compounds respectively.

To summarize this section, the laboratory experiments often in air and at room temperature strongly suggest that the photocatalytic destruction of Montreal gases and other halocarbons is possible at a much larger scale. Still the development of photocatalysts active under visible light might be helpful in this purpose.

4.3. Photocatalytic oxidation of hydrocarbons

This section reviews evidence showing that photocatalysis is a very powerful tool for oxidation of long chain and short chain hydrocarbons including methane.

D'Auria [222] performed photocatalysis during 100 h of crude oil from Basilicata (Southern Italy) and obtained extensive degradation: linear and branched alkanes were reduced by 98.8% and 97.3%, cyclic alkanes by 96%, aromatic compounds and alkenes were reduced by 99.5% and 98.5%, respectively. Meanwhile, direct irradiation during the same time (100 h) gave a reduction of 9% and 5% in the case of linear and branched alkanes respectively.

Djeghri, et al. [223] studied the photo-oxidation of alkanes, both normal and branched from ethane to octane, at room temperature under the influence of UV illumination (210–390 nm), on the surface of non-porous particles of TiO_2 anatase.

Brigden, et al. [224] proceed to the photo-oxidation of short-chain hydrocarbons (C2–C6) over TiO_2 with up to 4000 ppm hydrocarbon and up to 20% O_2 concentrations at 150 °C. Very little reaction was obtained without O_2, but the rate of hydrocarbon conversion increased with the O_2 concentration.

Wada, et al. [225] studied the activities of n-type solid metal oxide semiconductors (zinc oxide, titanium dioxide) at ambient temperature and up to 550 K for photo-oxidation of simple C_1—C_3 alkanes under aerobic conditions. The oxidation of CH_4 produced less than 10% methanol together with CO_2. For these reactions UV irradiation was indispensable. Low yields were obtained at ambient temperature, but they increased with temperature up to 550 K. TiO_2 photocatalyst has lower selectivity than ZnO for methanol production. Later Wada, et al. [226] studied the selective photo-assisted catalytic oxidation of CH_4 and ethane using silica supported vanadium oxide catalysts, where both a reaction temperature of 500 K and UV irradiation were essential. Photooxidation of methane using the V_2O_5/SiO_2- photocatalyst at 493 K gave 76% selectivity for methanol.

Complete photooxidation to CO_2 of ethane, propane and butane is also possible. TiO_2 exhibits fairly high activity but the deep oxidation is predominant [227]. Silica-supported vanadium oxide favors only a partial oxidation. For ethane, Twesme, et al. [228] tested TiO_2 and SiO_2/TiO_2, but obtained the best results with zirconium oxide (ZrO_2)/TiO_2 thin films. The reaction rates increase significantly with Twesme's operating conditions from 35 to 70 °C, but not anymore by warming till 100 °C.

4.3.1. Total oxidation of methane

The stability of the CH bond in CH_4 (104 kcal mol^{-1}) makes it very difficult to activate. Pioneering work [223,229] conducted by Fromenti, Teichner and Djeghriin in 1972–1974 describes the photo-oxidation under UV (210–390 nm), at room temperature, of linear and branched alkanes (C2–C8), on TiO_2 anatase particles.

Back in 1971, Fujita [230] studied the photo-decomposition mechanism of CH_4 on coated porous Vycor glasses at 77 K (−196 °C). When the Vycor glasses where coated with V_2O_5 and MoO_3 they showed the largest photo-sensitization of CH_4, meanwhile when coated with MnO_2 or Al_2O_3 they showed photo-desensitization.

HCOOH, CO, CO_2 and H_2O were obtained during the photooxidation of CH_4 over powered TiO_2 under UV by Lien, et al. [231] using $^{18}O_2$. At the beginning of the UV irradiation, the formate detected was $HC^{16}O^{16}O$ indicating that the TiO_2 lattice oxygen was involved.

Kaliaguine, et al. [232] studied the reactions of CH_4 and ethane by UV irradiation of V^{5+}/SiO_2 and stoichiometric TiO_2. They concluded that after completion of the oxidation of the hydrocarbon molecule a

reduced stable V^{4+} ion was left on the surface with a reactive behavior that gave the peculiarities to the system under UV light.

Some researchers like Kaliaguine used a vanadium derivative (V^{5+}/SiO_2) as photocatalyst, but very often researchers only used TiO_2 derivatives [224,228,233–237] to investigate the kinetics of the total oxidation of n-alkanes and alkenes (methane, ethane, ethane, propene. . .).

Minami and Kim [124] proceeded to the photocatalytic oxidation of CH_4, CHF_2Cl, and CCl_4 over TiO_2 because the similar structure of these compounds with different constituents. The highest decomposition rate was obtained with $CHClF_2$, then CH_4 and CCl_4 in decreasing order.

Other researchers like Krishna, et al. [117,238] discovered uranyl derivatives with high activity to perform at ambient temperature the total oxidation of CH_4 by photocatalysis under sunlight in the presence of air. No partial oxidation products (CH_3OH, CHO, HCOOH, CO) were detected by Krishna. The uranyl ions were anchored within a mesoporous silicate molecular sieve named MCM-41, which is easy to produce. Depleted uranium (with less radioactive isotopes) is an abundant by-product of the uranium enrichment for the nuclear energy and might be used without risks on this type of application. In Fig. 6 the kinetics of CH_4 oxidation obtained by Krishna [117] at different concentrations can be seen as a function of irradiation time versus conversion to CO_2. These concentrations are 4 orders or magnitude larger than current CH_4 concentration in the atmosphere.

At the Ecole Polytechnique Fédérale de Lausanne (EPFL), in Switzerland, the team of Graetzel [115], tested tungstosilicate $(SiW_{12}O_{40})^{4-}$ loaded on TiO_2 and on alumina (Al_2O_3) powders and found than the first one is active in the photoinduced oxidation of CH_4 at ambient temperature to give CO, CO_2, and H_2O. On TiO_2, in the absence of tungstosilicate, the total oxidation of CH_4 to CO_2 and H_2O occurs.

The same team by Graetzel, et al. [116] also tested TiO_2 supported on molybdenum under band gap illumination. In their experimental conditions, use of pure TiO_2 led to the complete oxidation of CH_4 to CO_2, in the presence of oxygen. Meanwhile molybdenum oxide (MoO_3) alone or supported on Al_2O_3 or on SiO_2 showed poor activity in the photoactivation of CH_4, the deposition of 4% MoO_3 on TiO_2 had a pronounced effect on CH_4 photoactivation, a competing reaction pathway produced CO by partial oxidation.

The TiO_2 photocatalysed total oxidation reaction of C1–C4 alkanes (CH_4, ethane, propane and isobutane) with oxygen was investigated by Haeger, et al. [235]. They studied the effects of the wavelength, the temperature, the irradiation intensity and the dependence of the reaction rate on the starting products concentration. Previously for olefin photooxidation, Haeger, et al. [234] observed some reversible photocatalyst deactivation and, due to a different reaction mechanism, they obtained a rate law differing from the one found for alkanes oxidation where no photocatalyst deactivation was observed.

Liu, et al. [239] investigated the photocatalytic degradation of low level CH_4 by TiO_2 under vacuum ultraviolet (VUV) light. These lamps generate ozone. Under certain experimental conditions Liu obtained 50% CH_4 removal rate using 15 W UV lamps (185 nm and 254 nm) as seen on Fig. 7.

The characteristics of the photocatalytic reactor used and of the photocatalyst preparation were described in a previous article [240]. A C-TiO_2 photocatalyst film was used in these studies and was prepared by a modified sol–gel method. By mixing at room temperature, tetrabutylorthotitanate ($Ti(OC_4H_9)_4$), acetyl acetone (a chelating agent used to control the hydrolysis of tetrabutylorthotitanate), deionized water, and n-propanol with a volumetric ratio of 1:0.3:0.4:7, a yellowish titanium dioxide solution was prepared. Then nanometric carbon black powder of 18 nm primary particle size and 265 m^2/g BET surface (Degussa Printex L6) was added in the solution at the ratio of 2.35 mg carbon black for 1 ml $Ti(OC_4H_9)_4$. According to the authors, the prepared mixture could remain stable for months at ambient temperature. The mixture was blended uniformly by ultrasound for 10 min before use for coating. Then the mixture was dipped and dried at room temperature on a polished aluminum sheet (440 mm length - 201 mm height and 0.18 mm thickness), and then baked for 2 h at 500 °C. The same operation (immersion-coating) was done 7 times (according to a previous optimization) to form a thin C-TiO_2 photocatalyst film. The authors found that the C-TiO_2 film was very stable and durable without any loss during application.

A cylindrical reactor of 1.4 l effective volume (64 mm diameter, 530 mm length, 1.7 l total volume) was used to conduct the photochemical reactions. The interior surface of the reactor was closely covered by the C-TiO_2 coated aluminum sheet. With an initial concentration 9 mg m^{-3} of CH_4, at a flow rate 8 L min^{-1}, 50% CH_4 removal rate was obtained (4.5 mg m^{-3} min^{-1}) with the C-TiO_2 photocatalyst using 15 W UV lamps (185 nm and 254 nm), with a relative humidity of nearly 30%. These laboratory scale experiments using a "small" reactor were interestingly done in a continuous flow reactor. At a 8 L min^{-1} flow rate, the CH_4 flux speed is 2.5 m min^{-1} (0.15 km h^{-1}), corresponding to a gas residence time in the reaction zone of about 10 s. It is the authors' opinion that this conditions and better can be obtained under a SCPP-PCR.

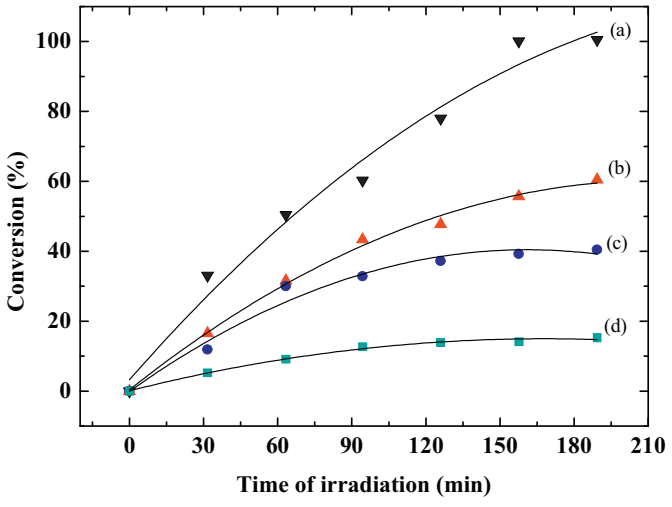

Fig. 6. Time dependent CO_2 production during CH_4 photooxidation obtained by Krishna [117] with Uranyl-Anchored on MCM-41 silicate molecular sieves. The reaction proceeds in air under sunlight irradiation. Curves (a) to (d) represent CH_4 concentrations in air varying at 0.15, 0.5, 1.25, and 2.3 vol %, respectively.

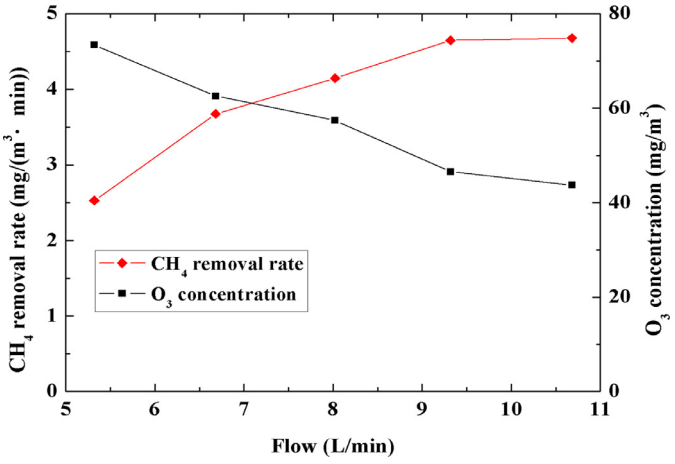

Fig. 7. Influence of the flow rate on the CH_4 removal and outlet ozone concentration (Liu, et al. [239]). Initial CH_4 concentration of 8.6–10.2 mg m^{-3}, and 27–30% RH%.

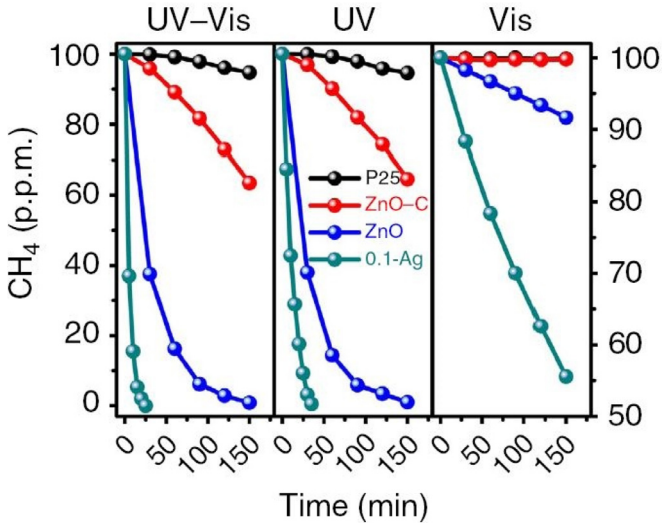

Fig. 8. UV and visible light activity of nano-photocatalysts ZnO, ZnO—C and 0.1% Ag—ZnO, during methane total oxidation experiments. The initial CH_4 concentration is of 100 p.p.m. commercial P25 TiO_2 photocatalyst is used for comparison (reproduced from Chen et al. [118]).

Several other experiments were carried on by Liu, et al. [239]: with TiO_2 the CH_4 removal was much higher than just with vacuum ultraviolet light. Addition of H_2O_2 and NO_x was not favorable for the CH_4 removal, but significantly reduced the outlet ozone concentration.

Numerous kinetics of CH_4 oxidation are given by Dreyer [241] and [242] using an ultra-low density UV-accessible aerogel photocatalyst.

Recently Pan et al. [243] demonstrated that $SrCO_3$ over $SrTiO_3$ nano-photocatalyst can proceed to complete oxidation of CH_4. Also Chen et al. [118] developed a very efficient Ag–ZnO photocatalyst with only 0.1% Ag which oxidizes CH_4 quickly, even in continuous flow reactor experiments. The next two Figs. 8 and 9, show respectively that this nano-photocatalyst exhibits visible light activity and that the lower the methane concentration, the faster the speed of the reaction. From Fig. 8, where CH_4 initial concentration is 100 p.p.m., it can be noted that simple ZnO nano-photocatalyst prepared under the same experimental conditions can also proceed to complete oxidation of CH_4 in 150 min (10 times more than with 0.1% Ag–ZnO), and more than 80% conversion in 50 min. Using only visible light, the 0.1% Ag–ZnO nano-photocatalyst can proceed to more than 90% oxidation of the CH_4 in 150 min. On Fig. 9, at a concentration of 100 p.p.m. it takes nearly 15 min to have 100% conversion of CH_4 into CO_2, while at 500 p.p.m. it takes nearly 40 min, and 100 min at 3000 p.p.m. The current concentration of CH_4 in the atmosphere is only 1.8 p.p.m. so it can be expected that the total oxidation will take an even shorter time.

As atomic chlorine is a sink for atmospheric CH_4 [244], another complementary strategy to reduce atmospheric levels of CH_4, can be the enhanced generation of °Cl thanks to photocatalytic Fe(II)/Fe (III) oxido-reduction in the atmosphere [245].

As seen from the examples above, the total oxidation of CH_4 is possible in air, at ambient temperature, under artificial illumination or under sunlight, using relatively simple and inexpensive photocatalysts like TiO_2, C-TiO_2 and Ag-ZnO.

4.3.2. *Partial oxidation of methane*

As previously mentioned, CH_4 is an abundant hydrocarbon, widely used as a fuel given its high calorific value. Mainly due to the fact that large amounts of natural gas are available in remote areas from the energy consumers with limited options to transport the gas, much work is being carried out in order to develop new catalysts and photocatalysts that can convert CH_4 into higher-value chemicals, often liquids easy to transport. From an environmental and energy perspective CH_4 transformation and direct oxidation into oxygenated products such as methanol is an attractive process. Consequently, nowadays an important amount of research is devoted to the selective CH_4 oxidation into products other than CO_2 and has been an on-going effort this last two decades.

In the photocatalytic approach, when ◦OH species oxidize CH_4, the formation of CH_3—OH is expected to occur from the generation of methyl radicals (CH_3), but then the subsequent oxidizing reactions can produce numerous other by-products. For this reason, currently the researchers try to avoid the complete oxidation of CH_4 and the formation of CO_2 and thus try to control the extent of the oxidation steps.

For instance Lopez and Martínez [246] studied the selective photo-assisted oxidation of methane into formaldehyde on mesoporous VO_x/SBA-15 photocatalysts that were seen to be more effective in terms of selectivity than VO_x / SiO_2 catalysts. SBA-15 are silica nanoparticles with much larger nanometre pores (4.6 to 30 nm) than the MCM-41 mesoporous silicate molecular sieve used by Krishna, et al. [117,238].

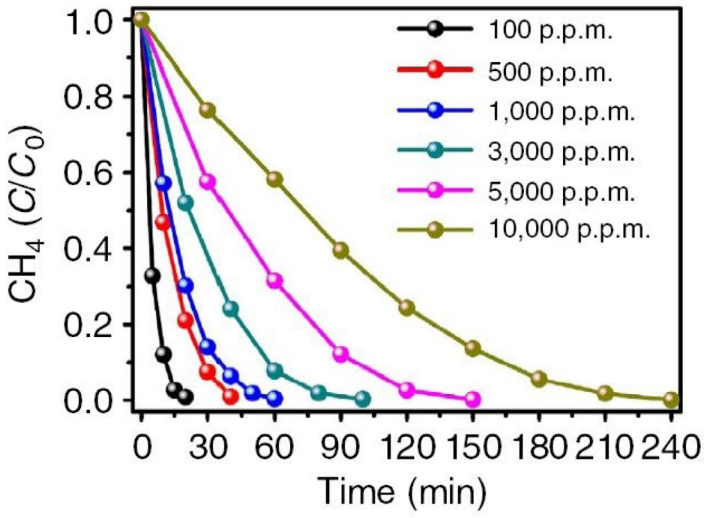

Fig. 9. Effects of initial concentration on methane total oxidation experiments under UV + visible light (reproduced from Chen et al. [118]).

Although few researchers reported the amount of undesired products obtained (CO_2) some information is available. For instance, Murcia-Lopez, et al. [247] wanted to selectively produce methanol and/or ethane from CH_4. They achieved an almost complete inhibition of undesired CO_2 by-product, with $BiVO_4$ photocatalyst in the presence of a low concentration of nitrite. But in these operating conditions after the first 60 min the highest CO_2 concentrations are reached then the CO_2 formation rates decreases. Nitrite increases the initial formation of CH_3OH at the expense of a decrease of CO_2 formation, which is expected as most of the CO_2 comes probably from oxidizing stages of methanol. For Murcia-Lopez, et al. [247], nitrite ions might act both as a UV filter and as a hydroxyl radical scavenger. A similar trend was observed when using an alternative photocatalyst Bi_2WO_6, in presence of nitrite, lower CO_2 production and higher selectivity for ethane production are observed. When Bi_2WO_6 was coupled with TiO_2, the methane conversion increased [248]; however, the undesired over-oxidation of CH_4 to CO_2 predominates. A similar effect is observed when electron scavengers such as Fe^{3+} are introduced in the photoreactor as a result of the formation of highly oxidant radicals. All the photocatalysts tested by these authors were synthesized by a facile hydrothermal method.

Xin [249] successfully oxidized CH_4 with niobium (1.4%) incorporated into silica-based mesoporous molecular sieves MCM-41. The reaction was carried out in the gas phase over 30 min, at 323 K, at atmospheric pressure with irradiation by a UV lamp (250–430 nm). The gas mixture tested was 45% CH_4, 5% O_2 and 50% He). As CH_4 is in excess compared to O_2, the CH_4 conversion yield was only of 10% with Nb_2O_5, to give mainly CO_2. The CH_4 conversion yield reached 18% with Nb-MCM-41 which was reacted after adsorption of water. Under these conditions some methanol (0.29 μmol) was obtained, but CO_2 is still the main product of the reaction (107.5 μmol or 370 times more than methanol).

Partial oxidation of CH_4 to methanol using bismuth-based photocatalysts Bi_2WO_6, $BiVO_4$, and Bi_2WO_6 coupled with TiO_2 was also succeeded by Murcia-López [248], in aqueous phase at 55 °C. All photocatalysts yield some small amount of ethane. The conversion rate is small with $BiVO_4$, and Bi_2WO_6 and the ratio of CO_2/CH_3OH obtained is respectively of approximately 1 and 2. Meanwhile with Bi_2WO_6/TiO_2 the conversion rate is nearly 4 fold, and the ratio is almost 12 in favor of CO_2.

Villa et al [250]. synthesized mesoporous WO_3 and explored the effect of the addition of electron scavengers (Fe^{3+}, Cu^{2+}, Ag^{+}) in aqueous phase at 55 °C. In the presence of Ag^{+} ions, the yields of ethane and methanol were the lowest and the CO_2 generation rates were the highest.

The same team also tested tungsten oxide (WO_3) and several derivatives [250,251]. They succeeded in improving the selectivity for the desired products, but the levels of CO_2 production were still high (nearly 3 times more than methanol and ethane, with the unmodified WO_3) at ~55 °C under UV–visible light irradiation, with 1 g catalyst L^{-1} under a continuous CH_4 flow of 4.5 mL min^{-1}.

So even if the on-going current research in this area is oriented towards the partial photocatalytic oxidation of CH_4, high amounts of complete oxidation to CO_2 are often observed (but not reported in publications) and small improvements to reach the goal of complete mineralization of CH_4 are feasible.

4.3.3. Other photocatalytic methane transformations

The conversion of CH_4 to more valuable chemicals is one of the most intensively studied topics in catalysis. CH_4 reforming or oxidation by thermal catalysis requires high temperatures [252] and is therefore out of the scope of this review. Nevertheless it is worth being mentioned that Walther [253] succeeded with CH_4 oxidation on 2 nm gold nanoparticles supported on various metal oxides at low temperature (130–250 °C). For full oxidation to CO_2, TiO_2 was found to be the best support for gold nanoparticles both in terms of activity and gold particle stability.

Partial oxidations of CH_4 by selective photocatalysis often produce CO_2 as a by-product, especially in the case of low selectivity or low yields. The high stability of CH_4 requires high energy levels for its conversion and remains a problem to be solved. In order to convert CH_4 into hydrogen and into more useful chemicals various efforts have been carried out [254]. For obtaining useful organic products like ethane and higher hydrocarbons, as well as formaldehyde, methanol or syngas, the selective photocatalytic conversion of CH_4 by coupling or partial oxidation is needed and has been reviewed [254,255] and the main reaction schemes are:

$$CH_4 + xO_2 \rightarrow \text{oxidation products } (CO_2 + CH_3OH + HCHO + HCOOH) + H_2O \quad (4)$$

or

$$xCH_4 \rightarrow C2 - C6 \text{ compounds} \quad (5)$$

As seen at the beginning of this section, to overcome the thermodynamic barrier photocatalysis has been proposed as one of the answers. New developments in the photocatalytic conversion of CH_4, such as CH_4 coupling and CH_4 conversion with other molecules is currently an intensive research topic.

Shimura [256] reviewed the three types of photocatalytic reactions for CH_4 conversion, that can be realized at a mild condition between ambient temperature and 473 K using semiconductor photocatalysis and photoenergy, i.e.:

- the photocatalytic non-oxidative coupling of methane also named dehydrogenative coupling of CH_4 to ethane;

$$2CH_4 \rightarrow C_2H_6 + H_2 \quad (6)$$

- the photocatalytic dry reforming of methane to produce syngas:

$$CH_4 + CO_2 \rightarrow 2CO + 2H_2 \quad (7)$$

- and the photocatalytic steam reforming of methane to produce hydrogen:

$$CH_4 + 2H_2O \rightarrow 4H_2 + CO_2 \quad (8)$$

Shimura et al [257,258] worked on photocatalytic steam reforming of CH_4, either with Pt-loaded or unmodified calcium titanate or sodium tantalate photocatalysts at nearly room temperature. They concluded that photocatalytic steam reforming of CH_4 and photocatalytic water decomposition proceeded simultaneously.

Although the goal of these processes is to photocatalytic conversion of concentrated CH_4 into liquid or gaseous fuels, these reactions should be kept in mind as they can also help to reduce the radiative forcing of atmospheric CH_4.

In summary, this section has highlighted the wealth of available catalytic reactions for mineralizing CH_4 or to transform it, not only using titania, but also using tungstosilicate, uranyl compounds and other semi-conductor metals like ZnO. The experience in this area is very promising for future applications in hybrid SCPP-PCRs.

5. Combination of SCPP with photocatalysis

5.1. Performance estimates of SCPPs and GHGs removal for the atmosphere

In order to give a preliminary assessment of the feasibility of the concept, estimates of performance of the hybrid device are reviewed here. All GHGR approaches require very scale equipment and it

is important to get an idea of the scale needed by way of first approximation.

The estimates may depend on the configuration of the system for which there are several options. For example, the photocatalyst can be installed on the ground of the SCPP (the GH is 38 km^2 for a model SCPP of 200 MW), but it can also be coated on the inner part of the glass (or plastic) of the canopy. A daily air flow of 17 km^3 passes through a 200 MW SCPP (>6000 km^3 yr^{-1}). Of course the relevant volume is only one third this amount, if the photocatalytic remediation takes place only 8 h day^{-1} under intense sunlight, but night operation strategies are proposed later. As the amount of CH_4 in the atmosphere is 1.83 ppm, if 17 km^3 of air passes every day under the GH of a 200 MW SCPP, this represents more than 31 000 m^3 of CH_4 per day and nearly 0.011 km^3 of atmospheric CH_4 per year passing under a single SCPP. With current atmospheric GHGs concentrations, per year this SCPP air flow contains (rounded numbers) 7900 tons of CH_4, 3900 tons of N_2O, and nearly 42 tons of halogenated compounds, representing all together more than 1.5 Mtons yr^{-1} eq-CO_2 [22].

In a canyon street (Fig. 4), as the buildings shadow moves during the day, and as pollution ($VOCs + NO_x$) levels depend on traffic intensity as well as on wind turbulences and direction, the area of photocatalyst receiving sunlight and pollution varies. Under the collector of a SCPP, which acts as a GH, the air flow direction will in contrast always be the in same direction (radial towards the center of the collector), and the airflow speed will be almost constant until arriving near the collector center (assuming that the collector height increases – see Section 2.3, and collector slope on Fig. 13). Thus in SCPPs the operation would be more like in indoor experiments, where the results are better than outdoors, as important parameters can be controlled.

Under the envisaged SCPP, the nano-sized photocatalytic coating on the inner side of the canopy is translucent, active under visible light and activated by the sunlight penetrating under the GH and reaching the floor, where other types of photocatalysts can be set up and activated by visible light [259]. As seen in Fig. 10, the best direct sunlight irradiation is mostly maintained, as there is almost no shadow. The partition walls under the GH prevent external rapid crosswind from disturbing the slow hot airflow under the GH, which thus moves radially towards the central tower [260]. Ambient crosswind entering under the GH by the front compartments is also guided by the partition walls to the turbines at the chimney entrance.

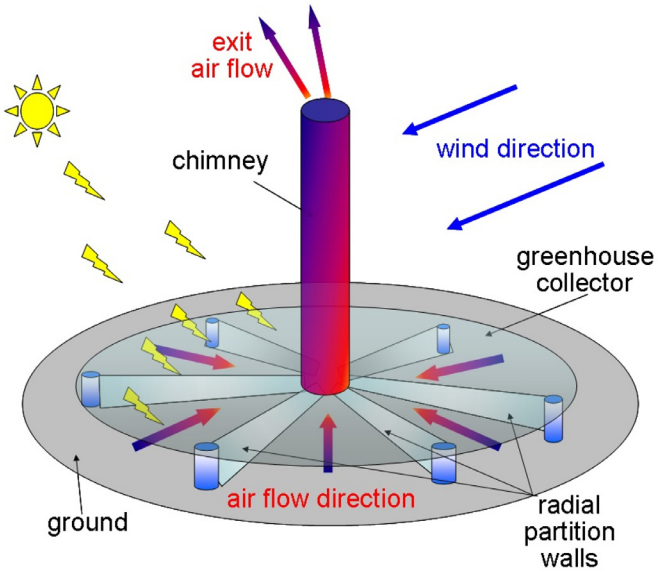

Fig. 10. Solar chimney with glass canopy, allowing sunlight to enter across the translucent photocatalytic coating and reaching the ground to activate other types of photocatalysts [260].

The temperature increases, and relative humidity (RH%) decreases, from collector entrance towards the bottom of the chimney. The RH% is at its maximum at tower exit, then during ascension in the chimney the temperature decreases and sometimes the condensation temperature is reached. Consequently, depending on the properties of the photocatalyst that will be used, its location under the SCPP GH can be adjusted so that several of the operating parameters are optimal.

The pressure drop is an important parameter in estimating airflow, and has been reviewed by several authors. Gannon et al. [261,262] evaluated the different pressure drops in SCPPs through a one-dimensional compressible flow approach and with wind tunnel experiments using a 0.63 m diameter small chimney model. The pressure drop associated with the vertical acceleration of the air and the loss due to the chimney internal bracing wheel and spokes (the tension system inside the chimney to prevent ovalization), was found to be much higher than the pressure drop associated with wall friction; thus smoothing the walls will have a small effect.

In order to maximize contact time between the molecules in air (CH_4, N_2O, CFCs and HFCs) and the photocatalyst coating, multiple translucent layers of photocatalyst spaced are proposed at the entrance of the SCPP as seen on Fig. 11. The pressure drop will depend on the layers spacing, as generally pressure drop is given by an equation of the form of Eq. (6):

$$\Delta p = f_D \cdot \frac{\rho \upsilon^2}{2} \cdot \frac{L}{D} \tag{6}$$

where L is the length of the channels between the layers and D is the hydraulic diameter), f_D is the Darcy friction factor (typically in the range 0.002–0.01 for turbulent flow) ρ the air–density and υ the flow velocity. Thus the local pressure drop should be determined from an optimization study to determine the requisite surface to volume ratio of catalyst, traded off against the pressure drop penalty. Nonetheless, at this stage it is noted that the velocity υ at the entrance is very much lower than at the center of the SCPP, and can be made even lower by increasing the height of the collector entrance as indicated in Fig. 11. As the pressure drop depends on the square of υ, it is therefore anticipated that the pressure drop penalty should not be too great (see also Section 5.3.2).

For reference, the pressure drops to perform the chemical removal of CO_2 directly from the atmosphere with a solid to air exchanger (using alkali solid resin) are in the order of 20–40 Pa, and with a liquid to air exchanger (similar to the ones in wet cooling towers) using an aqueous solution of alkalis the pressure drop is in the order of 100–150 Pa [39,263].This latter system is being used by the firm “Carbon Engineering” which proposes the “air contactor” of Fig. 12 [15,264], requiring hundreds of electrical fans and consuming electricity.

It is the authors’ opinion that the preferred configuration should be the one of Fig. 10, because the light penetration is more efficient than in Fig. 11 configuration (some losses occurs when crossing each of the multiple layers) and mass transfer of GHG from air to photocatalyst is similar in both configurations (same area of photocatalyst, the airflow puts much longer time to pass across the photocatalytic area under configuration of Fig. 10, allowing efficient mass transfer to occur).

If all our electrical energy needs (estimated at 8.8 TW electrical capacity or 31 PWh per year electricity generation [9] by 2030) were satisfied with 200 MW SCPPs, 50,000 such SCPPs would be required, and nearly one atmospheric volume would pass through them every 15 years. In this scenario of satisfying 100% of the electrical energy needs, no more CO_2 will be emitted for electricity production and oceans acidification will be slowed down. With 50 000 such SCPPs-PCRs, this amounts to total abatement of 80 Gt CO_2eq per

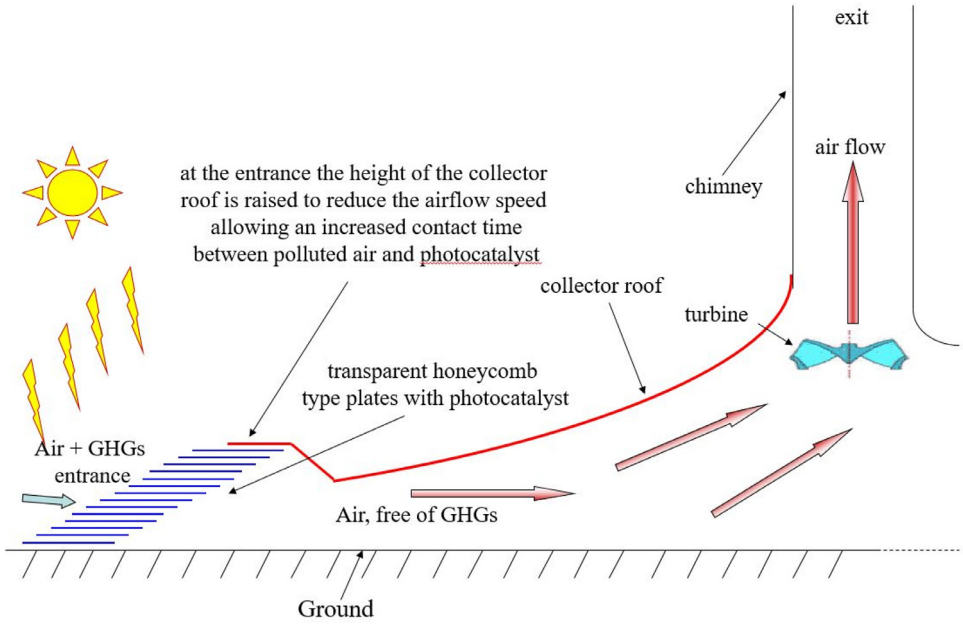

Fig. 11. under the GH around the circumference of the SCPP multiple layers of photocatalyst for GHGs mineralization can be installed [34].

year. For comparison, according to Williamson [29], it is necessary to remove in total 600 Gt eq-CO_2 to stabilize global warming to within 2 °C this century. Therefore, subject to the assumptions made, the proposed SCPP-PCR technology may indeed achieve mitigation and removal at the necessary rate and scale; and even 5 000 to 10 000 such negative emissions power plants could help to stay under the total carbon budget compatible with 2 °C goal.

10 000 SCPPs-PCRs can provide 2 TW amounting for 16 Gt CO_2-eq abatement per year. The total surface covered being 380,000 km^2, representing nearly 23 times the area of the city of Beijing; alternatively 4% of the entire Sahara Desert, 16% of the Arabian Desert, or 28% of the Australian deserts (which cover 18% of Australia).

Instead of being the only component of the energy portfolio, a reasonable aim for SCPPs is just to take a significant part (10–20%) on the energy mix of the future, which has to be diversified with increased use of most renewables. SCPPs are expected to require low maintenance [35], providing robust and long lasting power plants, producing electricity at almost zero cost after the repayment of loans and capital. According to Harte [36], their designed service-lives is of 100 years and more, which is 2 times longer than that of nuclear or fossil fuel power plants and 3 or 4 times longer than wind, PV, and CSP power plants. SCPPs provide a radical technological breakthrough: they are a non-CO_2 emitting source to produce renewable electricity from free-sunlight, presenting many synergies when associated with photocatalytic destruction of non-CO_2 GHGs.

5.2. Large-scale atmospheric photocatalytic transformation of GHGs

Previously work cited in this review was almost all done at the laboratory scale, but some articles mention the photo-elimination of CH_4 at a larger scale (Espagnol, et al. [265], Guarino, et al. [198], and Costa, et al. [199,266]). These works are especially interesting because they come closer to the focus area of the current review.

Promising results with CH_4 were presented in 2006 by Espagnol et al. [265]. To reduce gaseous emissions, Espagnol used a photocatalytic cover during the storage of slurry from 54 pigs. The slurry was split between two experimental vats each of 13 m^3 and stored outside. A pilot photocatalytic cover overlaid one of the vats and, using

Fig. 12. Air contactor device proposed by Carbon Engineering for direct capture of CO_2 from air [15].

a tracer method, gaseous emissions from the vats were measured continuously over 2 months. The photocatalytic covering was quite efficient with an oxidation rate of 59% for NH_3 and of 71% for CH_4.

Guarino and Costa [198,199,266] confirmed the results obtained with CH_4 by Espagnol, et al. [265] although with different experimental conditions. In order to reduce NH_3 and GHGs emissions from animal husbandries, Guarino and Costa used a TiO_2 photocatalytic low cost coating paint on the walls of a pig house. Two identical mechanical ventilated farrowing rooms were used to conduct the trials, and the gas concentrations and ventilation rate were continuously monitored in the two units over one month. The average concentration of CH_4 was reduced by 15–27% when lightening the walls by 36 W UV lamps. These results can be compared to the ones obtained by Liu et al. [239]. Thanks to a continuous flow reactor of 1.4 l, using 15 W UV lamps Liu et al. reached 50% CH_4 removal rate at a CH_4 flow rate 8 L min^{-1}.

The reaction speeds obtained by Melse and Hilhorst [267], during the photooxidation at 365 nm of CH_4 in exhaust air from of liquid manure storages and animal houses, were slow on TiO_2 coated on wool, but 20 times faster on TiO_2 coated on quartz fibers.

Bellobono, et al. [237,268,269] studied in laboratory-scale annular reactor, the photo-mineralization of (10–1000 ppm) CH_4 in air, by photocatalytic membranes immobilizing TiO_2, with flow rates from 4 $m^3 h^{-1}$ up to 400 $m^3 h^{-1}$. Bellobono also studied the photo-mineralization of CH_4 in water [270]. With standard flow rate of 300 $m^3 h^{-1}$, in presence of oxygen, in the gas phase saturated by water, Bellobono, et al. [269] found that at 318 K the mineralization of CH_4 with TiO_2 immobilized in photocatalytic membranes proceeds completely, as it occurs in the liquid phase.

The previous section demonstrated that successful research was carried out on the photocatalytic oxidation or reduction of CH_4, N_2O and HC in the gaseous phase. Almost all of the research experiments concerning HC and CH_4 were conducted at atmospheric pressure and in air (in presence of excess oxygen). So, direct photocatalytic oxido-reduction of HC and oxidation of CH_4 in air is possible. In the case of the photocatalytic reduction of N_2O, earlier articles describe experiments under reduced pressure sometimes with a neutral rare carrier gas like He [185]. Recent experiments conducted by Obalová [120,121] were done in the presence of excess oxygen and the photoreduction yield was slightly enhanced. The nitric oxide (NO) photodecomposition into N_2, and O_2 is well documented [137], but it also gives some amounts of N_2O. In presence of reducing agents like CO or NH_3 no N_2O is obtained. The selectivity of photoreduction of NO into N_2 and O_2 is favored by iron doping of TiO_2 [271] and transition metal oxides in zeolites [272]. As N_2 and O_2 readily desorb from the photocatalyst surface during this photoreduction reaction, no deactivation occurs; whereas NO_x removal by photooxidation produces nitrate species that need to be washed away for photocatalyst regeneration.

Once the best photocatalysts candidates are selected, it will be possible to use several of them under the SCPP collector at different locations, allowing selective transformation of several different non-CO_2 GHGs and ozone depleting gases. Judicious positioning of the different catalysts would allow optimization of the operating conditions for each one; for example, the temperature is lower (and the RH% higher) where the air enters at the SCPP perimeter, increasing towards the center.

On the one hand, the local surface-to-volume and mass transfer may be improved if multiple layers are used as shown in Fig. 11, but the visible-light intensity decreases progressively with the number of layers of coated glass or polymeric sheet. On the other hand, very large photocatalyst areas as shown on Fig. 10 may allow longer contact time and photocatalyst illumination, but with perhaps poorer mass transfer due to thicker boundary layers. In Fig. 13a SCPP-PCR system is shown that may overcome the disadvantages in each case, allowing installation of 4 different layers of photocatalyst at different locations under the GH, with varying temperatures and airflows. This arrangement also offers improved energy storage [273].

Because of its low cost, high stability, strong oxidizing power and non-toxicity (proved by many years of use in medicines and cosmetics) TiO_2 is widely used and studied, in particular for environmental applications and for the degradation of certain pollutants. Introduction of nano-particles has increased the surface area and light transparency; for example, composite nano-photocatalysts made of semiconductor oxides and high surface area adsorbents on supports such as silica, alumina, carbon or zeolites [274].

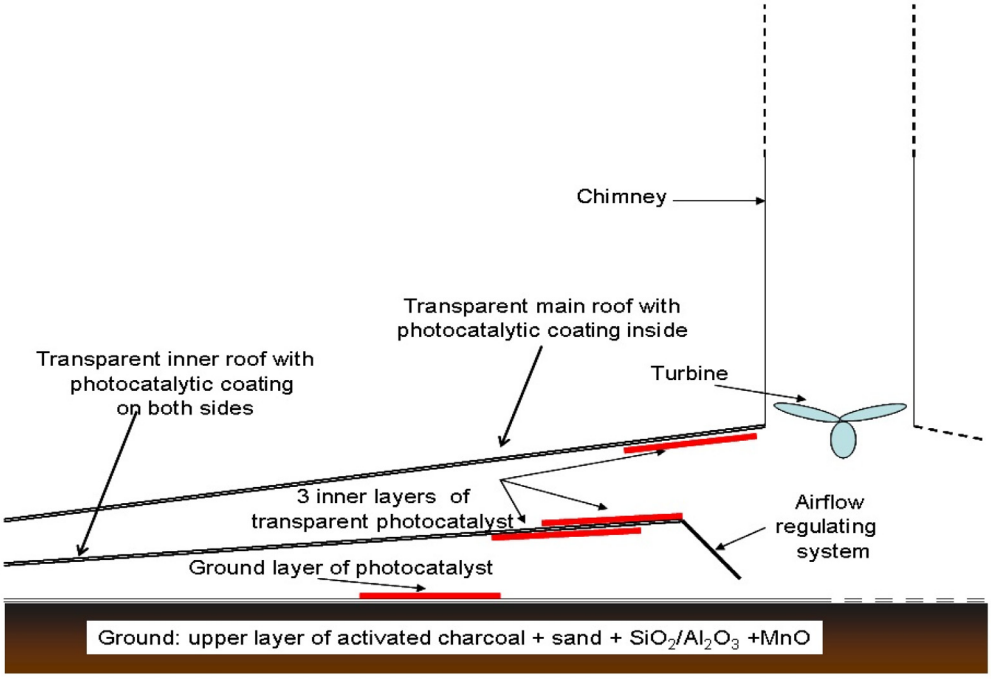

Fig. 13. A SCPP as proposed by Pretorius [273], with a double roof for energy storage, and providing 2 times more available surface for photocatalytic coating [34].

Considerable progress has been made by researchers to induce visible-light activity via numerous modification types [275,276], as it often increases the efficiency and quantum yield. Although the development of new non-toxic and low-cost visible–light active photocatalysts still seems interesting, the efficiency of available doped nano-sized TiO_2 photocatalysts is already satisfactory for practical use in mineralization of CFCs, HFCs and CH_4, and for N_2O reduction; and numerous cheap and abundant semiconductor oxides as well as modified zeolites [197] are also good candidates. A sustainable large-scale implementation needs also to address long-term stability and activity under strong solar irradiation, requiring further tests and research. Once the photocatalysts and the operating conditions are chosen, then the design specifications can be formulated and the economics worked out.

5.3. Mass transfer in the SCPP

5.3.1. Mass transfer for photocatalysis

Though there is valuable experience of energy conversion in SCPPs, and several models have been developed for this, there is no comparable experience of using SCPPs as photocatalytic reactors. Therefore it is important to review studies of other types of photocatalytic reactor to gain insights regarding mass transfer and photocatalytic performance.

Several processes may govern mass transfer in a photocatalytic reactor. In a study of photocatalytic air cleaners for the built environment, Zhong and Haghighat [154] identified as many as seven elemental mass transfer processes involved (Fig. 14):

(i) advection of reactants (e.g. methane) by the airflow;
(ii) mass transfer from the bulk flow to the exterior surface of the catalyst via boundary layers;
(iii) molecular or Knudsen diffusion through the pore structure of the catalyst;
(iv) adsorption at interior pore surfaces;
(v) photochemical reaction kinetics at interior surfaces;
(vi) desorption of reaction products;
(vii) mass transfer by diffusion and advection back to the bulk air stream and outlet (Fig. 12).

Since these processes occur in series, any one may in principle limit the overall rate of reaction. Light availability and penetration to the catalyst can present a further limitation, according to the quantum efficiency of the photocatalytic reaction [277].

Zhong et al. [278] represented multiple processes of boundary layer mass transfer and reaction kinetics at interior surfaces, together with light penetration, in an integrated model of an indoor UV photocatalytic air cleaner that they verified by experiment. Their reactor was only 0.76 m long. In comparison, outdoor reactors are large in scale (tens of meters typically), suggesting that advection and bulk mass transfer through boundary layers will be limiting the limiting processes, as assumed by Sikkema in a study of photocatalytic paving [158]. These processes are represented non-dimensionally by Sherwood (Sh) number correlations, typically of the form $Sh = \text{constant} \times Re^m\ Sc^{\ n}$, where *Re* and *Sc* are the Reynolds and Schmidt number respectively, and m and n are constants usually less than one. Examples of Sherwood correlations used in photocatalytic studies and elsewhere are included in Table 5. The definition of the Sherwood number is Sh = KL/D where K ($m\ s^{-1}$) is the mass transfer coefficient to be determined, *L* (m) is the characteristic length and *D* ($m^2\ s^{-1}$) is the diffusion coefficient of the reacting species moving through the air. Table 5 is useful to illustrate the general form of the applicable relationships, which can also lead to preliminary predictions of mass transfer performance as discussed next.

5.3.2. Dimensional analysis of transfer processes

Extension of the function of the SCPP to that of a photocatalytic chemical reactor requires effective design with respect to heat, mass and momentum transfer. Heat transfer to the moving air will promote energy conversion by increasing collector efficiency; and mass transfer will promote photocatalytic performance. On the other hand, momentum transfer may be detrimental to energy conversion if it increases pressure drop significantly. Dimensional analysis is very useful technique to show the relations among these three processes. It enables simple and general estimates of performance, prior to more detailed and time-consuming analyses for specific design cases [282].

Based on the fundamental similarity between diffusion of heat and mass, correlations for Nusselt and Sherwood numbers (of the kind shown in Table 5) are expected to be similar in forced convective flow. With the addition of buoyancy terms, Grashof number (Gr) terms should be also be included [283]. If the Prandtl number (Pr) and Schmidt number (*Sc*) are equal, then Nu = Sh. The ratio *Sc*/Pr, called the Lewis number, is shown in Table 6 for trace gases of interest, confirming that Le≈1. This means that measures to enhance heat transfer – such as extensions to surfaces or turbulence promoters – could be expected to increase Sh and Nu by the same percentage. For example, if the photocatalytic material were coated on the ground surface of the collector, corrugations in the surface could be useful to enhance both heat transfer to the air and the mass transfer by similar amounts. On the other hand, the equivalence between Nu and Sh is only valid to the extent that the same surfaces are being used for both heat transfer and for photocatalysis. For example, it could well be the case in practice that heat transfer occurs mainly at the ground and photocatalysis at the glazed surface above.

The fact that, in the correlations of Table 5, *Re* is raised to a power less than unity suggests a sub-linear dependence of heat and mass transfer on flow velocity: a doubling in velocity would be expected to increase heat and mass transfer by less than 2. We also note that, since the characteristic length *L* appears in the numerator of Sh, a decrease of *L* will help to achieve an increase in mass transfer in inverse proportion to *L* at given *Re*. This is because the distance over which molecules have to be transferred is decreased.

Momentum transfer occurs through shear stress at flow boundaries. According to the Reynolds analogy, skin friction coefficient (C=wall shear stress/$\rho\ u^2$) and the Stanton number ($St = h/\rho\ c_p\ u$) assume proportionate values (ρ is air density, c_p is heat capacity, *u* is

Table 5
Sherwood (Sh) and Nusselt (Nu) number correlations from the literature, as used in photocatalysis and other more general applications. According to principles of dimensional analysis, Nu may be substituted by Sh with Pr substituted by *Sc*.

Configuration	Correlations	References	Comments
Honeycomb or fibrous filter	$Sh = 0.705\ (Re\ D/L_f)^{0.43}\ Sc^{0.56}$	[279], used in [154]	L_f is thickness of TiO_2 film coated on glass fibers, L the characteristic length of the fibrous medium
Concrete paving slabs	$Sh = 0.664 Re_{tr}^{1/2} Sc^{1/3} + 0.036 Re_L^{0.8} Sc^{0.43}\left[1-\left(\frac{Re_{tr}}{Re_L}\right)^{0.8}\right]$	used in [158]	Re_L is based on the roadway width, R_{tr} is for a transition region
Turbulent boundary layer	$Nu = 0.032 Re^{0.8} Pr^{0.43}$	[280]	Valid for $2\times10^5 < Re < 5\times10^6$
Turbulent pipe flow	$Nu = 0.0243\ Re^{0.8}\ Pr^{0.4}$	[281], p.360	Dittus–Boelter correlation
Turbulent pipe flow	$Nu = 0.023\ Re^{0.8}\ Pr^{0.33}$	[281], p.360	Colburn correlation $2\times10^4 < Re < 3\times10^5$

Table 6
Schmidt number for trace gases in air and Lewis number (Le = *Sc*/Pr) on basis of Pr = 0.71 for air; values for diffusivities from [284]; at 25 °C.

Gas mixture	Diffusion coefficient ($\times 10^{-5}$ m^2 s^{-1})	*Sc*	Le = *Sc*/Pr	Le$^{0.33}$
H_2O vapour in air	2.55	0.61	0.87	0.95
CH_4 in air	2.29	0.69	0.97	0.99
N_20 in air	1.68	0.93	1.31	1.09

air velocity and h is heat transfer coefficient). Various forms of the Reynolds analogy exist e.g., that due to Žukauskas [280,281]:

$$St = (C/2)Pr^{-0.57}$$

suggesting that St and *C* will increase proportionately with changes to geometry or dimensions. With the mass transfer coefficient K = Sh.D/H and following again the simplification due to Le≈1, provides the approximation of St ≈ K/u. The appearance of u^2 in the denominator of *C*, in contrast to u in the denominator of St, suggests that for given *C* and St, lowering of u will result in a large reduction of wall shear stress accompanied by only modest penalty in K. Therefore, to mitigate potential conflict between maximizing mass transfer and minimizing pressure drop, we should choose a large contact area of catalyst (to maximize the action area of action for both K and C) and small u to give low *C* (a similar principle to that used in a micro-channel heat exchanger). This would be favored by positioning any additional photocatalytic surfaces away from regions of higher flow velocity, that is to say away from regions near the center of the solar collector or in the vicinity of the turbine and chimney inlet. To minimize u, additional surfaces could be positioned instead towards the outer rim of the solar collector (as in Fig. 11).

The Reynolds analogy is only applicable when flow resistance is dominated by skin friction and not by profile drag [281,283]. Profile drag is induced by pressure variations against bluff surfaces facing the flow, asymmetries, or separation of flows behind surfaces. Photocatalytic surfaces in the solar collector should therefore be aerodynamically designed to minimize profile drag, if such drag is found to be significant in magnitude.

Based on the above considerations, a preliminary dimensional analysis of the effectiveness of a SCPP as a photocatalytic reactor is presented in Table 7 below, based on the assumption that the floor of the solar collector is coated with catalyst to provide zero concentration of methane at this boundary. Accordingly, the estimate Sh = Nu = 1340 enables a mass transfer coefficient $K = 0.0166$ m s^{-1} to be calculated readily, resulting in a number of mass transfer units of 1.1, and mass transfer effectiveness of a 67% – indicating that two out of every three molecules of methane entering the SCPP would be removed.

Table 7
Preliminary dimensional analysis of the Manzanares SCPP modified for photocatalysis by coating the floor with TiO_2, predicting a removal effectiveness of 67% for methane; input parameters from [40,285].

Calculated parameters	
Collector area	46,760 m^2
Volume flow	707 m^3/s
Air density at chimney inlet	1.1 kg/m^3
Mass flow	777 kg/s
Rate of heat transfer (based on temperature rise)	24,300 kW
Log mean temp difference	30 °C
Heat transfer coefficient	0.0173
Nu = Sh	1340
Diffusion coefficient CH_4 (D)	2.29×10^{-5} m^2 s^{-1}
Mass transfer coefficient *K* = Sh.D/H	0.0166 m/s
Number of transfer units (NTU)	1.1
Mass transfer effectiveness $\varepsilon = 1 - e^{-NTU}$	0.67

The calculation ignores the issue that coating the floor with TiO_2 would increase the reflectivity and reduce the optical absorption and thus solar collector efficiency. More realistically, the TiO_2 would be applied to the underside of the glazing. Nonetheless, this would provide the same surface area subject to similar mass transfer regime. Therefore, subject to the assumed condition of zero concentration at the flow boundary, the calculation gives a preliminary indication that a reasonable photocatalytic performance is possible, and that further study and optimization is justified.

5.3.3. Quantitative experimental studies of PCR performance

Liu et al [239] conducted photochemical reactions in a 64 mm diameter cylindrical reactor of 530 mm length (total volume 1.7 l, effective volume of 1.4 l). The C-TiO_2 coated 0.18 mm thick aluminium sheet used (440 mm length - 201 mm height) was attached closely on the interior reactor surface.

With an initial concentration 9 mg m^{-3} of CH_4, at a flow rate 8 L min^{-1}, 50% CH_4 removal rate was obtained (4.5 mg m^{-3} min^{-1}) with the C-TiO_2 photocatalyst using 15 W UV lamps (185 nm and 254 nm), with a relative humidity of nearly 30%. These laboratory scale experiments using a "small" reactor were interestingly done in a continuous flow reactor. At a 8 L min^{-1} flow rate, the CH_4 flux speed is 2,5 m min^{-1} (0.15 km h^{-1}), corresponding to about 10 s gas residence time in the reaction zone.

The photocatalytic CH_4 decomposition performance of vertically aligned TiO_2 nanotube arrays grown by a one-step anodic oxidation technique was reported by In, et al. [286]. At typical experimental conditions, 2 vol% of CH_4 gas (in a 2:5 gas mixture of He and atmospheric air), through the reaction zone the gas flow is around 6×10^{15} molcules s^{-1}, corresponding to about 1 s gas residence time in the reaction zone.

Photocatalytic measurements were carried out under UV irradiation at 367 nm (410 mW cm^{-2}, 250 mW total power). The optimal nanotube photocatalyst thickness for CH_4 oxidation under 367 nm illumination was estimated by the authors to be about 575 nm. The CH_4 conversion was about 24×10^{-9} mmol s^{-1} (1.4×10^{13} CH_4 s^{-1}) and the absorbed photon to product conversion efficiency obtained by the authors was about 2.5×10^{-4} CO_2 molecules per photon.

Nielsen et al. [287] studied the total oxidation of CH_4 in a microreactor of 240 nl allowing experiments to be carried out at 1 bar with 2% CH_4 in air on small amounts of catalyst (ranging from 10 to 350 μg) with on the order of 5.10^9 molcules/s and a residence time of 1 s.

With the assumption that the height of the entrance of the GH of a SCPP is 3 m, the air flow speed under the GH is nearly 3 m s^{-1} (for an air flow speed of 15 m s^{-1} inside the tower at the turbines). The gas residence time in the reaction zone is about 833 s (almost 14 min) if the photocatalysts covers 20 km^2, to be compared to about 1 s in the case of Nielsen et al. [287], and to about 10 s for Liu et al. [239]. If the height at the entrance of the collector is higher (Figs. 10, 11 and 13), the air flow speed is lower and the gas residence time in the reaction zone is longer.

Taranto [288] compared the photocatalytic efficacy of two types of photocatalytic purifiers under development for treating gaseous effluents employing TiO_2-coated materials either as planar or folded fibrous filters, or as honeycomb monoliths. Taranto tested a 0.4 m^3 closed-loop, air tight, photocatalytic reactor with a loop through which the airflow can go from 16 to 1800 m^3/h. This reactor comprised a parallelepiped accommodating alternate banks of U-shaped lamps emitting at 254 nm and TiO_2 coated-materials. Methanol was chosen as the test pollutant, because contrary to CH_4 it is easily mineralized and two materials were tested: (i) a thin, folded tissue impregnated with commercial TiO_2 and colloidal SiO_2 used as a binder and (ii) an aluminum honeycomb-shaped material coated with the same commercial TiO_2. The interest of using honeycomb

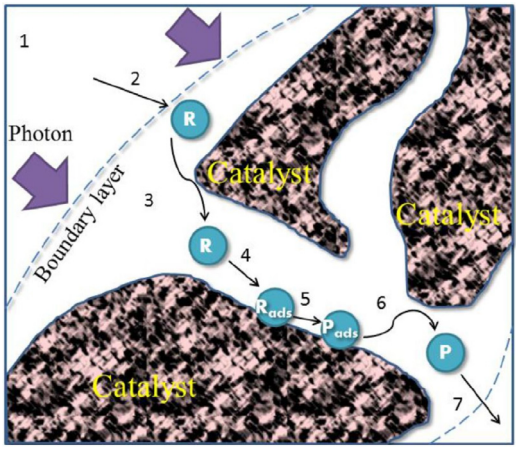

Fig. 14. Elemental mass transfer processes in the photocatalytic reactor (reproduced from [154]).

shapes was clearly demonstrated by the considerable differences in pressure drop between the two materials.

5.4. Materials, economics and nocturnal operation

Commercial photocatalytic coatings or paints contain after application 50 to 100 g m^{-2} of nano-sized TiO_2. Making the assumption of using 1000 tons of photocatalyst (256 m^3, as TiO_2 density is nearly 3900 kg m^{-3}) in a single layer of 50 g m^{-2}, an area of 20 km^2 can be covered under the GH of a SCPP. If the photocatalyst is applied in the centre of the GH, a radius of 2.5 km can be covered. At the current prices of bulk nano-sized TiO_2 (i.e. more or less USD $3300 per ton) 1000 tons represents USD$ 3–4 million, the total cost of the coating process can be estimated to USD$ 20 million, less than 2% of the cost of the SCPP [289].

Non-CO_2 GHGs removal by photocatalysis has the potential to provide not only significant climatic benefits by countering global warming, but also environmental benefits as halocarbons and N_2O have deleterious effects on the ozone layer.

The driving parameters for a large scale PCR for atmospheric remediation will be the visible light absorption for good solar energy-conversion efficiencies and reaction rates, and the photocatalyst cost and lifetime. Of course many other important parameters can be cited, like: flow rate, mass transfer rate, pressure drop, catalyst amount, illuminated area, light efficiency, intrinsic reaction kinetics, catalyst specific area and particle size, doping element or co-catalyst if any, temperature, absorption wavelength, alkalinity, etc.

The mineralization of N_2O and CH_4 (Eq. (1) and Eq. (3)) does not produce deleterious by-products. The oxido-reduction of CFCs and HFCs produces halo acids that can be neutralized by cheap alkalis which can be part of the photocatalytic coating or of the SCPP soil. But even with the assumptions that (i) 100% of the halogenated compounds passing through the SCPP per year are destroyed, (ii) each mole giving 4 mol of acids (although phosgene and chlorine gas are also possible products) and (iii) that 100% of the halogenated acids stay on the photocatalyst, deactivating it stoichiometrically by adsorption or by reaction (metal oxides are alkalis), only $^1/_9$ of the TiO_2 per year will be consumed.

Photocatalysed reactions can only be done when the photocatalysis are activated by light illumination. Under a SCPP they can only take place during the day, but strategies have been proposed [33,34] to overcome this restriction.

Using artificial illumination at night is not recommended due to additional costs, although possible with low cost energy-saving compact fluorescent lamps, which emit UV light, s converted inside the bulb into visible light when it strikes the fluorescent inner coating.

Several other alternatives during night time have been proposed like non-CO_2 GHGs adsorption on a substrate (metal organic frameworks, zeolites, activated carbon, sands…), taking advantage of reduced temperatures and reduced airspeed at night, with possible desorption during the day when sunlight activates the photocatalyst and increasing temperature releases the pollutant from the adsorption substrate.

MOFs are studied for methane storage and delivery [290], while the CH_4 adsorption capacity of carbonaceous solids is studied like for granular activated carbon (3.21 mol kg^{-1}) and wood-derived biochars (0.05–0.9 mol kg^{-1}) [291]. Some decomposition at room temperature of HFCs and CFCs upon adsorption over zeolites was discovered by Hannus [292]. According to Saha et al. [293], zeolite 5A is a good adsorbent to remove CO_2 and N_2O from air, meanwhile to remove CH_4 from air the metal organic framework MOF-177 is the adsorbent of choice. The potential of soils as a sink of CFCs was demonstrated by Khalil and Rasmussen [294] and by Benzoni [295]. Four sands from different locations (Mecca, Oman, Egypt and USA) were studied by Gäb [296], together with alumina and molecular sieves of known composition. Only modest mineralization of CCl_2F_2 was generally observed (0% to 9%) whatever the substrate, but 87% CCl_4 mineralization was obtained on basic alumina, 92% on neutral alumina, 41% on molecular sieves (containing 32.2% $A1_2O_3$, 38% SiO_2 and K_2O) and up to 46% CCl_4 on Mecca sand (containing 13.6% $A1_2O_3$, 69.3% SiO_2, and Fe_2O_3, CaO, NaO, MgO). The conclusion is that some halocarbons can be mineralized on sand, on alumina and on several metal oxides, even in the dark. As SCPPs are located in desert regions, the natural sandy soil composition can therefore be of benefit for GHGR.

6. Discussion

This review has been motivated by the limitations of current approaches to tackling global warming. It has been argued that hybrid SCPP-photocatalytic reactors present a possible complementary solution, alongside clean and efficient conversion technologies and carbon capture and storage as discussed elsewhere [297–299].

However, though the landmark 50 kW prototype SCPP constructed in Spain enabled promising subsequent design studies [300], the 4000-fold scale up to 200 MW is challenging. Scales of 200 MW (or even 400 MW) will be needed for significant contribution to a solution, with airflow around 17×10^9 m^3 day^{-1}. In contrast, in the largest laboratory scale photocatalytic reactions conducted for CH_4 removal, the airflow rate was a mere 11.5 m^3 day^{-1} (8 L min^{-1}) [239]. Can the methods proposed in this review article effectively remove non-CO_2 GHGs from the atmosphere at sufficient scale to have an effect on global warming? Though it is too soon to answer this question decisively, some interesting initial observations can be made. In Section 5.3.2 we are able to extrapolate from the Manzanares trials a mass transfer effectiveness of 67%; in other words for every 3 molcules of CH_4 entering the reactor, 2 will get converted to CO_2 with relatively low GWP.

In a scenario where future energy needs of 10,000 GW were satisfied by 50,000 SCPPs each of 200 MW output (or 680 GWh, with 39% capacity factor), close to one atmospheric volume would pass through the SCPPs collectors every 15 years, which could help to clean up indefinitely the atmosphere from several non-CO_2 GHGs. Making the assumption that the effectiveness of mass transfer allows the elimination of 67% of the CH_4, halocarbons and N_2O in the air flux under the PCR [115–117, 239], each photocatalytic SCPP can eliminate nearly 1000 kt eq-CO_2 yr^{-1}, and avoid a further 600 ktCO_2 yr^{-1} of emissions (assuming a reference scenario in which electricity is generated with carbon intensity of 0.88 tCO_2 MWh^{-1})

or even 900 $ktCO_2\,yr^{-1}$ based on Australian carbon intensity [301], thus helping to limit the Earth's temperature rise.

One important question is safety and security of use. Photocatalysis has been shown to be a source of N_2O (when starting from NO_x) [302] and incomplete oxidation of VOCs in terms of emissions of harmful by-products (such as aldehydes) can be of concern, for instance for the use of commercial photocatalytic air-purifiers sold for indoors domestic use [154,303]. In all cases, the photocatalyst has to be chosen for its activity but also its lowest side-reactions and by-products. This review proposes to perform removal of GHGs in very sparsely populated deserts, where there will be almost no VOCs or NO_x pollution. Often, intermediate by-products like aldehydes or alcohols react more rapidly in the atmosphere with the °OH radical, thus are more rapidly eliminated that the parent pollutant. In the cases of methane, CFCs and HFCs, the reaction intermediates are the same as the ones that currently arise from the natural oxidation processes by the °OH radical, or by photolysis, thus no new risk is presented. Also all the products obtained will be released quite high in the atmosphere by the chimney of the SCPP and with some kinetic energy allowing them to go even higher, so the risks for life and environment are lower than the advantages.

Another important question concerns whether the SCPP provides an effective approach to contacting photocatalysts with the atmosphere, compared to the other approaches reported in the literature. For example, it is interesting to compare against the approach of Stolaroff [28] who proposed several geoengineering strategies like dispersion of catalytic aerosols in the atmosphere. We feel that dispersion of aerosols would entail many governance issues, risking unforeseen side effects, in common with atmospheric injection technologies suggested for SRM. Stolaroff thinks that industrial technologies cannot process of the order of 1/10 of the atmosphere each year. This review suggests the contrary.

Despite several drawbacks [304,305], some researchers [306,307] have proposed the deliberate injection of titania or alumina particles into the stratosphere to scatter solar radiation back to space as a possible climate engineering scheme. But global warming is caused by longwave radiation, thus reducing the shortwave radiation will not solve the problem; neither will it reduce ocean acidification. This review paper proposes to address the underlying causes of climate change. Reducing the amount of GHGs in the atmosphere allows more thermal energy to escape to the outer space: this mitigation strategy, called Earth Radiation Management by Ming [308], is not SRM [309]. SRM by stratospheric sulphate aerosols might increase the ozone hole, or might delay its recovery, while N_2O, CFCs and HFCs removal by SCPPs-PCRs might decrease the ozone hole and provide both health and financial benefits [310].

Based on the important urban photocatalytic experiments of Folli [136] and some others, as analyzed by Kleffmann [159], some points can be made:

- for NO_x degradation, the photocatalyst employed in those experiments was only active under UV, meanwhile for CH_4 total oxidation and for the removal of the other non-CO_2 GHGs it is proposed to use photocatalysts active under both UV and visible light, taking profit of a larger range of the sunlight energy;
- the irradiation for NO_x degradation was of 3 $W\,m^{-2}$ [136] and 0.6 or 1.6 $W\,m^{-2}$ [140,156]; while under a SCPP it will be of 600–800 $W\,m^{-2}$, more than two orders of magnitude larger, with UV intensity in the order of 30 $W\,m^{-2}$; suggesting that the SCPP-PCR will not fail due to insufficient radiation;
- urban NO_x photooxidation trials were performed inside cities and there are many shadows of buildings (or even of the cars, buses and trucks passing on the streets), thus, as illustrated in fig. 4, the illumination of the photocatalyst is not constant; while under a SCPP the daily illumination of the collector is permanent and more intense (excepting the shadow from the chimney and sometimes from clouds);
- the NO_x concentration at vehicles' exhaust is high and dilution occurs rapidly with distance, thus there is a gradient that could impair performance; while concentration of well mixed GHGs in the atmosphere is considered constant, making for consistent performance of the SCPP-PCR;
- in an urban environment, the air speed varies with crosswind direction and the turbulences close to passing vehicles (buses, trucks, cars) at different speeds is important and variable; while under the SCPP collector the air flow will be almost constant over all the area of the photocatalyst coating;
- on the canyon street the photocatalyst was only on the sidewalks at the bottom near the road; on the tunnel the photocatalyst was only at the top of the walls and on the ceiling; while under a SCPP the photocatalyst is proposed on both ground and canopy;
- the area of the UV active photocatalyst used in Folli experiments was not sufficient (400 m^2) to transform significant amounts of the pollutant targeted, while for the SCPP-PCR proposal it is in excess (20 km^2), 50,000 times larger.

In SCPP-PCR, several tons of photocatalytic materials are proposed to be used under intense sunlight to destroy ppb levels of CH_4, N_2O and p.p.t. levels of halocarbons.

In fact, whereas the SCPP-PCR has certain distinct advantages over the urban photocatalysis approaches; it can also be argued that it follows the recommendations following from such experiments. The international team that conducted the field campaigns in one Brussels tunnel and in a model street canyon [140,156] made "*recommendations for the proper use of photocatalytic materials, such as:*

1. optimized application of the photocatalytic coating on a regular substrate, in order to obtain a low surface roughness minimizing dust adsorption;
2. high UV light intensity levels ideally around 10 W/m^2, to avoid surface passivation;
3. adequate design of the illumination system (visible plus UV light), to reach acceptable investments in terms of cost-benefit ratio;
4. low average relative humidity of tunnel air (<60%);
5. high photocatalytic activity of the de-polluting material, with a photocatalytic deposition velocity for NO of at least 0.1 cm/s measured under tunnel conditions;
6. low average tunnel wind speed, for increased reaction time of pollutants;
7. two-way tunnels, for increased reaction time and turbulent mixing;
8. high active surface-to-volume ratio (smaller-sized tunnel tubes); in absolute terms, the length of the tunnel should be adequate to have an appreciable de-pollution effect."

Taking these recommendations one by one, it can be noted that: (1) the canopy cover of the SCPP is a smooth and flat ceiling with low roughness and the gravity prevents dusts deposition in the inner part; (2 & 3) the sunlight visible-light intensity under a SCPP will be almost 2 orders of magnitude larger as the UV intensity recommended in these publications; and (4) the humidity level is by definition quite low in hot and arid countries. The photocatalytic surface passivation by urban VOC pollutants will be several orders of magnitude lower in the deserts where SCPP can be installed and CH_4 total photooxidation and N_2O photoreduction are not supposed to produce by-products; the acids by-products of the photocatalytic oxido-reduction of halogenated compounds can easily be neutralized and, their amount is limited, as Montreal gases concentration in the atmosphere is at the p.p.t. level. Regarding point (5), the

proposed photocatalysts are active both under UV and visible-light. Regarding (6 & 7), it is possible to optimize the airflow speed under the GH of a SCPP by varying the collectors entrance height; the GHG reactants are already well mixed and the flow is turbulent, and can be optimized [311]. The long reaction time of pollutants, and (8) the high active surface-to-volume ratio, is likely to be the case for 200 MW SCPPs with a greenhouse cover radius of 3.5 km and the photocatalyst coating covering a radius of about 2.5 km (20 km^2).

The photocatalytic deposition velocity for N_2O, CH_4, and of every individual CFC and HFC, has still to be measured for the non-CO_2 GHGs targeted in this review [312,313] and is part of the urgently research needed to go further in future with the SCPP-PCR open perspectives to slow down global warming and to fight climate change.

Clearly there are also disadvantages of SCPP-PCRs compared to urban photocatalysis. The latter generally make use of existing structures, as such are expected to be of lower cost, be less visually intrusive, and have lower environmental impact in their construction. The Life Cycle Assessment of SCPP will be an important topic for further work.

Before implementation, field studies are necessary to validate and understand better how photocatalytic coatings under a SCPP collector will perform under real-world conditions.

Future research does not need to start by building a large SCPP, as PCR can start by being tested in existing structures which have to deal with larger GHGs concentrations, for instance photocatalytic CH_4 total oxidation from coal mine ventilation, although according to some articles, photocatalysis works better at low concentrations [118]. Future research can also focus on other GHGs photocatalytic removal, such as ventilation of greenhouses used in agriculture where sewage sludge from treatment plants or pig manure are drying; then by measuring the amount of some other GHGs inside and outside large agricultural greenhouses, after passing through a large surface area of photocatalyst exposed to sunlight [289]. These applications provide economic incentives in themselves to perform the photocatalytic tests and then construct some pilot plants. Estimating the scalability of the process will then be possible.

Some further possible benefits of photocatalytic removal of non-CO_2 GHGs from the atmosphere may be mentioned.

1. *Simultaneous removal of ozone depleting substances, through elimination of residual CFCs being phased out by the Montreal protocol.* The benefits of the photocatalytic removal of non-CO_2 GHGs from the atmosphere are not limited to tackling global warming. Environment Canada estimated in 1997 [310] that, by the year 2060, the economic benefits of the Montreal protocol will totalize $459 billion, for a cost of $235 billion to achieve CFC phase-out. For atmospheric clean-up, the use of SCPP-PCR may provide benefits of comparable value. The benefits of the Montreal protocol [314] came from reduced UV damage to fisheries, agriculture and materials like outdoors plastics and paints. The decreased health care costs savings were not evaluated, but the number of fewer cases of cataracts, melanoma and non-melanoma skin cancer and deaths worldwide were estimated. Accelerating the removal of halocarbons from the atmosphere, as well as the removal of N_2O (a powerful ozone layer depleting compound) will provide similar benefits for the ozone layer as well as for climate and human, animal and vegetal health is also affected by global warming. Clearly there are also some downsides and risks to the SPCC-PCR concept. For example, mineralization of halogenated compounds produces acids that might have to be neutralized, but CFCs and HFCs concentration in the atmosphere is more than 5 orders of magnitude lower than CO_2 concentration, thus easier to deal with and to manage.
2. *Positive feedback in decreasing methane lifetime.* As the concentration of methane will be lower, its atmospheric lifetime will decrease, and thus the amount of $^{\circ}OH$ radical will increase (IPCC AR5 [315]: a 1% increase in CH_4 leads to a 0.32% decrease in $^{\circ}OH$), making it available for the destruction of other GHGs in the troposphere, like HFCs. The $^{\circ}OH$ radical is also called the detergent of the atmosphere as many anthropogenic and biogenic chemicals emitted into the atmosphere do not reach the stratosphere, thanks to their reaction with $^{\circ}OH$ that breaks them down efficiently. Recently Howarth [316] wrote that by reducing CH_4 emissions, society buys some critical decades of lower temperatures, as the climate system responds much more quickly to reducing CH_4 than to CO_2. Howarth said: *"society needs to wean itself from the addiction to fossil fuels as quickly as possible. . . . We should embrace the technologies of the 21st century and convert our energy systems to ones that rely on wind, solar and water power."* SCPPs together with photocatalysis could help to reach this goal.

7. Conclusion

This review shows that a large scale method of removal of GHGs other than CO_2 is possible, as these GHGs can be mineralized by photocatalysis, using simple metal oxides like MgO or ZnO, cheap TiO_2 derivatives and zeolites.

A giant PCR supported by the infrastructure of a SCPP is proposed as a device able to:

- transform CH_4 into CO_2 which has GWP >10 times lower per mole on a 100 years' basis;
- transform several CFCs and HFCs into $CO_2 + HCl$ and HF and neutralize the halo-acids by-products;
- reduce the atmospheric concentrations of CH_4, N_2O and halocarbons, thus achieving GHG removal;
- require minimum additional investment for the PCR.

The development perspectives are promising, as each 200 MW SCPP can at the same time:

- produce annually 680 GWh of non-intermittent renewable electricity, preventing from 0.6 to 0.9 million tons of CO_2 emissions per year [301];
- and allow negative emissions energy production thanks to the PCR.

SCPP-PCR is a negative emissions technology which might help to fight global warming and tackle climate change by preventing or removing nearly 1600 ktons eq-CO_2 yr^{-1} (for each 200 MW plant). Advances in photocatalysis science and technology, as well as in industrial applications, point out the promising potential of photocatalysis for reducing the levels of GHGs in the atmosphere, with a positive impact on climate change effects.

Scale up to 200 MW is highly challenging, in terms of the techno-economic risks involved: 200 MW is a 4000 times larger than the largest SCPP prototype built to date. Beyond that, however, risks and uncertainties will be more manageable – as the system is essentially modular and the process of replication up to say several 1000 SCPPs would benefit from a learning curve. Though costly, SCPPs can also provide socio-economic benefits in developing countries, mainly by using local raw materials: desert sand for the glass canopy, cement and iron for the chimney. They could help to create employment and economic investment in sunny countries that have growing populations and fragile economies. Unlike a number of SRM technologies,

SCPPs do not require aerospace or ballistics technology – as such they are relatively free from concerns about militarization.

Unlike sequestration approaches (CCS, BECCS, DAC), non-CO_2 GHGs removal by SCPPs-PCRs does not require gas capture, purification, compression, and transport – avoiding the risks associated with these processes and avoiding the costs associated to disposal or sequestration of CO_2: no disposal is required for non-CO_2 GHGR.

Non-CO_2 GHGs have poor to no-utility in the atmosphere; removing part of them to cool the Earth will have few drawbacks. Whereas maintaining relatively elevated levels of CO_2 might have positive effects on photosynthesis of some plants and crops species (although in a warmer world there will be a limit to such benefits [317]). Thus non-CO_2 GHG removal is complementary with CDR [39,245].

Emissions must fall to zero to stabilize the global climate (Fig. 1) and achieve 'net zero' or 'climate neutrality' by the second half of the century [10]. Among the many measures on the table to achieve these goals that are discussed in this paper, one has further attraction not already mentioned, which is the ease of monitoring the changes in atmospheric concentrations it provides. Sensors installed at the inlets and outlets of the SCPPs would give real-time information on removal rates, essential for verification and economic justification of such measures in future implementation schemes for GHG reduction. Last but not least, in case of destabilization of methane hydrates [318,319], SCPPs-PCRs can destroy CH_4 and thus be an insurance in the future to prevent a potential climate tipping point [320].

It is the authors' opinion that instead of SRM, ground level methods for removing GHGs other than CO_2 from the atmosphere should be quickly brought into the climate policy debate, as they add vital flexibility to the efforts to tackle climate change at the needed scale.

Acknowledgments

The authors would like to deeply thank the anonymous reviewers for taking the time to review this manuscript and for their very constructive comments and questions that greatly helped to improve the quality of this review.

This research work was supported by the National Key Basic Research Program of China (973 Program; 2013CB228302), the National Natural Science Foundation of China (No. 51106060), the ESI Discipline Promotion Foundation of Wuhan University of Technology (WUT No. 35400664), and the Scientific Research Foundation of WUT (No. 40120237).

References

[1] Butler J, Montzka S. The NOAA annual greenhouse gas index (AGGI). NOAA/ESRL Global Monitoring Division; 2015.
[2] Matthews HD, Caldeira K. Stabilizing climate requires near–zero emissions. Geophys Res Lett 2008;35.
[3] Vichi M, Navarra A, Fogli P. Adjustment of the natural ocean carbon cycle to negative emission rates. Clim Change 2013;118:105–18.
[4] Tian H, Lu C, Ciais P, Michalak AM, Canadell JG, Saikawa E, et al. The terrestrial biosphere as a net source of greenhouse gases to the atmosphere. Nature 2016;531:225–8.
[5] Cao L, Caldeira K. Atmospheric carbon dioxide removal: long-term consequences and commitment. Environ Res Lett 2010;5:024011.
[6] Leung DY, Caramanna G, Maroto-Valer MM. An overview of current status of carbon dioxide capture and storage technologies. Renew Sustain Energy Rev 2014;39:426–43.
[7] Kuramochi T, Ramírez A, Turkenburg W, Faaij A. Comparative assessment of CO_2 capture technologies for carbon-intensive industrial processes. Prog Energy Combust Sci 2012;38:87–112.
[8] Koornneef J, Ramírez A, Turkenburg W, Faaij A. The environmental impact and risk assessment of CO_2 capture, transport and storage–An evaluation of the knowledge base. Prog Energy Combust Sci 2012;38:62–86.
[9] 'International Energy Agency'. Energy and climate change World Energy Outlook Special Report 2015. France: International Energy Agency; 2015. p. 200.
[10] UNEP. The Emissions Gap Report 2015. United Nations Environment Programme (UNEP), ISBN: 978-92-807-3491-1. Nairobi. 2015. p. 98.
[11] Robbins MP, Evans G, Valentine J, Donnison IS, Allison GG. New opportunities for the exploitation of energy crops by thermochemical conversion in Northern Europe and the UK. Prog Energy Combust Sci 2012;38:138–55.
[12] Heidenreich S, Foscolo PU. New concepts in biomass gasification. Prog Energy Combust Sci 2015;46:72–95.
[13] Nigam PS, Singh A. Production of liquid biofuels from renewable resources. Prog Energy Combust Sci 2011;37:52–68.
[14] Huang H-J, Yuan X-Z. Recent progress in the direct liquefaction of typical biomass. Prog Energy Combust Sci 2015;49:59–80.
[15] Holmes G, Nold K, Walsh T, Heidel K, Henderson MA, Ritchie J, et al. Outdoor prototype results for direct atmospheric capture of carbon dioxide. Energy Proc 2013;37:6079–95.
[16] Bobicki ER, Liu Q, Xu Z, Zeng H. Carbon capture and storage using alkaline industrial wastes. Prog Energy Combust Sci 2012;38:302–20.
[17] Shepherd J. Geoengineering the climate: science, governance and uncertainty http://eprints.soton.ac.uk/156647/1/Geoengineering_the_climate.pdf accessed 02-06-2015 Royal Society 2009.
[18] Smith P, Davis SJ, Creutzig F, Fuss S, Minx J, Gabrielle B, et al. Biophysical and economic limits to negative CO_2 emissions. Nat Clim Change 2016;6:42–50.
[19] Smeets EM, Faaij AP, Lewandowski IM, Turkenburg WC. A bottom-up assessment and review of global bio-energy potentials to 2050. Prog Energy Combust Sci 2007;33:56–106.
[20] Hamilton C. Earthmasters: the dawn of the age of climate engineering. Yale University Press; 2013.
[21] de_Richter R, Davies P, Ming T. An unusual renewable energy device for atmospheric removal of GHGs. Oxford, UK: The Oxford Greenhouse Gas Removal Conference In: School OM, editor; 2015.
[22] de_Richter R, Caillol S. Can airflow and radiation under the collector glass contribute to SCPPs' profitability? In: Proceedings of the second international conference on solar chimney power technology SCPT; 2012. p. 28–30. Bochum, Germany: Ruhr-Universität; 2013.
[23] Schlaich J. The solar chimney: electricity from the sun. Edition Axel Menges; 1995.
[24] Myhre G, Shindell D, Bréon F, Collins W, Fuglestvedt J, Huang J, et al. Anthropogenic and natural radiative forcing. Clim Change 2013: 423.
[25] Ruddiman W, Vavrus S, Kutzbach J, He F. Does pre-industrial warming double the anthropogenic total? Anthropocene Rev 2014;1:147–53.
[26] ISBN: 978-1-4419-7990-2 Kuo J. Technological options for reducing non-CO_2 GHG emissions. In: Chen Wei-Yin, Seiner John, Suzuki Toshio, Lackner Maximilian, editors. Handbook of climate change mitigation. Springer; 2012. p. 1781–819. ISBN: 978-1-4419-7990-2 .
[27] Boucher O, Folberth GA. New directions: atmospheric methane removal as a way to mitigate climate change? Atmos Environ 2010;44:3343–5.
[28] Stolaroff JK, Bhattacharyya S, Smith CA, Bourcier WL, Cameron-Smith PJ, Aines RD. Review of methane mitigation technologies with application to rapid release of methane from the Arctic. Environ Sci Technol 2012;46:6455–69.
[29] Williamson P. Emissions reduction: scrutinize CO_2 removal methods. Nature 2016;530:153.
[30] Kemper J. Biomass and carbon dioxide capture and storage: a review. Int J Greenh Gas Control 2015;40:401–30.
[31] Kraxner F, Aoki K, Leduc S, Kindermann G, Fuss S, Yang J, et al. BECCS in South Korea—Analyzing the negative emissions potential of bioenergy as a mitigation tool. Renew Energy 2014;61:102–8.
[32] Vaughan N., Gough C. Synthesising existing knowledge on feasibility of BECCS: Workshop Report. 2015.
[33] de Richter R, Ming T, Shen S, Caillol S. Fighting global warming by greenhouse gas removal: destroying atmospheric nitrous oxide thanks to synergies between two breakthrough technologies. Environ Sci Pollut Res 2016;23:6119–38.
[34] de Richter R, Ming T, Caillol S, Liu W. Fighting global warming by GHG removal: destroying CFCs and HCFCs in solar-wind power plant hybrids producing renewable energy with no-intermittency. Int J Greenh Gas Control 2016.
[35] Schlaich J, Bergermann R, Schiel W, Weinrebe G. Design of commercial solar updraft tower systems - Utilization of solar induced convective flows for power generation. J Sol Eng-T Asme 2005;127:117–24.
[36] Harte R, Höffer R, Krätzig WB, Mark P, Niemann H-J. Solar updraft power plants: engineering structures for sustainable energy generation. Eng Struct 2013;56:1698–706.
[37] Zongker JD. Life cycle assessment of solar updraft tower power plant: EROEI and GWP as a design tool. Wichita State University; 2013.
[38] Cao Q, Pui DY, Lipiń ski W. A concept of a novel solar-assisted large-scale cleaning system (SALSCS) for urban air remediation. Aerosol Air Qual Res 2015;15:1–10.
[39] Kiesgen de_Richter R, Ming T, Caillol S. Fighting global warming by photocatalytic reduction of CO_2 using giant photocatalytic reactors. Renew Sustain Energy Rev 2013;19:82–106.
[40] Haaf W, Friedrich K, Mayr G, Schlaich J. Solar chimneys part I: principle and construction of the pilot plant in Manzanares. Int J Solar Energy 1983;2:3–20.
[41] Haaf W. Solar chimneys: part ii: preliminary test results from the Manzanares pilot plant. Int J Sustain Energy 1984;2:141–61.
[42] Deodhe NP, Raut SG. The floating solar chimney technology. Int J Res 2016;3:479–85.
[43] Papageorgiou CD. Floating solar chimney technology: a solar proposal for China. In: Goswami DZ, YW, editors. Solar world congress of the international-solar-energy-society. Haidianqu, Beijing, People Republic of China: Beijing, People Republic of China: Tsinghua University Press; 2007. p. 172–6.

[44] Zhou X, Yang H, Wang F, Xiao B. Economic analysis of power generation from floating solar chimney power plant. Renew Sustain Energy Rev 2009;13:736–49.
[45] Ming T, Liu W, Pan Y, Xu G. Numerical analysis of flow and heat transfer characteristics in solar chimney power plants with energy storage layer. Energy Convers Manag 2008;49:2872–9.
[46] Pasumarthi N, Sherif SA. Experimental and theoretical performance of a demonstration solar chimney model-part I: mathematical model development. Int J Energy Res 1998;22:277–88.
[47] Padki MM, Sherif SA. On a simple analytical model for solar chimneys. Int J Energy Res 1999;23:345–50.
[48] Pasumarthi N, Sherif SA. Experimental and theoretical performance of a demonstration solar chimney model - Part II: experimental and theoretical results and economic analysis. Int J Energy Res 1998;22:443–61.
[49] Bernardes MAD, Voss A, Weinrebe G. Thermal and technical analyses of solar chimneys. Sol Energy 2003;75:511–24.
[50] Ming T, Meng F, Liu W, Pan Y, Kiesgen de Richter R. Analysis of output power smoothing method of the solar chimney power generating system. Int J Energy Res 2013;37:1657–68.
[51] Pastohr H, Kornadt O, Gürlebeck K. Numerical and analytical calculations of the temperature and flow field in the upwind power plant. Int J Energy Res 2004;28:495–510.
[52] Ming T. Solar chimney power plant generating technology. Academic Press and Zhejiang University Press; 2016.
[53] Lodhi MAK. Application of helio-aero-gravity concept in producing energy and suppressing pollution. Energy Convers Manag 1999;40:407–21.
[54] Tingzhen M, Wei L, Guoliang X. Analytical and numerical investigation of the solar chimney power plant systems. Int J Energy Res 2006;30:861–73.
[55] Gannon AJ, vB TW. Solar chimney turbine performance. J Sol Eng-T Asme 2003;125:101–6.
[56] von Backstrom TW, G AJ. Solar chimney turbine characteristics. Sol Energy 2004;76:235–41.
[57] Fluri TP, Von Backstrom TW. Performance analysis of the power conversion unit of a solar chimney power plant. Sol Energy 2008;82:999–1008.
[58] Pastohr H, Kornadt O, Gurlebeck K. Numerical and analytical calculations of the temperature and flow field in the upwind power plant. Int J Energy Res 2004;28:495–510.
[59] Ming TZ, Liu W, Xu GL, Xiong YB, Guan XH, Pan Y. Numerical simulation of the solar chimney power plant systems coupled with turbine. Renew Energy 2008;33:897–905.
[60] Nizetic SK B. A simplified analytical approach for evaluation of the optimal ratio of pressure drop across the turbine in solar chimney power plants. Appl Energy 2010;87:587–91.
[61] Guo P, Li J, Wang Y, Liu Y. Numerical analysis of the optimal turbine pressure drop ratio in a solar chimney power plant. Sol Energy 2013;98:42–8.
[62] Guo P, Li J, Wang Y, Wang Y. Evaluation of the optimal turbine pressure drop ratio for a solar chimney power plant. Energy Convers Manage 2016;108:14–22.
[63] Schlaich J. The solar chimney. Stuttgart, Germany: Edition Axel Menges; 1995.
[64] Li W, Wei P, Zhou X. A cost-benefit analysis of power generation from commercial reinforced concrete solar chimney power plant. Energy Convers Manag 2014;79:104–13.
[65] Gholamalizadeh E, Kim MH. Thermo-economic triple-objective optimization of a solar chimney power plant using genetic algorithms. Energy 2014;70:204–11.
[66] Cao F, Li H, Zhao L, Guo L. Economic analysis of solar chimney power plants in Northwest China. J Renew Sustain Energy 2013;5:021406.
[67] Harte R, Hoffer R, Krä tzig WB, Mark P, Niemann HJ. Solar updraft power plants: A structural engineering contribution for sustainable and economic power generation. Bautechnik 2012;89:173–81.
[68] Bernardes MAD, von Backstrom TW. Evaluation of operational control strategies applicable to solar chimney power plants. Sol Energy 2010;84:277–88.
[69] Fluri TP, Pretorius JP, Van Dyk C, Von Backstrom TW, Kroger DG, Van Zijl GPAG. Cost analysis of solar chimney power plants. Sol Energy 2009;83:246–56.
[70] Onyango FN, Ochieng RM. The potential of solar chimney for application in rural areas of developing countries. Fuel 2006;85:2561–6.
[71] Papageorgiou CD. Solar turbine power stations with floating solar chimneys. In: Bourkas PDH P, editor. 4th IASTED international conference on power and energy systems. Rhodes, Greece: Int Assoc Sci & Technol Dev; Tech Comm Energy & Power Syst; World Modelling & Simulat Forum; 2004. p. 151–8.
[72] Papageorgiou CD. External wind effects on floating solar chimney. In: Bourkas P, DH P, editors. 4th IASTED international conference on power and energy systems. Rhodes, Geece. Calgary, Alberta, Canada: Acta Press; 2004. p. 159–63.
[73] Papageorgiou CD. Floating solar chimney power stations with thermal storage. In: Bourkas P, editor. 6th IASTED international conference on european power and energy Systems. Rhodes, Greece. Anaheim, CA, USA: Acta Press; 2006. p. 325–31.
[74] Papageorgiou CD, et al. Floating solar chimney technology for desertec. In: Mastorakis NP, M, Mladenov V, Bojkovic Z, Simian D, Kartalopoulos S, editors. 2nd WSEAS/IASME international conference on renewable energy sources. Corfu. AG Loannou Theologou, Athens, Greece: Greece World Scientific and Engineering Academy and Society; 2008. p. 216–22.
[75] Papageorgiou CD, K Petros. A modular solar collector for desert floating solar chimney technology. In: Mastorakis NH, C, Papageorgiou CD, Panagopoulos T, editors. 5th international conference on energy, environment, ecosystems and sustainable development / 2nd international conference on landscape architecture. Vouliagmeni. AG Loannou Theologou, Athens, Greece: Greece World Scientific and Engineering Academy and Society; 2009. p. 126–32.
[76] Cao F, Zhao L, Guo LJ. Simulation of a sloped solar chimney power plant in Lanzhou. Energy Convers Manag 2011;52:2360–6.
[77] Panse SV, Jadhav AS, Gudekar AS, Joshi JB. Inclined solar chimney for power production. Energy Convers Manag 2011;52:3096–102.
[78] Koonsrisuk A. Mathematical modeling of sloped solar chimney power plants. Energy 2012;47:582–9.
[79] Cao F, Zhao L, Li H, Guo L. Performance analysis of conventional and sloped solar chimney power plants in China. Appl Therm Eng 2013;50:582–92.
[80] Koonsrisuk A. Comparison of conventional solar chimney power plants and sloped solar chimney power plants using second law analysis. Sol Energy 2013;98:78–84.
[81] Zhou XP, Yuan S, Bernardes MAD. Sloped-collector solar updraft tower power plant performance. Int J Heat Mass Transf 2013;66:798–807.
[82] Li QL, Fan XY, Xin X, Chao J, Zhou Y. Performance study of solar chimney power plant system with a sloped collector. Special Collect 2015: 1826–32.
[83] Gholamalizadeh E, Kim MH. CFD (computational fluid dynamics) analysis of a solar-chimney power plant with inclined collector roof. Energy 2016;107:661–7.
[84] Maghrebi M, Masoudi Nejad R, Masoudi S. Performance analysis of sloped solar chimney power plants in the southwestern region of Iran. Int J Ambient Energy 2016: 1–8.
[85] Kalash S, Naimeh W, Ajib S. Experimental investigation of the solar collector temperature field of a sloped solar updraft power plant prototype. Sol Energy 2013;98:70–7.
[86] Ming T, Richter RK, Meng F, Pan Y, Liu W. Chimney shape numerical study for solar chimney power generating systems. Int J Energy Res 2013;37:310–22.
[87] Tingzhen M, Wei L, Guoling X, Yanbin X, Xuhu G, Yuan P. Numerical simulation of the solar chimney power plant systems coupled with turbine. Renew Energy 2008;33:897–905.
[88] Fasel HF, Meng F, Shams E, Gross A. CFD analysis for solar chimney power plants. Sol Energy 2013;98:12–22.
[89] Krätzig WB. Physics, computer simulation and optimization of thermo-fluidmechanical processes of solar updraft power plants. Sol Energy 2013;98:2–11.
[90] Patel SK, Prasad D, Ahmed MR. Computational studies on the effect of geometric parameters on the performance of a solar chimney power plant. Energy Convers Manag 2014;77:424–31.
[91] Zhou X, Wang F, Ochieng RM. A review of solar chimney power technology. Renew Sustain Energy Rev 2010;14:2315–38.
[92] Lupi F, Borri C, Harte R, Krätzig W, Niemann HJ. Facing technological challenges of solar updraft power plants. J Sound Vib 2015;334:57–84.
[93] Francke W, de Richter R, Petersen O, Petersen J. A realistic growth path for solar wind power. Appl Mech Mater 2013: 57–64.
[94] Fluri T, Pretorius J, Van Dyk C, Von Backström T, Kröger D, Van Zijl G. Cost analysis of solar chimney power plants. Sol Energy 2009;83:246–56.
[95] Krätzig WB. Solar updraft power technology: fighting global warming and rising energy costs. J Technol Innovat Renew Energy 2015;4:52.
[96] MacKay DJC. Sustainable energy - withou the hot air. www.withouthotair.com; 2008.
[97] Kost C, Mayer JN, Thomsen J, Hartmann N, Senkpiel C, Philipps S, et al. Levelized cost of electricity renewable energy technologies. Fraunhofer Institute for Solar Energy Systems ISE2013.
[98] Bergermann R, Weinrebe G. Realization and costs of solar updraft towers. In: Proceedings of the international conference on solar chimney power technology SCPT; 28–30 Sept., 2010. p. 63–8. 2010.
[99] Ong S, Campbell C, Denholm P, Margolis R, Heath G. Land-use requirements for solar power plants in the United States Technical Report NREL/TP -6A20-56290. Golden, CO: National Renewable Energy Laboratory wwwnrelgov/docs/fy13osti/56290pdf; 2013.
[100] Negishi N, Sano T. Photocatalytic solar tower reactor for the elimination of a low concentration of VOCs. Molecules 2014;19:16624–39.
[101] Cao F, Li H, Ma Q, Zhao L. Design and simulation of a geothermal–solar combined chimney power plant. Energy Convers Manag 2014;84:186–95.
[102] Braslavsky SE, Braun AM, Cassano AE, Emeline AV, Litter MI, Palmisano L, et al. Glossary of terms used in photocatalysis and radiation catalysis (IUPAC Recommendations 2011). Pure Appl Chem 2011;83:931–1014.
[103] Fujishima A, Hashimoto K, Watanabe T. TiO2 photocatalysis: fundamentals and applications: BKC Incorporated; 1999.
[104] Paz Y. Photocatalytic treatment of air: from basic aspects to reactors. Adv Chem Eng 2009;36:289–336.
[105] Zhang Y, Yang R, Zhao R. A model for analyzing the performance of photocatalytic air cleaner in removing volatile organic compounds. Atmos Environ 2003;37:3395–9.
[106] Alfano OM, Cassano AE. Scaling-up of photoreactors: applications to advanced oxidation processes. Adv Chem Eng 2009;36:229–87.
[107] Ray AK. Photocatalytic reactor configurations for water purification: experimentation and modeling. Adv Chem Eng 2009;36:145–84.
[108] Braham RJ, Harris AT. Review of major design and scale-up considerations for solar photocatalytic reactors. Ind Eng Chem Res 2009;48:8890–905.
[109] Hoffmann MR, Martin ST, Choi W, Bahnemann DW. Environmental applications of semiconductor photocatalysis. Chem Rev 1995;95:69–96.

[110] Qu Y, Duan X. Progress, challenge and perspective of heterogeneous photocatalysts. Chem Soc Rev 2013;42:2568–80.
[111] Wang J-L, Wang C, Lin W. Metal–organic frameworks for light harvesting and photocatalysis. ACS Catal 2012;2:2630–40.
[112] Kisch H, Macyk W. Visible–light photocatalysis by modified titania. ChemPhysChem 2002;3:399–400.
[113] Anpo M, Takeuchi M, Ikeue K, Dohshi S. Design and development of titanium oxide photocatalysts operating under visible and UV light irradiation.: the applications of metal ion-implantation techniques to semiconducting TiO_2 and Ti/zeolite catalysts. Curr Opin Solid State Mater Sci 2002;6:381–8.
[114] Coronado JM, Fresno F, Hernández-Alonso MD, Portela R. Design of advanced photocatalytic materials for energy and environmental applications. Springer; 2013.
[115] Graetzel M, Thampi K, Kiwi J. Methane oxidation at room temperature and atmospheric pressure activated by light via polytungstate dispersed on titania. J Phys Chem 1989;93:4128–32.
[116] Thampi KR, Kiwi J, Grätzel M. Room temperature photo-activation of methane on TiO_2 supported molybdena. Catal Lett 1988;1:109–16.
[117] Krishna V, Kamble VS, Selvam P, Gupta NM. Sunlight-assisted photocatalytic oxidation of methane over uranyl-anchored MCM-41. Catal Lett 2004;98:113–6.
[118] Chen X, Li Y, Pan X, Cortie D, Huang X, Yi Z. Photocatalytic oxidation of methane over silver decorated zinc oxide nanocatalysts. Nat Commun 2016;7.
[119] Matsuoka M, Anpo M. Local structures, excited states, and photocatalytic reactivities of highly dispersed catalysts constructed within zeolites. J Photochem Photobiol C 2003;3:225–52.
[120] Obalová L, Reli M, Lang J, Matě jka V, Kukutschová J, Lacný Z, et al. Photocatalytic decomposition of nitrous oxide using TiO_2 and Ag-TiO_2 nanocomposite thin films. Catal Today 2013;209:170–5.
[121] Obalová L, Šihor M, Praus P, Reli M, Koč í K. Photocatalytic and photochemical decomposition of N_2O on ZnS-MMT catalyst. Catal Today 2014;230:61–6.
[122] Tennakone K, Wijayantha K. Photocatalysis of CFC degradation by titanium dioxide. Appl Catal B 2005;57:9–12.
[123] Filby W, Mintas M, Güsten H. Heterogeneous catalytic degradation of chlorofluoromethanes on zinc oxide surfaces. Berichte der Bunsengesellschaft für physikalische Chemie 1981;85:189–92.
[124] Minami W, Kim HJ. Decomposition of halocarbons using TiO2 photocatalyst. Kagaku Kogaku Ronbunshu 2006;32:310–3.
[125] Ragesh P, Ganesh VA, Nair SV, Nair AS. A review on 'self-cleaning and multifunctional materials'. J Mater Chem A 2014;2:14773–97.
[126] Midtdal K, Jelle BP. Self-cleaning glazing products: a state-of-the-art review and future research pathways. Sol Energy Mater Sol Cells 2013;109:126–41.
[127] Chabas A, Lombardo T, Cachier H, Pertuisot M, Oikonomou K, Falcone R, et al. Behaviour of self-cleaning glass in urban atmosphere. Build Environ 2008;43:2124–31.
[128] Spasiano D, Marotta R, Malato S, Fernandez-Ibañez P, Di Somma I. Solar photocatalysis: materials, reactors, some commercial, and pre-industrialized applications. A Compr Approach. Appl Catal B: Environ 2015;170:90–123.
[129] Guan K. Relationship between photocatalytic activity, hydrophilicity and self-cleaning effect of TiO_2/SiO_2 films. Surf Coat Technol 2005;191:155–60.
[130] Lee S-K, McIntyre S, Mills A. Visible illustration of the direct, lateral and remote photocatalytic destruction of soot by titania. J Photochem Photobiol A 2004;162:203–6.
[131] Shindell D, Kuylenstierna JC, Vignati E, van Dingenen R, Amann M, Klimont Z, et al. Simultaneously mitigating near-term climate change and improving human health and food security. Science 2012;335:183–9.
[132] Wong M-S, Chu W-C, Sun D-S, Huang H-S, Chen J-H, Tsai PJ, et al. Visible-light-induced bactericidal activity of a nitrogen-doped titanium photocatalyst against human pathogens. Appl Environ Microbiol 2006;72:6111–6.
[133] Sadowski R, Strus M, Buchalska M, Heczko PB, Macyk W. Visible light induced photocatalytic inactivation of bacteria by modified titanium dioxide films on organic polymers. Photochem Photobiol Sci 2015;14:514–9.
[134] Liu Q, Liu Q, Zhu Z, Zhang J, Zhang B. Application of TiO2 photocatalyst to the stone conservation. Mater Res Innovations 2015;19 S8-51-S8-4.
[135] Pichat P, Disdier J, Hoang-Van C, Mas D, Goutailler G, Gaysse C. Purification/deodorization of indoor air and gaseous effluents by TiO_2 photocatalysis. Catal Today 2000;63:363–9.
[136] Folli A, Strøm M, Madsen TP, Henriksen T, Lang J, Emenius J, et al. Field study of air purifying paving elements containing TiO_2. Atmos Environ 2015;107:44–51.
[137] Lasek J, Yu Y-H, Wu JC. Removal of NOx by photocatalytic processes. J Photochem Photobiol C 2013;14:29–52.
[138] Ibusuki T. Cleaning atmospheric environment. In: Kaneko M, Okura I, editors. Photocatalysis: science and technology (356p), Chapter 8. Springer; 2002. p. 123–59..
[139] Riderelli L, Bocci E, Bocci M, Fava G. Airborne pollutant inside a highway tunnel coated with a photocatalytic mortar. Energy Environ Eng 2015;3:23–31.
[140] Gallus M, Akylas V, Barmpas F, Beeldens A, Boonen E, Boréave A, et al. Photocatalytic de-pollution in the Leopold II tunnel in Brussels: NO_x abatement results. Build Environ 2015;84:125–33.
[141] Paz Y. Application of TiO_2 photocatalysis for air treatment: patents' overview. Appl Catal, B 2010;99:448–60.
[142] Gallus M, Ciuraru R, Mothes F, Akylas V, Barmpas F, Beeldens A, et al. Photocatalytic abatement results from a model street canyon. Environ Sci Pollut Res 2015: 1–12.
[143] Boonen E, Beeldens A. Recent photocatalytic applications for air purification in Belgium. Coatings 2014;4:553–73.
[144] Maggos T, Plassais A, Bartzis J, Vasilakos C, Moussiopoulos N, Bonafous L. Photocatalytic degradation of NO_x in a pilot street canyon configuration using TiO_2-mortar panels. Environ Monit Assess 2008;136:35–44.
[145] Moussiopoulos N, Barmpas P, Ossanlis I, Bartzis J. Comparison of numerical and experimental results for the evaluation of the depollution effectiveness of photocatalytic coverings in street canyons. Environ Model Assess 2008;13:357–68.
[146] Dylla H, Hassan M, Osborn D. Field evaluation of ability of photocatalytic concrete pavements to remove nitrogen oxides. Transp Res Rec: J Transp Res Board 2012: 154–60.
[147] Folli A, Pochard I, Nonat A, Jakobsen UH, Shepherd AM, Macphee DE. Engineering photocatalytic cements: understanding TiO_2 surface chemistry to control and modulate photocatalytic performances. J Am Ceram Soc 2010;93:3360–9.
[148] Osburn L. Literature review on the application of titanium dioxide reactive surfaces on urban infrastructure for depolluting and self-cleaning applications. 5th Post Graduate Conference on Construction Industry Development, Bloemfontein. South Africa; 2008.
[149] Maggos T, Bartzis J, Liakou M, Gobin C. Photocatalytic degradation of NOx gases using TiO2-containing paint: a real scale study. J Hazard Mater 2007;146:668–73.
[150] Chen DH, Li K, Yuan R. Photocatalytic coating on road pavements/structures for NO_x abatement. Beaumont: Texas air research center, Lamar University annual project report submitted to houston advanced research centre and office of air quality planning and standards US environmental protection agency; 2007.
[151] de_Richter R, Caillol S. Fighting global warming: the potential of photocatalysis against CO_2, CH_4, N_2O, CFCs, tropospheric O_3, BC and other major contributors to climate change. J Photochem Photobiol C 2011;12:1–19.
[152] Mo J, Zhang Y, Xu Q, Lamson JJ, Zhao R. Photocatalytic purification of volatile organic compounds in indoor air: a literature review. Atmos Environ 2009;43:2229–46.
[153] Tejasvi R, Sharma M, Upadhyay K. Passive photo-catalytic destruction of airborne VOCs in high traffic areas using TiO_2-coated flexible PVC sheet. Chem Eng J 2015;262:875–81.
[154] Zhong L, Haghighat F. Photocatalytic air cleaners and materials technologies–Abilities and limitations. Build Environ 2015;91:191–203.
[155] Ochiai T, Fujishima A. Photoelectrochemical properties of TiO2 photocatalyst and its applications for environmental purification. J Photochem Photobiol C 2012;13:247–62.
[156] Boonen E, Akylas V, Barmpas F, Boréave A, Bottalico L, Cazaunau M, et al. Construction of a photocatalytic de-polluting field site in the Leopold II tunnel in Brussels. J Environ Manag 2015;155:136–44.
[157] Guerrini GL. Photocatalytic performances in a city tunnel in Rome: NO_x monitoring results. Constr Build Mater 2012;27:165–75.
[158] Sikkema JK. Photocatalytic degradation of NO_x by concrete pavement containing TiO_2. Iowa State University; 2013.
[159] Kleffmann J. Discussion on "Field study of air purification paving elements containing TiO2 "by Folli et al.(2015) Atmos Environ 2016.
[160] Ohtani B. Photocatalysis A to Z—What we know and what we do not know in a scientific sense. J Photochem Photobiol C 2010;11:157–78.
[161] Folli A, Bloh JZ, Strøm M, Pilegaard Madsen T, Henriksen T, Macphee DE. Efficiency of solar-light-driven TiO_2 photocatalysis at different latitudes and seasons. Where and when does TiO_2 really work. J Phys Chem Lett 2014;5:830–2.
[162] Folli A, Macphee D. Future challenges for photocatalytic concrete technology. In: 34th cement and concrete science conference. . University of Sheffield; 2014. p. 209.. Paper Number.
[163] Zhao Z, Zhang W, Lv X, Sun Y, Dong F, Zhang Y. Noble metal-free bi nanoparticles supported on TiO_2 with plasmon-enhanced visible light photocatalytic air purification. Environ Sci: Nano 2016.
[164] Bloh JZ, Folli A, Macphee DE. Photocatalytic NO_x abatement: why the selectivity matters. RSC Adv 2014;4:45726–34.
[165] Bloh JZ, Folli A, Macphee DE. Adjusting nitrogen doping level in titanium dioxide by codoping with tungsten: properties and band structure of the resulting materials. J Phys Chem C 2014;118:21281–92.
[166] Macphee D, Bloh J, Folli A, Greenhalgh DJ. A method of photocatalytically oxidising nitrogen oxides Patent WO2016005760. 2016.
[167] Chabas A, Alfaro S, Lombardo T, Verney-Carron A, Da Silva E, Triquet S, et al. Long term exposure of self-cleaning and reference glass in an urban environment: a comparative assessment. Build Environ 2014;79:57–65.
[168] Murata Y, Tobinai K. Influence of various factors on NO_x removal performance of permeability interlocking block based on photocatalysis. J Struct Constr Eng (Trans Archit Inst Jpn) 2002: 9–15.
[169] Yu C-M. Deactivation and regeneration of environmentally exposed titanium dioxide (TiO_2) based products. Department of Chemistry, Chinese University of Hong Kong; 2003.
[170] Todorova N, Giannakopoulou T, Karapati S, Petridis D, Vaimakis T, Trapalis C. Composite TiO_2/clays materials for photocatalytic NO_x oxidation. Appl Surf Sci 2014;319:113–20.
[171] Beeldens A, Cassar L, Murata Y. Applications of TiO_2 photocatalysis for air purification. Applications of titanium dioxide photocatalysis to construction materials. Netherlands: Springer; 2011. p. 23–35.
[172] Sikkema J, Ong S, Alleman J. Photocatalytic concrete pavements: laboratory investigation of NO oxidation rate under varied environmental conditions. Constr Build Mater 2015;100:305–14.
[173] Sikkema JK, Alleman JE, Cackler T, Taylor PC, Bai B, Ong SK, et al. Photocatalytic pavements. Climate change, energy, sustainability and pavements. Springer; 2014. p. 275–307.

[174] Cunningham J, Kelly JJ, Penny A. Reactions involving electron transfer at semiconductor surfaces. I. Dissociation of nitrous oxide over n-type semiconductors at 20. deg. J Phys Chem 1970;74:1992–2000.

[175] Cunningham J, Kelly JJ, Penny A. Reactions involving electron transfer at semiconductor surfaces. II. Photoassisted dissociation of nitrous oxide over illuminated ferric oxide and zinc oxides. J Phys Chem 1971;75:617–25.

[176] Reli M, Huo P, Šihor M, Ambrožová N, Troppová I, Matějová L, et al. Novel TiO_2/C_3N_4 Photocatalysts for photocatalytic reduction of CO_2 and for photocatalytic decomposition of N_2O. J Phys Chem A 2016;120:8564–73.

[177] Ebitani K, Hirano Y, Morikawa A. Rare earth ions as heterogeneous photocatalysts for the decomposition of dinitrogen monoxide (N_2O). J Catal 1995;157:262–5.

[178] Ebitani K, Morokuma M, Kim J-H, Morikawa A. Evidence for the role of monovalent copper ions in the photocatalytic N_2O decomposition on excessively copper ion-containing ZSM-5 zolite. Bull Chem Soc Jpn 1993;66:3811–2.

[179] Ebitani K, Morokuma M, Morikawa A. Active state of copper in copper-containing ZSM-5 zeolites for photocatalytic decomposition of dinitrogen monoxide. Stud Surf Sci Catal 1994;84:1501–6.

[180] Ebitani K, Morokuma M, Kim J, Morikawa A. Photocatalytic decomposition of nitrous oxide on Cu ion-containing ZSM-5 catalyst. J Catal 1993;141:725–8.

[181] Ebitani K, Morokuma M, Kim J-H, Morikawa A. Photocatalytic decomposition of dinitrogen oxide on Cu-containing ZSM-5 catalyst. J Chem Soc, Faraday Trans 1994;90:377–81.

[182] Matsuoka M, Takahashi K, Yamashita H, Anpo M. Local structures of copper ion catalysts anchored onto various oxide supports and their photocatalytic reactivities for the decomposition of N_2O at 298 K. In Situ XAFS, photoluminescence, EPR Investigations. J Phys IV 1997;7 C2-943-C2-4.

[183] Matsuoka M, Ju W-S, Takahashi K, Yamashita H, Anpo M. Photocatalytic decomposition of N_2O into N_2 and O_2 at 298 K on Cu (I) ion catalysts anchored onto various oxides. The effect of the coordination state of the Cu (I) ions on the photocatalytic reactivity. J Phys Chem B 2000;104:4911–5.

[184] Kočí K, Matějová L, Obalová L, Čapek L, Wu JC. Preparation, characterization and photocatalytic performance of TiO_2 prepared by using pressurized fluids in CO_2 reduction and N_2O decomposition. J Sol−Gel Sci Technol 2015: 1–9.

[185] Kočí K, Krejčíková S, Šolcová O, Obalová L. Photocatalytic decomposition of N_2O on Ag-TiO_2. Catal Today 2012;191:134–7.

[186] Matějová L, Šihor M, Brunátová T, Ambrožová N, Reli M, Čapek L, et al. Microstructure-performance study of cerium-doped TiO_2 prepared by using pressurized fluids in photocatalytic mitigation of N_2O. Res Chem Intermed 2015: 1–15.

[187] Kočí K, Reli M, Troppová I, Šihor M, Kubková J, Kustrowski P, et al. Photocatalytic decomposition of N_2O over TiO_2/gC_3N_4 photocatalysts heterojunction. Appl Surf Sci 2017 http://dx.doi.org/10.1016/j.apsusc.2016.11.242 (in press).

[188] Ju W-S, Matsuoka M, Anpo M. The photocatalytic reduction of nitrous oxide with propane on lead (II) ion-exchanged ZSM-5 catalysts. Catal Lett 2001;71:91–3.

[189] Ju W-S, Matsuoka M, Yamashita H, Anpo M. Local structure of Pb (II) ion catalysts anchored within zeolite cavities and their photocatalytic reactivity for the elimination of N2O. J Synchrotron Radiat 2001;8:608–9.

[190] Ju W-S, Matsuoka M, Anpo M. Incorporation of silver (I) ions within zeolite cavities and their photocatalytic reactivity for the decomposition of N_2O into N_2 and O_2. Int J Photoenergy 2003;5:17–9.

[191] Ju W-S, Matsuoka M, Iino K, Yamashita H, Anpo M. The local structures of silver (I) ion catalysts anchored within zeolite cavities and their photocatalytic reactivities for the elimination of N_2O into N_2 and O_2. J Phys Chem B 2004;108:2128–33.

[192] Matsuoka M, Ju W-S, Yamashita H, Anpo M. Investigations on the local structure of Ag+/ZSM-5 catalysts and their photocatalytic reactivities for the decomposition of N_2O at 298 K. J Synchrotron Radiat 2001;8:613–5.

[193] Matsuoka M, Ju W-S, Yamashita H, Anpo M. In situ characterization of the Ag+ ion-exchanged zeolites and their photocatalytic activity for the decomposition of N_2O into N_2 and O_2 at 298 K. J Photochem Photobiol A 2003;160:43–6.

[194] Rakhmawaty D, Matsuoka M, Anpo M. Photocatalytic decomposition of N_2O in the presence of CO on Ti/USY photocatalysts. Proc Int Seminar on Chem 2008: 342–5 http://chemistry.unpad.ac.id/isc-proceeding/2008/Pdf/OP/0342-0345%20Diana.pdf ISBN 978-979-18962-0-7. Jatinangor.

[195] Sano T, Negishi N, Mas D, Takeuchi K. Photocatalytic decomposition of N2O on highly dispersed Ag+ ions on TiO_2 prepared by photodeposition. J Catal 2000;194:71–9.

[196] Kudo A, Sakata T. Photocatalytic decomposition of N_2O at room temperature. Chem Lett 1992: 2381–4.

[197] Anpo M, Matsuoka M, Hano K, Mishima H, Ono T, Yamashita H. Photocatalytic decomposition of N_2O on Cu+/Y-zeolite catalysts prepared by ion-exchange. Korean J Chem Eng 1997;14:498–501.

[198] Guarino M, Costa A, Porro M. Photocatalytic TiO2 coating—to reduce ammonia and greenhouse gases concentration and emission from animal husbandries. Bioresour Technol 2008;99:2650–8.

[199] Costa A, Chiarello GL, Selli E, Guarino M. Effects of TiO2 based photocatalytic paint on concentrations and emissions of pollutants and on animal performance in a swine weaning unit. J Environ Manag 2012;96:86–90.

[200] Zabloudilova P, Pecen J, Petrackova B, Dolejs J. Influence of photocatalytic TiO_2 coating on gaseous emissions, odour and microbiological contamination in stable environment within animal husbandries. NANOCON International Conference; 2010. p. 258–63 http://konsys-t.tanger.cz/files/proceedings/nanocon_10/lists/papers/573.pdf;.

[201] Tanaka K, Hisanaga T. Photodegradation of chlorofluorocarbon alternatives on metal oxide. Sol Energy 1994;52:447–50.

[202] Kutsuna S, Takeuchi K, Ibusuki T. Adsorption and reaction of trichlorofluoromethane on various particles. J Atmos Chem 1992;14:1–10.

[203] Wylie DJ, Cooney RP, Seakins JM, Millar GJ. Spectroscopic studies of the adsorption and reactions of chlorofluorocarbons (CFC-11 and CFC-12) and hydrochlorofluorocarbon (HCFC-22) on oxide surfaces. Vib Spectrosc 1995;9:245–56.

[204] Sangchakr B, Hisanaga T, Tanaka K. Photocatalytic degradation of 1, 1-difluoroethane (HFC-152a). Chemosphere 1998;36:1985–92.

[205] Jo W-K, Park KH. Heterogeneous photocatalysis of aromatic and chlorinated volatile organic compounds (VOCs) for non-occupational indoor air application. Chemosphere 2004;57:555–65.

[206] Zhou X-L, Cowin J. Photodestruction of CCl4 on MgO films with/without water. J Phys Chem 1996;100:1055–65.

[207] Balko BA, Tratnyek PG. Photoeffects on the reduction of carbon tetrachloride by zero-valent iron. J Phys Chem B 1998;102:1459–65.

[208] Choi W, Hoffmann MR. Photoreductive mechanism of CCl4 degradation on TiO_2 particles and effects of electron donors. Environ Sci Technol 1995;29:1646–54.

[209] Wiltowski T, Howerton R, Lalvani S, Zamansky V. Photocatalytic oxidation of trichloroethylene and carbon tetrachloride using titanium dioxide filter as a catalyst. Energy Sources 2001;23:845–52.

[210] Hsu T-LC, Chang I-J, Ward DL, Nocera DG. Photoreduction of 1, 2-dichloroalkanes and 1, 2-dichloroalkenes by Tetrakis (diphenyl phosphato) dimolybdenum (II, II). Inorg Chem 1994;33:2932–7.

[211] Alberici RM, Jardim WF. Photocatalytic destruction of VOCs in the gas-phase using titanium dioxide. Appl Catal B 1997;14:55–68.

[212] Calza P, Minero C, Hiskia A, Papaconstantinou E, Pelizzetti E. Photocatalytic transformations of CCl_3Br, CBr_3F, $CHCl_2Br$ and CH_2BrCl in aerobic and anaerobic conditions. Appl Catal B 2001;29:23–34.

[213] Calza P, Minero C, Hiskia A, Papacostantinou E, Pelizzetti E. Photolytic and photocatalytic decomposition of bromomethanes in irradiated aqueous solutions. Appl Catal B 1999;21:191–202.

[214] Yin LF. Photocatalytic degradation of hydrofluorocarbon under visible light irradiation. Appl Mech Mater 2014: 1357–60.

[215] Nguyen T, Ollis D. Complete heterogeneously photocatalyzed transformation of 1, 1-and 1, 2-dibromoethane to carbon dioxide and hydrogen bromide. J Phys Chem 1984;88:3386–8.

[216] Martin CA, Baltanas MA, Cassano AE. Photocatalytic reactors. 3. Kinetics of the decomposition of chloroform including absorbed radiation effects. Environ Sci Technol 1996;30:2355–64.

[217] Borisch J, Pilkenton S, Miller ML, Raftery D, Francisco JS. TiO2 photocatalytic degradation of dichloromethane: an FTIR and solid-state NMR study. J Phys Chem B 2004;108:5640–6.

[218] Choi W, Hoffmann MR. Novel photocatalytic mechanisms for $CHCl_3$, $CHBr_3$, and CCl_3CO_2-degradation and the fate of photogenerated trihalomethyl radicals on TiO2. Environ Sci Technol 1996;31:89–95.

[219] Imamura S, Higashihara T, Jindai H. Reactivating effect of water on freon 12 decomposition catalysts. Chem Lett 1993: 1667–70.

[220] Ohko Y, Nakamura Y, Fukuda A, Matsuzawa S, Takeuchi K. Photocatalytic oxidation of nitrogen dioxide with TiO_2 thin films under continuous UV-light illumination. J Phys Chem C 2008;112:10502–8.

[221] Portela R, Suárez S, Rasmussen S, Arconada N, Castro Y, Duran A, et al. Photocatalytic-based strategies for H_2S elimination. Catal Today 2010;151:64–70.

[222] D'Auria M, Emanuele L, Racioppi R, Velluzzi V. Photochemical degradation of crude oil: comparison between direct irradiation, photocatalysis, and photocatalysis on zeolite. J Hazard Mater 2009;164:32–8.

[223] Djeghri N, Formenti M, Juillet F, Teichner S. Photointeraction on the surface of titanium dioxide between oxygen and alkanes. Faraday Discuss Chem Soc 1974;58:185–93.

[224] Brigden CT, Poulston S, Twigg MV, Walker AP, Wilkins AJ. Photo-oxidation of short-chain hydrocarbons over titania. Appl Catal B 2001;32:63–71.

[225] Wada K, Yoshida K, Takatani T, Watanabe Y. Selective photo-oxidation of light alkanes using solid metal oxide semiconductors. Appl Catal A 1993;99:21–36.

[226] Wada K, Yamada H, Watanabe Y, Mitsudo TA. Selective photo-assisted catalytic oxidation of methane and ethane to oxygenates using supported vanadium oxide catalysts. J Chem Soc Faraday Trans 1998;94:1771–8.

[227] Tanaka T, Ito T, Takenaka S, Funabiki T, Yoshida S. Photocatalytic oxidation of alkane at a steady rate over alkali-ion-modified vanadium oxide supported on silica. Catal Today 2000;61:109–15.

[228] Twesme TM, Tompkins DT, Anderson MA, Root TW. Photocatalytic oxidation of low molecular weight alkanes: observations with ZrO_2−TiO_2 supported thin films. Appl Catal B 2006;64:153–60.

[229] Formenti M, Juillet F, Meriaudeau P, Teichner S, Vergnon P. Preparation in a hydrogen-oxygen flame of ultrafine metal oxide particles. Oxidative properties toward hydrocarbons in the presence of ultraviolet radiation. J Colloid Interface Sci 1972;39:79–89.

[230] Fujita Y, Hatano K, Yanagita M, Katsu T, Sato M, Kwan T. The photosensitized decomposition of methane adsorbed on porous vycor glasses coated with metal oxides at 77° K. Bull Chem Soc Jpn 1971;44:2884.

[231] Lien CF, Chen MT, Lin YF, Lin JL. Photooxidation of methane over TiO_2. J Chin Chem Soc 2004;51:37–42.

[232] Kaliaguine S, Shelimov B, Kazansky V. Reactions of methane and ethane with hole centers O−. J Catal 1978;55:384–93.

[233] Kleinschmidt O, Hesse D. Kinetics of the photocatalytic total oxidation of different alkanes and alkenes on TiO_2 powder. Can J Chem Eng 2002;80:71–8.

[234] Haeger A, Kleinschmidt O, Hesse D. Kinetics of photocatalyzed gas reactions using titanium dioxide as the catalyst–part i: photocatalyzed total oxidation of olefines with oxygen. Chem Eng Technol 2004;27:181–8.

[235] Haeger A, Kleinschmidt O, Hesse D. Kinetics of photocatalyzed gas reactions using titanium dioxide as the catalyst Part II: photocatalyzed total oxidation of alkanes with oxygen. Chem Eng Technol 2004;27:1019–26.

[236] Finger M, Haeger A, Hesse D. Kinetics and mechanisms of photocatalyzed total oxidation reaction of hydrocarbon species with titanium dioxide in the gas phase. Chem Eng Technol 2005;28:783–9.

[237] Bellobono IR, Stanescu R, Costache C, Canevali C, Morazzoni F, Scotti R, et al. Laboratory-scale photomineralization of n-alkanes in gaseous phase by photocatalytic membranes immobilizing titanium dioxide. Int J Photoenergy 2006;2006.

[238] Krishna V, Kamble VS, Gupta NM, Selvam P. Uranyl-anchored MCM-41 as a highly efficient photocatalyst in the oxidative destruction of short chain linear alkanes: an in situ FTIR study. J Phys Chem C 2008;112:15832–43.

[239] Liu D, P-y Zhang, Wang J. Photocatalytic degradation of methane under irradiation of vacuum ultraviolet light. China Environ Sci 2006;26:653–6.

[240] Pengyi Z, Fuyan L, Gang Y, Qing C, Wanpeng Z. A comparative study on decomposition of gaseous toluene by O_3/UV, TiO_2/UV and O_3/TiO_2/UV. J Photochem Photobiol A 2003;156:189–94.

[241] Dreyer M, Newman G, Lobban L, Kersey S, Wang R, Harwell J. Enhanced oxidation of air contaminants on an ultra-low density UV-accessible aerogel photocatalyst. MRS Proceedings. Cambridge Univ Press; 1996. p. 141.

[242] Newman GK, Harwell JH, Lobban L. Enhanced oxidation of air contaminants on an ultra-low density UV-accessible aerogel photocatalyst. U.S. Patent No. 6,241,856.: Google Patents; 2001.

[243] Pan X, Chen X, Yi Z. Photocatalytic oxidation of methane over $SrCO_3$ decorated $SrTiO_3$ nanocatalysts via a synergistic effect. Phys Chem Chem Phys 2016.

[244] Allan W, Lowe D, Gomez A, Struthers H, Brailsford G. Interannual variation of 13C in tropospheric methane: implications for a possible atomic chlorine sink in the marine boundary layer. J Geophys Res: Atmos 2005;110 (1984–2012).

[245] Oeste FD, de Richter R, Ming T, Caillol S. Climate engineering by mimicking the natural dust climate control: the iron salt aerosols method. Earth Syst Dynam Discuss (in review) 2016 doi:105194/esd-2016-32.

[246] López HH, Martínez A. Selective photo-assisted oxidation of methane into formaldehyde on mesoporous VO x/SBA-15 catalysts. Catal Lett 2002;83:37–41.

[247] Murcia-López S, Villa K, Andreu T, Morante J. Improved selectivity for partial oxidation of methane to methanol in the presence of nitrite ions and $BiVO_4$ photocatalyst. Chem Commun 2015;51:7249–52.

[248] Murcia-López S, Villa K, Andreu T, Morante JR. Partial oxidation of methane to methanol using bismuth-based photocatalysts. ACS Catal 2014;4:3013–9.

[249] Xin J, Chen X-H, Suo J-S, Zhang X-M, Yan L, Li S-B. Photocatalytic oxidation of methane over Nb-MCM-41 mesoporous molecular sieve catalyst under mild conditions. J Mol Catal (China) 2001;15:219–21.

[250] Villa K, Murcia-López S, Andreu T, Morante JR. Mesoporous WO_3 photocatalyst for the partial oxidation of methane to methanol using electron scavengers. Appl Catal B 2015;163:150–5.

[251] Villa K, Murcia-López S, Andreu T, Morante JR. On the role of WO_3 surface hydroxyl groups for the photocatalytic partial oxidation of methane to methanol. Catal Commun 2015;58:200–3.

[252] Li Z, Hoflund GB. A review on complete oxidation of methane at low temperatures. J Nat Gas Chem 2003;12:153–60.

[253] Walther G, Cervera-Gontard L, Quaade U, Horch S. Low temperature methane oxidation on differently supported 2 nm Au nanoparticles. Gold Bull 2009;42:13–9.

[254] Yuliati L, Yoshida H. Photocatalytic conversion of methane. Chem Soc Rev 2008;37:1592–602.

[255] Taylor CE. Methane conversion via photocatalytic reactions. Catal Today 2003;84:9–15.

[256] Shimura K, Yoshida H. Semiconductor photocatalysts for non-oxidative coupling, dry reforming and steam reforming of methane. Catal Surv Asia 2014;18:24–33.

[257] Shimura K, Kato S, Yoshida T, Itoh H, Hattori T, Yoshida H. Photocatalytic steam reforming of methane over sodium tantalate. J Phys Chem C 2010;114:3493–503.

[258] Shimura K, Yoshida T, Yoshida H. Photocatalytic activation of water and methane over modified gallium oxide for hydrogen production. J Phys Chem C 2010;114:11466–74.

[259] Pelaez M, Nolan NT, Pillai SC, Seery MK, Falaras P, Kontos AG, et al. A review on the visible light active titanium dioxide photocatalysts for environmental applications. Appl Catal B 2012;125:331–49.

[260] Ming T, Wu Y, De_Richter R, Liu W, Sherif S. Solar updraft power plant system: A brief review and a case study on a new system with radial partition walls in its collector. Renew Sustain Energy Rev 2017;69:472–87.

[261] von Backström TW, Gannon AJ. Compressible flow through solar power plant chimneys. J Sol Energy Eng 2000;122:138–45.

[262] von Backström TW, Bernhardt A, Gannon AJ. Pressure drop in solar power plant chimneys. J Sol Energy Eng 2003;125:165–9.

[263] Lackner KS, Brennan S, Matter JM, Park A-HA, Wright A, Van Der Zwaan B. The urgency of the development of CO_2 capture from ambient air. Proc Natl Acad Sci 2012;109:13156–62.

[264] Carbon, Engineering. Industrial-scale capture of CO_2 from ambient air accessed https://www.youtube.com/watch?t=374&v=GkEAA7VnyhE; 28 June 2015 accessed .

[265] Espagnol S, Hassouna M, Robin P, Levasseur P, Vallet C, Guyomard F. Incidence d'une couverture photocatalytique au stockage de lisier porcin sur les émissions gazeuses (NH_3, N_2O, Ch_4, CO_2). Journées Recherche Porcine 2006;38:27–34.

[266] Costa A, Guarino M. Photocatalytic TIO_2 treatment effects on ammonia, greenhouse gases, dust concentration and emission in a weaning room. Agricultural and biosystems engineering for a sustainable world International Conference on Agricultural Engineering, Hersonissos, Crete, Greece, 23-25 June 2008. European Society of Agricultural Engineers (AgEng); 2008. p. OP–1260.

[267] Melse R, Hilhorst M. Photocatalytic oxidation on TiO2 of methane from exhaust air of animal houses and liquid manure storages= Fotokatalytische oxidatie op TiO2 van methaan uit stallen en drijfmestopslagen: Agrotechnology & Food innovations; 2003.

[268] Bellobono IR, de Martini G, Tozzi PM, Canevali C, Morazzoni F, Scotti R, et al. Modelling of quantum yields in photocatalytic membrane reactors immobilising titanium dioxide. Int J Photoenergy 2006: 73167. 2006:Article ID.

[269] Bellobono IR, Rossi M, Testino A, Morazzoni F, Bianchi R, de Martini G, et al. Influence of irradiance, flow rate, reactor geometry, and photopromoter concentration in mineralization kinetics of methane in air and in aqueous solutions by photocatalytic membranes immobilizing titanium dioxide. Int J Photoenergy 2008:283741 2008:Article ID.

[270] Bellobono IR, Morazzoni F, Bianchi R, Mangone ES, Stanescu R, Costache C, et al. Laboratory-scale photomineralisation of n-alkanes in aqueous solution, by photocatalytic membranes immobilising titanium dioxide. Int J Photoenergy 2005;7:79–85.

[271] Wu Q, van de Krol R. Selective photoreduction of nitric oxide to nitrogen by nanostructured TiO2 photocatalysts: role of oxygen vacancies and iron dopant. J Am Chem Soc 2012;134:9369–75.

[272] Anpo M, Zhang SG, Mishima H, Matsuoka M, Yamashita H. Design of photocatalysts encapsulated within the zeolite framework and cavities for the decomposition of NO into N2 and O2 at normal temperature. Catal Today 1997;39:159–68.

[273] Pretorius JP. Optimization and control of a large-scale solar chimney power plant [PhD, Dr.-ME Tesis]. South Africa: University of Stellenbosch; 2007.

[274] Paz Y. Composite titanium dioxide photocatalysts and the" adsorb & shuttle" approach: a review. Solid state phenomena. Trans Tech Publ; 2010. p. 135–62.

[275] Park H, Park Y, Kim W, Choi W. Surface modification of TiO_2 photocatalyst for environmental applications. J Photochem Photobiol C 2013;15:1–20.

[276] Rabani J, Goldstein S. Mechanisms of reactions induced by photocatalysis of titanium dioxide nanoparticles. Environmental photochemistry part III. The handbook of environmental chemistry, 35; 2013. p. 2013115–57.

[277] Minero C, Bedini A, Minella M. On the standardization of the photocatalytic gas/solid tests. Int J Chem Reactor Eng 2013;11:717–32.

[278] Zhong L, Haghighat F, Lee CS. Ultraviolet photocatalytic oxidation for indoor environment applications: experimental validation of the model. Build Environ 2013;62:155–66.

[279] Votruba J, Mikuš O, Nguen K, Hlaváček V, Skřivánek J. Heat and mass transfer in honeycomb catalysts—II. Chem Eng Sci 1975;30:201–6.

[280] Zukauskas A, Slanciauskas A. Heat transfer in turbulent fluid flows. 1987.

[281] Lienhard JH. A heat transfer textbook: Courier Corporation; 2013.

[282] Cussler E. Diffusion: mass transfer in fluid systems. Cambridge University Press; 1984.

[283] Monteith J, Unsworth M. Principles of environmental physics: plants, animals, and the atmosphere. Academic Press; 2013.

[284] Massman W. A review of the molecular diffusivities of H_2O, CO_2, CH_4, CO, O_3, SO_2, NH_3, N_2O, NO, and NO_2 in air, O_2 and N_2 near STP. Atmos Environ 1998;32:1111–27.

[285] Schlaich Jr, Bergermann R, Schiel W, Weinrebe G. Design of commercial solar updraft tower systems—utilization of solar induced convective flows for power generation. J Sol Energy Eng 2005;127:117–24.

[286] In S-I, Nielsen MG, Vesborg PC, Hou Y, Abrams BL, Henriksen TR, et al. Photocatalytic methane decomposition over vertically aligned transparent TiO_2 nanotube arrays. Chem Commun 2011;47:2613–5.

[287] Nielsen MG, In S-I, Vesborg PC, Pedersen T, Almtoft KP, Andersen IH, et al. A generic model for photocatalytic activity as a function of catalyst thickness. J Catal 2012;289:62–72.

[288] Taranto J, Frochot D, Pichat P. Photocatalytic air purification: comparative efficacy and pressure drop of a TiO_2-coated thin mesh and a honeycomb monolith at high air velocities using a 0.4 m3 close-loop reactor. Sep Purif Technol 2009;67:187–93.

[289] Deich N, de_Richter R. Expert dialogue: should we be pursuing strategies to remove non-CO2 greenhouse gases from the air? 2016.

[290] He Y, Zhou W, Qian G, Chen B. Methane storage in metal–organic frameworks. Chem Soc Rev 2014;43:5657–78.

[291] Sadasivam BY, Reddy KR. Adsorption and transport of methane in biochars derived from waste wood. Waste Manag 2015.

[292] Hannus I. Adsorption and transformation of halogenated hydrocarbons over zeolites. Appl Catal A 1999;189:263–76.

[293] Saha D, Bao Z, Jia F, Deng S. Adsorption of CO_2, CH_4, N_2O, and N_2 on MOF-5, MOF-177, and zeolite 5A. Environ Sci Technol 2010;44:1820–6.

[294] Khalil M, Rasmussen R. The potential of soils as a sink of chlorofluorocarbons and other man–made chlorocarbons. Geophys Res Lett 1989;16:679–82.

[295] Benzoni L, Garbassi F. Reactivity of fluorochloromethanes with desert sands. Berichte der Bunsengesellschaft für physikalische Chemie 1984;88:379–82.

[296] Gäb S, Schmitzer J, Turner WV, Korte F. Mineralization of CCl_4 and CCl_2F_2 on solid surfaces. Z Naturforschung B 1980;35:946–52.

[297] Rubin ES, Mantripragada H, Marks A, Versteeg P, Kitchin J. The outlook for improved carbon capture technology. Prog Energy Combust Sci 2012;38:630–71.
[298] Nakata T, Silva D, Rodionov M. Application of energy system models for designing a low-carbon society. Prog Energy Combust Sci 2011;37:462–502.
[299] Zeman FS, Keith DW. Carbon neutral hydrocarbons. Philos Trans R Soc Lond A: Math, Phys Eng Sci 2008;366:3901–18.
[300] Schindelin H. Entwurf eines 1500 m hohen Turms eines Solar-Aufwindkraftwerkes Parameteruntersuchung zur Geometrieoptimierung (Design of a 1500 m high tower of a Solar Updraft Chimney: Parameter study of the geometry optimization), PhD thesis. Univ of Wuppertal; 2002.
[301] Enviromission. accessed http://www.enviromission.com.au/EVM/ShowStaticCategory.aspx?CategoryID=226; 30 May 2015 accessed .
[302] Lasek J, Yu Y-H, Wu JC. Removal of NO_x by photocatalytic processes. J Photochem Photobiol C 2013;14:29–52.
[303] Costarramone N, Cantau C, Desauziers V, Pécheyran C, Pigot T, Lacombe S. Photocatalytic air purifiers for indoor air: european standard and pilot room experiments. Environ Sci Pollut Res 2016: 1–9.
[304] Ferraro AJ, Charlton−Perez AJ, Highwood EJ. Stratospheric dynamics and midlatitude jets under geoengineering with space mirrors and sulfate and titania aerosols. J Geophys Res: Atmos 2015;120:414–29.
[305] Tang M, Telford P, Pope F, Rkiouak L, Abraham N, Archibald A, et al. Heterogeneous reaction of N_2O_5 with airborne TiO_2 particles and its implication for stratospheric particle injection. Atmos Chem Phys 2014;14:6035–48.
[306] Pope F, Braesicke P, Grainger R, Kalberer M, Watson I, Davidson P, et al. Stratospheric aerosol particles and solar-radiation management. Nat Clim Change 2012;2:713–9.
[307] Weisenstein DK, Keith DW, Dykema J. Solar geoengineering using solid aerosol in the stratosphere. Atmos Chem Phys 2015;15:11835–59.
[308] Ming T, de_Richter R, Liu W, Caillol S. Fighting global warming by climate engineering: is the Earth radiation management and the solar radiation management any option for fighting climate change? Renew Sustain Energy Rev 2014;31:792–834.
[309] Lomax G, Workman M, Lenton T, Shah N. Reframing the policy approach to greenhouse gas removal technologies. Energy Policy 2015;78:125–36.
[310] Smith D, Vodden K, Rucker L, Cunningham R. Global benefits and costs of the montreal protocol on substances that deplete the ozone layer. Ottawa: Environment Canada; 1997.
[311] Nia ES, Ghazikhani M. Numerical investigation on heat transfer characteristics amelioration of a solar chimney power plant through passive flow control approach. Energy Convers Manag 2015;105:588–95.
[312] Mills A, Burns L, O'Rourke C, Elouali S. Kinetics of the photocatalysed oxidation of NO in the ISO 22197 reactor. J Photochem Photobiol A 2016;321:137–42.
[313] Engel A, Glyk A, Hülsewig A, Große J, Dillert R, Bahnemann DW. Determination of the photocatalytic deposition velocity. Chem Eng J 2015;261:88–94.
[314] Programme UNE. Environmental effects of ozone depletion and its interactions with climate change: progress report, 2015. Photochem Photobiol Sci 2016;15:141–74.
[315] Stocker T, Qin D, Plattner G, Tignor M, Allen S, Boschung J, et al. IPCC WG1 AR5: climate change 2013: the physical science basis. Contribution of working group I to the fifth assessment report of the intergovernmental panel on climate change; 2013.
[316] Howarth RW. A bridge to nowhere: methane emissions and the greenhouse gas footprint of natural gas. Energy Sci Eng 2014;2:47–60.
[317] Tomimatsu H, Tang Y. Effects of high CO_2 levels on dynamic photosynthesis: carbon gain, mechanisms, and environmental interactions. J Plant Res 2016: 1–13.
[318] Behl R, Kennett J, Cannariato K, Hendy I. Methane hydrates and climate change; the clathrate gun hypothesis. AAPG Bull 2003;87:1693.
[319] de Garidel-Thoron T, Beaufort L, Bassinot F, Henry P. Evidence for large methane releases to the atmosphere from deep-sea gas-hydrate dissociation during the last glacial episode. Proc Natl Acad Sci USA 2004;101:9187–92.
[320] Lenton TM. Early warning of climate tipping points. Nat Clim Change 2011;1:201–9.